MECHANICAL PROPERTIES AND SUPERMOLECULAR STRUCTURE OF AROMATIC CARBOXYLATE IONOMERS AND THEIR NON-IONIC PRECURSORS

by

Erica Besso

A thesis submitted to the Faculty of Graduate Studies and Research in partial fulfilment of the requirements for the degree of Doctor of Philosophy.

Department of Chemistry
McGill University
Montreal, Quebec, Canada

May 1984

Short title for thesis (Ph.D.) of ERICA BESSO , Dept. of Chemistry to appear along the spine of the bound copy:

Physical Properties of Aromatic Carboxylate Ionomers

MECHANICAL PROPERTIES AND SUPERMOLECULAR STRUCTURE OF AROMATIC CARBOXYLATE IONOMERS AND THEIR NON-IONIC PRECURSORS

Abstract

This thesis describes the investigation of the physical properties of an aromatic carboxylate ionomer system and its non-ionic precursor. The study is focused on microporous films (ca. 150 μm in thickness) of 600 equivalent weight. These materials were studied with the dual objectives of investigating the structure-property relations in a novel ionomer system and of exploring its viability as a separator in alkaline water electrolysis.

The presence of ionic interactions was confirmed in this relatively rigid ionomer of high glass transition temperature (>400°C). The ionic groups do not appear to form large aggregates. Their presence imparts good wettability to the films. These are extremely brittle in the dry state but become ductile in aqueous environments. At 80°C, hydrated ionomer films are characterized by a tensile modulus of ca. 100 MPa, tensile strength of 100 MPa and elongation to break of 30 %.

STRUCTURE ET PROPRIETES PHYSIQUES D'UN SYSTEME D'IONOMERES AROMATIQUES CARBOXYLES ET DE LEURS PRECURSEURS

Résumé

Cette étude porte sur les propriétés physiques d'un nouvel ionomère, un aromatique carboxylé, ainsi que son précurseur. Seul le système ayant un poids équivalent de 600 fut étudié en profondeur, sous forme de membranes d'une épaisseur de ca. 150 µm.

Cette étude fut entreprise afin de satisfaire les objectifs suivants: premièrement, caractériser la structure et les propriétés physiques d'un nouveau système d'ionomères à température de transition vitreuse élevée; deuxièmement, étudier la possibilité de son utilisation comme membrane séparatrice dans l'électrolyse de l'eau en milieu alcalin.

La présence d'intéractions ioniques fut confirmée, bien que les ions ne semblent former que de petits agrégats. Les membranes sont très cassantes à l'état sec mais deviennent ductiles dans un milieux aqueux. Dans un milieux aqueux de haute basicité, à 80°C, elles sont caractérisées par un module tensile de 100 MPa, une force tensile de 10 MPa et une élongation à la rupture de 30%.

ACKNOWLEDGMENTS

It is with sincere appreciation that the contributions of the following individuals are acknowledged:

Professor A. Eisenberg - for the opportunity to conduct this research, for his direction and enlightening discussions

C. G. Bazuin - for steadfast encouragement and valuable discussions, and for being largely responsible for the program in Appendix V

Dr. E. D. Salin - for advice and guidance pertaining to the computer interfacing work

Dr. R. Legras - for cheerful and enlightening discussions

Dr. D. Simkin - for help in making the printed circuit for the temperature controller

Fellow Graduate Students and Post-Doctoral Fellows - for contributing to an excellent working environment

Dr. A. E. Steck - for helpful discussion and for his determination of hydrolysis conditions

Mr. P. Smith and Dr. T. Van de Ven - for help in making the contact angle measurements

Dr. R. St.John Manley - for helpful discussion and permission to use the X-ray diffraction apparatus

Mr. J. F. Revol - for assistance with performing X-ray diffraction measurements

Mr. R. Gaulin - for his help with troubleshooting and set-up of electrical and electronic systems

Mr. Fred Kluck - for his invaluable assistance in the design of instrumental components and his excellent construction thereof

Finally, thanks are due to the National Research Council of Canada for financial support during the past four years.

FOREWORD

This thesis is organized in the following manner :

Chapter 1	Introduction
Chapter 2	Experimental Procedure
Chapter 3	Results
Chapter 4	Discussion
Chapter 5	Contribution to original knowledge and suggestions for future work

References are followed by :

Appendix I	Synthetic method
Appendix II	Interface of the AIM-65 microcomputer to a vibrating reed mechanical spectrometer
Appendix III	Instrumental additions to Instron stress-strain tester
Appendix IV	Instrumental modifications of high temperature stress relaxometer
Appendix V	Software written for temperature control system built into the stress relaxometer
Appendix VI	Supporting data for figures

TABLE OF CONTENTS

LIST OF FIGURES

LIST OF TABLES

1. INTRODUCTION

1.1 High Performance Polymeric Materials

Polymeric materials which retain good mechanical properties in extreme conditions of use, such as high temperatures (>200°C) or corrosive chemical environments, have recently been the subject of extensive and stimulating research. A very recent symposium focused on the latest advances in the area of high performance polymers (Vandenberg, 1984). They have been of interest in the field of chemistry, both synthetic and physical, as well as in that of engineering, where their properties promise wide-ranging applications for specialized requirements.

1.1.1 High Temperature Resistance

The thermal stability of polymers is dependent on several factors. Since the bond energy between the atoms forming the backbone is usually of the order of 80 kcal/mole for most covalent bonds, it is not the main determinant of stability. Rather, structural features which slow down the kinetics of bond dissociation, such as the presence of aromatic groups or heterocyclic rings, succeed in imparting a measure of thermal stability. Hydrogen-bonding, dipole-dipole interactions, Van der Waals forces and the electron delocalization inherent in resonance stabilization also influence the stability of a polymer system. Although these forces are generally of lower energy than those of covalent

bonding, their stabilizing effect is nonetheless significant. Crosslinking and multiple bonding, such as that found in double-stranded or ladder-type polymers, are among other factors which contribute to increased stability.

On the basis of comparative weight loss data described for a variety of high temperature resistant polymers, Arnold (1979) deduced the following structure-property generalizations: The highest stabilities are observed with ladder-type polymers which contain heterocyclic rings and fully conjugated aromatic systems. The stability of flexible linking groups is, in decreasing order: aliphatics with complete substitution of the hydrogens by phenyl groups or fluorine atoms, -O-, -S-, C=O, alkyl and amide linkages and, lastly, chlorine containing groups. Some examples of high temperature resistant systems are the polyesters, polyamides and -imides, polycarbonates, polyphenylene oxides and sulfides, polyquinoxalines and pyrrones. A more comprehensive treatment of such systems can be found in the literature (Mark, 1979; Frazer, 1978).

1.1.2 Hydrolytic Stability

For some applications, high temperature stability is the principal requirement. However, chemical stability is often a co-requisite of importance. The addition of a requirement for oxidative and hydrolytic stability in a high temperature resistant polymer narrows the number of candidate systems significantly. It leads to the elimination of such groups as polyesters, polyamides,

polycarbonates, etc., on the basis of their anticipated hydrolytic instability under the service conditions. Polymers of high oxidative and thermal stability often decompose before softening and are of low solubility in most common solvents, thus making them difficult to work with. Incorporation of flexible linking groups makes them easier to handle but usually brings a concomitant decrease in stability. For example, in the unsubstituted poly-p-phenylene series, the following decreasing order of stability for interconnecting groups is observed: single bond, -O-, SO_2, CH_2, C_2H_4 and $C(CH_3)_2$ (Arnold, 1979). Despite these limitations, polymers which can survive demanding thermal and hydrolytic conditions can be found, provided that the necessary compromises are made.

1.1.3 Electrolyzer Application

One of the applications for high performance polymers which incorporate the characteristics described in the above sections is as a separator material for alkaline water electrolysis. The growing awareness of the limited extent of hydrocarbon oil reserves has recently fuelled an extensive effort in various fields of energy research. The production of hydrogen via the electrolysis of water holds the promise of a clean fuel source which could find widespread use for heating, transportation and energy storage. Water electrolysis, with the electricity provided either by hydroelectric generation or nuclear power,

presently stands as the only viable means for hydrogen production from non-fossil energy sources. For a more comprehensive treatment of the subject, the reader is referred to a recent book (Casper, 1978).

A basic electrolyzer cell is shown schematically in Figure 1. An electrolyzer consists of a stack of these cells in unipolar or bipolar arrangement. The function of a separator is to prevent the mixing of the product gases (H_2 and O_2) while still allowing current throughput by means of ionic movement. The principal requirements for a good separator are thermal and chemical stability, mechanical strength under the conditions of use, wettability and high ionic conductivity.

Current electrolyzers operate at a maximum temperature of 90°C at ambient pressures, using concentrated KOH as the electrolyte and asbestos mats as the separator. For both thermodynamic and kinetic reasons, electrolyzer efficiency could be significantly improved by increasing the operating temperature and pressure to 150-200°C and 3 MPa, respectively. The high pressures are desirable in order to decrease the bubble size of evolved gases and thus raise the conductivity. Currently, no separator is available which withstands these conditions in concentrated KOH electrolytes. Among the materials with potential utility as high performance separators are Nafion, Teflon-bonded potassium titanate, polysulfone, reinforced asbestos (Renaud and Leroy, 1982) and sulfonated polyphenylene sulfide (Giuffre et.al., 1981), none of which are entirely satisfactory.

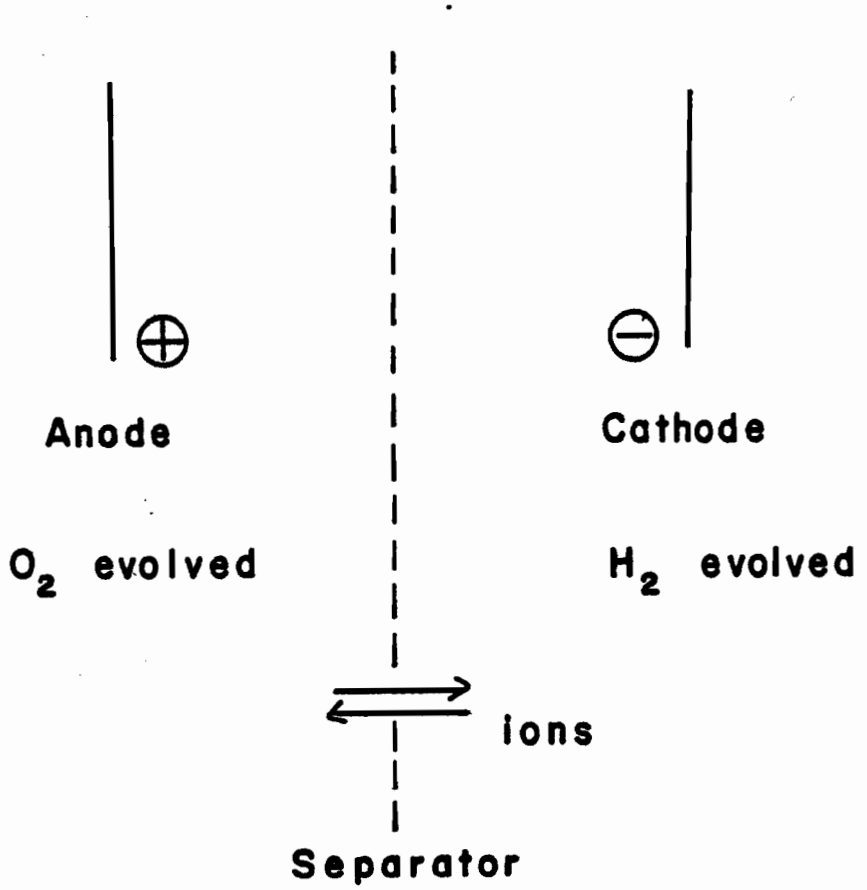

Figure 1: Schematic representation of a basic electrolyzer cell

Cathode Reaction: $4H_2O + 4e^- \longrightarrow 2H_2 + 4OH^-$

Anode Reaction: $4OH^- \longrightarrow O_2 + 2H_2O + 4e^-$

Overall Reaction: $2H_2O \longrightarrow 2H_2 + O_2$

The investigation of the physical properties of a novel group of polymers, the carboxylated polyphenylene ethers, as potential separator materials, was one of the aims of this study. Polyphenylene ethers are systems which have shown a combination of thermal and chemical resistance, thus satisfying two important requirements of a separator material. However, they lack another essential property required of a separator: ionic conductivity. The incorporation of carboxylate groups in the non-ionic phenylene ether backbone imparts to the system this capacity for ion transport. These new systems of relatively low ion content belong to the ionomer family.

1.2 Ionomers

Ionomers constitute a distinctive family of ion-containing polymers. In the past two decades, they have gained increasing recognition as strong, versatile materials which offer a convenient handle for property modification through variation of parameters such as their ion content, as well as the position and type of ion and counterion. Ionomers are copolymers of non-ionic and ionic moieties, the latter usually comprising carboxylic or sulfonic acid groups partially or completely neutralized to form salts. The concentration of ionic groups generally does not exceed 20 mol %, thus imparting a hydrophilic character to materials which remain water insoluble.

Although most of the ionomers studied to date

consist of hydrocarbon backbones, the tetrafluoroethylene-based system known as Nafion, which was developed by Du Pont, is a notable exception. The general chemical formula of Nafion is shown in Figure 2, the ionic moiety consisting of a perfluorosulfonic acid side chain. The Nafions have found extensive use as electrochemical separator membranes (Vaughan, 1973; Nuttall, 1975; Harrar and Sherry, 1975; Grot, 1978; Eisenberg and Yeager, 1982), particularly in the chlor-alkali industry, due to their selectivity in ion transport. They show permeability towards cations while presenting an effective barrier to anionic species.

The structure and mechanical properties of ionomers differ significantly from those of other polymer systems. Unlike polyelectrolytes, they are insoluble in water despite their hydrophilic character. In the systems studied to date, ion incorporation has been found to raise the glass transition temperature, rubbery modulus and melt viscosity significantly and, in some cases, to introduce thermorheological complexity. A brief review of the properties characteristic of ionomers is presented here for the convenience of the reader.

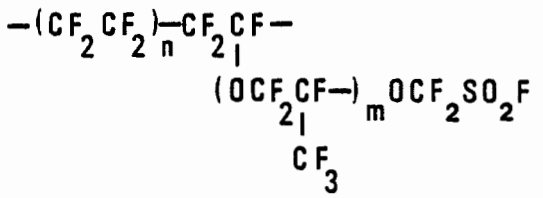

Figure 2: General chemical formula of Nafion

1.2.1 Glass Transition

One of the fundamental characteristics of a polymeric material, the glass transition temperature (T_g) range is defined as that at which a polymer goes from a glassy state to a viscous liquid or rubbery state. The glass transition is not a thermodynamic phase transition, principally due to its dependence on the experimental rate of heating or cooling used in its determination. Significant changes in other physical properties occur near T_g, the mechanical properties of a polymer being dependent on the proximity of the test temperature to the T_g of the material. The glass transition can be thought of as the upper limit of the range in which the system retains its mechanical integrity in the absence of crosslinks.

A typical effect displayed on ion incorporation into polymers is a striking rise in T_g. The magnitude of this increase depends on the concentration of ionic groups and on the nature of the ions, the effect increasing in proportion to the strength of the interaction between anion and cation. Analysis of the results in terms of the cation-anion interaction leads to the relationship

$$T_g \propto cq / a$$

where c is the concentration of ionic repeat units in the backbone, q is the cation charge and a is the distance of closest approach between the centers of charge of cation and anion. For most organic systems, T_g increases with ion

incorporation at rates ranging from 2 to 10°C per mol % ionic repeat unit.

1.2.2 Modulus

An index of material stiffness, the modulus is defined as the ratio of stress to strain. The elastic modulus (E, Young's modulus) is obtained from experiments applying a tensile stress to the sample, whereas the shear modulus (G) is obtained in the case of an applied shear stress. For a one-component non-crystalline system, a single relaxation mechanism is observed in the primary transition zone as the polymer chains rearrange to minimize the stress induced by the deformation.

The effect of temperature is usually to accelerate or decelerate the relaxation process. The modulus goes from a glassy plateau region at temperatures below T_g, through a sharp drop at T_g, to another plateau associated with the rubbery state at temperatures above T_g. At constant temperature in the transition and plateau zones, the moduli of ionomer systems show a dramatic increase relative to those of their non-ionic precursors.

The behaviour of a polymeric system is conveniently studied through a series of isothermal stress relaxation experiments spanning the temperature range of interest. By making use of the principle of time-temperature superposition, it is possible to characterize the behaviour of a material over much longer periods of time

than those attainable experimentally. The principle states that the effect of temperature on linear viscoelastic properties is equivalent to multiplying the time scale by a factor appropriate to that temperature. This factor is given by the equation for temperature dependence of the viscosity derived by Williams, Landel and Ferry (1955), the reference temperature usually taken to be that of the glass transition. In this manner, a series of isothermal stress relaxation curves can be converted to a single master curve covering several decades of time.

Stress relaxation studies of ionomer systems near T_g show a significant broadening of the transition region of the master curve, indicating a much broader distribution of relaxation times than in the parent polymer. Again, the effect is strongly dependent on the concentration of ionic comonomer in the system. A second inflection point appears in both the master curve and modulus-temperature curves. Furthermore, in some systems above a critical ion content, time-temperature superposition breaks down. This breakdown is indicative of the presence of more than one relaxation mechanism, a situation found in phase-separated systems, for example. Materials exhibiting this behaviour are termed thermorheologically complex.

1.2.3 Loss Tangent

Dynamic mechanical testing, either of the resonance or of the free decay type, is another classical method for characterizing viscoelastic materials. The

dynamic modulus measured, G^*, is expressed as the complex sum of the storage modulus G' and the loss modulus G''. The loss tangent, tan δ, is defined as the ratio of these moduli, G''/G', and is a measure of the energy lost and energy stored per cycle of deformation. Loss tangents are conveniently measured at a constant frequency as a function of temperature. The peaks in such a curve indicate the presence of a molecular energy-dissipating mechanism which proceeds at the measuring frequency at that temperature. The glass transition manifests itself by a large, sharp peak in the tan δ - temperature curve of most polymers.

Loss tangent curves of many ionomer systems feature two peaks in the glass transition region, as opposed to the single peak typical of homopolymers or of compatible polymer blends. Peak position and intensity along the temperature axis appear to be a function of ion content. In most systems studied to date, the intensity of the low temperature peak decreases with increasing ion content whereas the high temperature peak shows the opposite behaviour. Both peaks shift to higher temperature with increasing ion content. These observations are consistent with the stress relaxation data which indicate at least two separate relaxation processes above a critical ion content.

1.2.4 Structure

Ion aggregation is the structural feature underlying the properties characteristic of ionomer systems.

Two basic types of aggregates have been postulated (Eisenberg, 1970): small aggregates consisting of a few ion pairs termed multiplets and larger aggregates termed clusters which comprise non-ionic backbone material as well as many ion pairs. The structure of ionomers which contain an ion content above the critical level previously mentioned can broadly be described as that of a microphase-separated system in which a matrix of low ion content (due to multiplets) is interspersed with ion-rich domains (clusters). The structure of the larger ionic aggregates remains controversial and several models have been proposed, particularly for the Nafion systems. For a more exhaustive treatment of general structure-property relations and of molecular parameters influencing ion aggregation, the reader is referred to several reviews which have recently appeared in the literature (Longworth, 1983; Bazuin and Eisenberg, 1981; MacKnight and Earnest, 1981).

1.3 Polyphenylene Ether System

1.3.1 Non-Ionic Polymers

The results of a number of investigations of the viscoelastic and material properties of the poly-p-phenylene ether systems have been published in the past twenty years (Cayrol, 1973; Wrasidlo, 1971). Although a variety of these polymers has been synthesized (Hay et.al., 1969), only poly(2,6-dimethyl p-phenylene ether) has attained commercial importance and consequently has been studied more extensively. Substituted polyphenylene oxides

have been prepared by a Diels-Alder condensation reaction (H. Mukamal et.al., 1967). These showed reasonable processability properties, unlike most other aromatic conjugated polymers. More recently, the phenyl substituted polyphenylene ethers incorporating pendant carboxylate groups were synthesized by Harris and coworkers (Harris et.al., 1976, 1978a, 1978b) and thus introduced a new member to the ionomer family.

1.3.2 Polyphenylene Ether Ionomers

Originally prepared for possible use as windshield materials on supersonic aircraft, these systems of high glass transition temperature display, among other attributes, good thermal and hydrolytic stability. These ionomers are the subject of this work.

The structural formulae of the non-ionic ester precursor and of the ionomer are shown in Figure 3. The molar ratio of X to Y, controlled by the proportion of co-monomers used, determines the ionic content of the polymer. Details of the synthetic procedure are given in Appendix I.

A convenient way of expressing the ion contents is in the form of equivalent weight (EW), a quantity which denotes the weight of polymer in grams which will neutralize one equivalent of base. The equivalent weights and corresponding ionic contents for various molar ratios are

Figure 3: General chemical formula of the aromatic poly-phenylene ether in the non-ionic (ester) precursor and potassium ionomer (salt) form

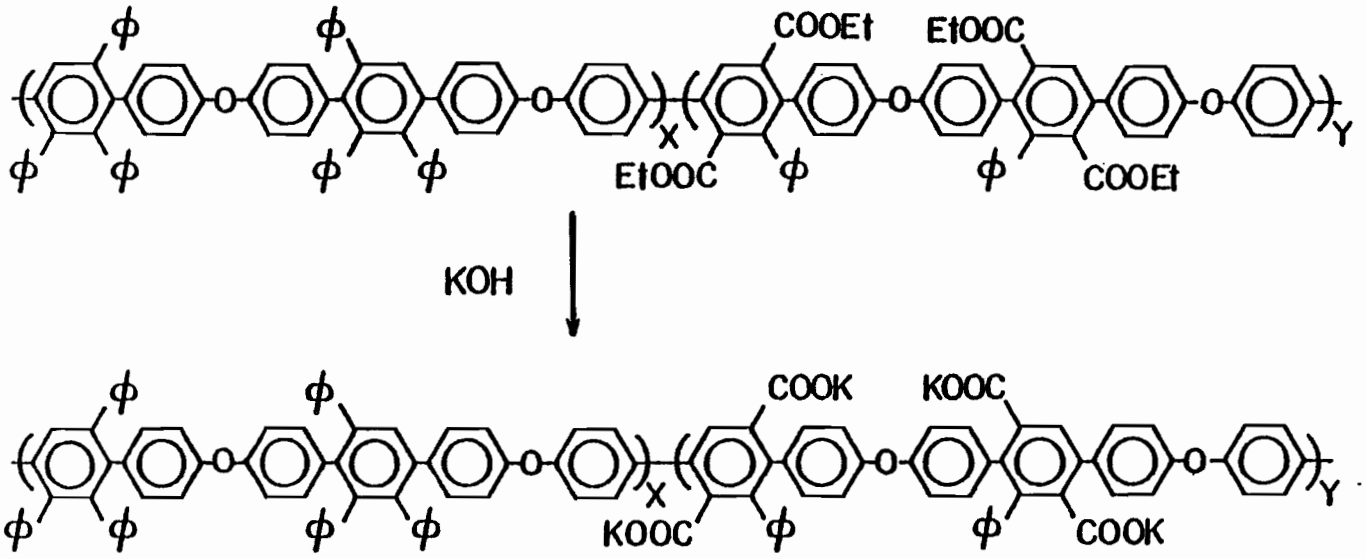
COOEt
EtOOC
EtOOC
COOEt
KOH
COOK
KOOC
KOOC
COOK

Table 1 Nomenclature and ionic content of aromatic ionomers

Designation	X	Y	% ionic groups pendant phenyl groups
1200EW	0.8	0.2	10
800EW	0.7	0.3	15
600EW	0.6	0.4	20
400EW	0.4	0.6	30

shown in Table 1. The present work focuses on material of equivalent weight 600. The terminology used in subsequent discussion will be as follows. Mention of equivalent weight alone (e.g. 600EW) will be used to designate the ionomer (potassium salt), whereas the precursor will be denoted by the addition of the word "ester" (e.g. 600EW ester).

A study of the viscoelastic behaviour of two aromatic ionomer systems of very low ion content was published recently (Rigdahl et.al., 1980). Systems of 1200EW were studied in the bulk form. Mechanical loss tangent measurements indicated that the glass transition temperature was of the order of 300°C.

The aim of that work had been to explore, on a preliminary basis, whether the ionic interactions which give rise to the viscoelastic behaviour described in section 1.2 are present in materials of very high glass transition temperature. Ionic interactions were found to persist at temperatures exceeding 350°C, with the effect of broadening the distribution of relaxation times. It was concluded that

this broadening was mainly due to the crosslinking action of multiplets since no evidence of cluster formation could be found. This is the only study reported to date on the subject of ionomers of very high glass transition temperature. One of the aims of the present work was to expand the investigation of the physical and mechanical properties of these novel systems to higher ion contents.

1.3.3 Material Processability

The 1200EW materials were studied in the bulk, using compression-molded samples. Based on sample darkening, it was even then concluded that minor degradation occurred despite the use of rather low molding temperature (250-285^{o}C). Early work with ionomers of lower equivalent weight (i.e. higher ion content) showed a greater degree of decomposition on molding. Although a molded sample of 800EW material was obtained, it was not possible to mold 600EW and 400EW material. It was thus imperative that the ionomers of higher ion content be studied in film form.

Attempts to cast ionomer films from solution led to an extensive solubility study of the 600EW material. The ionomer was known to be soluble in dimethyl sulfoxide (DMSO), but the high boiling point of this solvent made the casting conditions unpleasant and difficult to optimize. The search for a more convenient solvent, based on a solubility parameter approach, yielded few alternatives. Among these were N-methyl pyrrolidinone, dimethyl formamide

and a 4:1 mixture of DMSO and toluene. None of these enhanced the solubility of 600EW relative to pure DMSO and the latter unfortunately remained the solvent of choice.

It was known that the non-ionic precursors could be cast into tough, flexible films. The alternative method of casting ester precursor films and of subsequently hydrolyzing these to the ionomer form was finally adopted as the standard approach.

1.4 Aims of the Study

This study was undertaken with two major objectives. The first was to investigate the mechanical properties and structure of this new ionomer system, which is characterized by its relative rigidity and high glass transition temperature, especially at relatively high ion contents. In a fully aromatic polymer, rotational mobility is greatly restricted due to resonance and steric effects, especially barriers to rotation arising from ortho substituents. Obtaining experimental evidence for the existence of transitions and relaxations in both the non-ionic aromatic precursor and the ionomer, and the subsequent correlation with material structure and properties, was the first aim of this work.

The second and parallel objective was to investigate these materials as possible separators in alkaline water electrolysis. It was thus necessary to ascertain whether their mechanical properties remained adequate in concentrated alkaline solution at high

temperature, whether they showed good wettability and whether films made of these materials could withstand electrolyzer operating conditions for a reasonable period of time.

Concurrently with this study of the mechanical properties of these systems, the electrochemical and transport properties of the aromatic ionomers in film form were also investigated in another laboratory. For example, the specific conductance of 600EW ionomer film in 30% sodium hydroxide at 5 kA m^{-2} and 160°C was found to be ca. 0.1 Ω^{-1} cm^{-1} (Steck, 1983; Eisenberg et.al., 1984).

1.5 Methods Used

The techniques used to perform this study were wide-ranging. The classical methods of stress relaxation, stress-strain and dynamic mechanical analysis were supplemented by differential scanning calorimetry (DSC), infrared spectroscopy (IR), scanning electron microscopy (SEM), wide angle X-ray diffraction (WAXD) and contact angle measurements.

1.5.1 Experimental Techniques

Stress relaxation was used to investigate material behaviour over long periods of time. In the case of the ionomer, the results would indicate whether or not clusters form in these systems. Dynamic mechanical testing was performed primarily as a means of obtaining the glass

transition temperature. It was also used to investigate the occurrence of other dispersions and to obtain their activation energy via the performance of experiments at different frequencies. Stress-strain testing was used to obtain such material parameters as the elastic modulus and tensile strength.

The necessity of testing the materials in conditions approaching those of the projected use led to the design and construction of two additions to the standard stress-strain tester. The first chamber allowed stress-strain testing in a liquid environment at temperatures ranging from 20 to 200°C. No such adaptation exists commercially. The second chamber was essentially a tube furnace which permitted stress-strain testing at elevated temperatures ranging up to 500°C.

Taken together, it was hoped that the results of these methods would yield a comprehensive survey of the mechanical properties of the material, particularly in the form of films.

The surface and internal structure of the films were investigated by SEM, WAXD and qualitative contact angle studies. X-ray diffraction was used as a probe to establish orientation effects and the existence of crystallinity. Electron microscopy of surfaces and fractures of the film samples was useful in the identification of structural differences resulting from various preparation methods and pretreatments. Measurement of the contact angle of water on fresh film surfaces was a simple means of investigating

wettability and surface energy, in a preliminary manner. Since most of these methods have been described in the literature, they will not be discussed here but will simply be referred to in the next chapter, where appropriate.

It is assumed that the reader is familiar with the terms which have come to be associated with the study of polymer systems. Accordingly, they will not be defined here. However, some terms used to discuss the results of stress-strain testing are not considered to belong to the "classical" vocabulary of polymer chemistry and these will be treated in the next section.

1.5.2 Definition of Materials Science Terms

Since a significant part of the discussion will entail the use of terminology associated more with a materials science approach than with that of classical physical chemistry, a few terms pertaining to the characterization of materials are now defined.

A material is said to yield if it undergoes a maximum stress shortly after the elastic region, as depicted in the schematic stress-strain curve shown in Figure 4. This maximum in stress is termed the yield strength. The yield point sometimes appears as an inflection point or a plateau on the curve rather than as a well defined maximum. It stands as a boundary between elastic (reversible) and plastic deformation. It indicates the activation of a new molecular mechanism of deformation and, in practice,

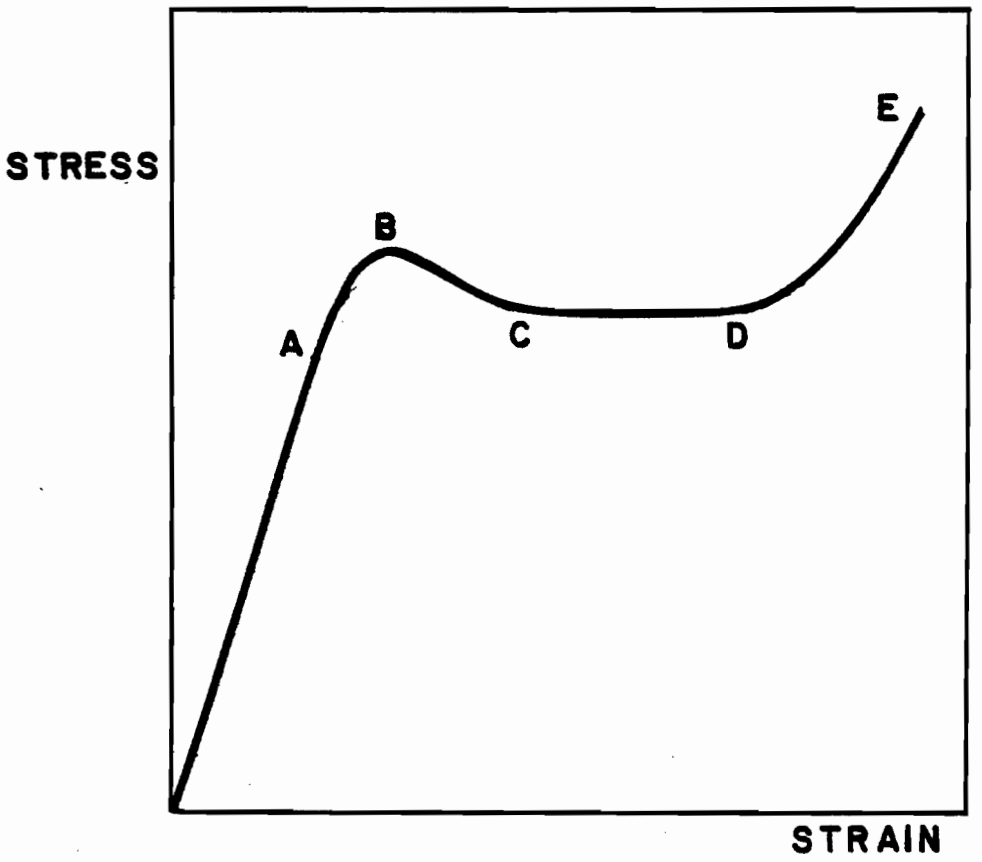

Figure 4: Schematic representation of a typical stress-strain curve

A - limit of the elastic region of linear deformation

B - yield point

C - beginning of region of cold drawing

D - beginning of strain hardening

E - fracture or break point

determines the resistance to fracture of the material. When yield is followed by a region of virtually constant stress which often increases again near break, the process is defined as strain hardening. Physically initiated by the formation of a constriction called a neck (Vincent, 1960), it is indicative of significant increases in the strength of the drawn sample. Cold drawing designates the large extensions achieved at relatively low stress as the result of the increased orientation of the polymer chains. Materials which yield and undergo plastic flow are described as ductile or tough. The fact that plastics can be tough even in regions of high modulus is a facet of their non-linear viscoelastic behaviour.

This non-linear viscoelastic behaviour is also the reason for which plastics are so useful. For although a rubber exhibits a tensile strength which is ten times lower than that of a glass, it can absorb on the order of a thousand times more energy before breaking. This may be stored as elastic energy, it may be used to effect a rearrangement of the polymer chains, or it may simply be dissipated as heat as in the permanent deformation of a crystalline material.

A brittle material is defined as one which breaks at maximum load and at low strains, of the order of a few percent. The energy to break, calculated as the area under the stress-strain curve, is much lower for a brittle material than for a tough, ductile one. A change in

fracture mode from brittle to ductile can be brought about by changing experimental conditions such as temperature, strain rate or pressure. It can also be effected by the use of plasticizers or additives.

Although it has been suggested that the brittle-to-ductile transition always occurs near a modulus transition, the bulk of more recent evidence indicates no correlation with mechanical relaxation phenomena. The brittle-to-ductile transition is influenced by such basic material variables as molecular weight, crosslinking and degree of crystallinity. It should be noted that, at temperatures below the glass transition, some amorphous polymers such as polycarbonate and poly(ethylene terephthalate) show ductile failure while others such as poly(vinyl chloride) and polystyrene show brittle failure.

The mechanism of the brittle-to ductile transition remains poorly understood. The transition, which also occurs in metals, had been explained phenomenologically by the Ludwik-Davidenkov-Orowan (L-D-O) hypothesis (Davidenkov and Wittman, 1937; Orowan, 1948). This treatment assumes that the brittle fracture and plastic flow are independent processes and that brittle fracture stress and yield stress become equal at the transition temperature. By "independent" is meant that they both vary with temperature, but not in the same manner, yield strength being more dependent on temperature than brittle strength. The L-D-O hypothesis was adapted to polymers by Vincent (1960). However, this interpretation does not consider microstructu-

ral features such as porosity or the crazing and shear banding phenomena. More recently, the brittle-to-ductile transition has been described in terms of a competition between crazing and shear-banding (Matsushige et.al.,1976; B.Z.Jang et.al.,1983). A model for the transition based on free volume considerations (Bouda, 1982) has also been proposed. For a complete discussion of fracture processes in polymers, the reader is referred to a book authored by Andrews (1968).

2. EXPERIMENTAL

The materials investigated in this work were synthesized by a condensation polymerization reaction. The synthetic procedure is summarized in Appendix I. The resulting alkoxycarbonyl-substituted polyphenylene oxide precursors were converted to the ionomers by further reaction with potassium hydroxide (KOH) as described below. The Nafion film used was kindly supplied by E.I. Du Pont de Nemours & Co.; it was a sodium-neutralized ionomer of equivalent weight 1200.

2.1 SAMPLE PREPARATION

The 600EW ester precursor used in this study came from a single batch, identified as 2. The ionomer films were prepared by one of the following two methods.

2.1.1 Hydrolysis of Precursor in Powder Form

The precursor material in powder form was placed in a solution of 25% KOH in ethylene glycol and kept under reflux at 190°C for a period of 50 hours. The reaction was carried out in a Teflon vessel to prevent the introduction of ions due to etching of the glass container by the alkaline reaction medium. Alternatively, the reaction was carried out in a Teflon-lined pressure vessel at 190°C. The reaction medium in that case was 10% KOH in a 1:1 mixture of de-ionized water and ethylene glycol. The reaction was

allowed to proceed for three days under a pressure of 0.3 MPa, after which conversion to the ionomer form was complete.

The ionomer was subsequently dissolved in hot dimethyl sulfoxide (DMSO) to form a solution of ca. 0.2% solids. It was then hot-filtered through a fritted glass disc of medium porosity. The filtrate was brought to a concentration of ca. 5% then cast on a hot, clean glass plate. The surface temperature of the plate was maintained at 140°C until the solvent was evaporated. Best results were obtained when the evaporating solution was shielded from ambient air currents by overlaying it with a porous cover such as a paper towel or a perforated piece of aluminum foil.

Once evaporation was complete, the glass plate was removed from heat and allowed to cool to ca. 70°C. The amber-coloured film was detached with the help of a sharp knife blade. The film was dried further under reduced pressure until constant weight was achieved. The product of this method will be designated by the equivalent weight followed by the suffix p (e.g. 600EW-p).

2.1.2 Hydrolysis of Precursor in Film Form

The precursor material was dissolved in chloroform to form a 4 - 5 % solution. This solution was filtered through a fritted glass disc of medium porosity and immediately cast onto a levelled glass surface. The dimensions of the surface were delimited by an aluminum

strip which was bonded to the glass plate (using a high-temperature curing epoxy adhesive) to form a rectangular perimeter. It was thus possible to estimate the amount of solution necessary to obtain a desired film thickness. The solution was protected from air currents in the manner described above and solvent evaporation was allowed to proceed at room temperature. Once evaporation was complete, the film was easily detached from the glass substrate by using a few drops of de-ionized water to initiate the lifting of a corner.

The amber-coloured transparent film of ca. 130 micrometers in thickness was then hydrolyzed in a pressure reactor at 190°C for ca. 5 days. The reaction medium consisted of freshly prepared 10 % KOH in 1:1 ethylene glycol/de-ionized water solution. This 150-ml pressure reactor was completely lined with Teflon and was designed to withstand pressures of 30 MPa. The temperature of an external heating jacket was regulated to ± 0.2°C by an automatic controller (D921 temperature controller, Omega Engineering). The assembly is shown schematically in Figure 5. On completion of hydrolysis, the reactor was allowed to cool and the films were removed, briefly rinsed and then stored in de-ionized water. These films will be designated by the ___EW-f nomenclature (e.g. 600EW-f).

The pressure used in the first successful hydrolysis of a large amount of material was ca. 3 MPa. Material from this hydrolysis batch will subsequently be

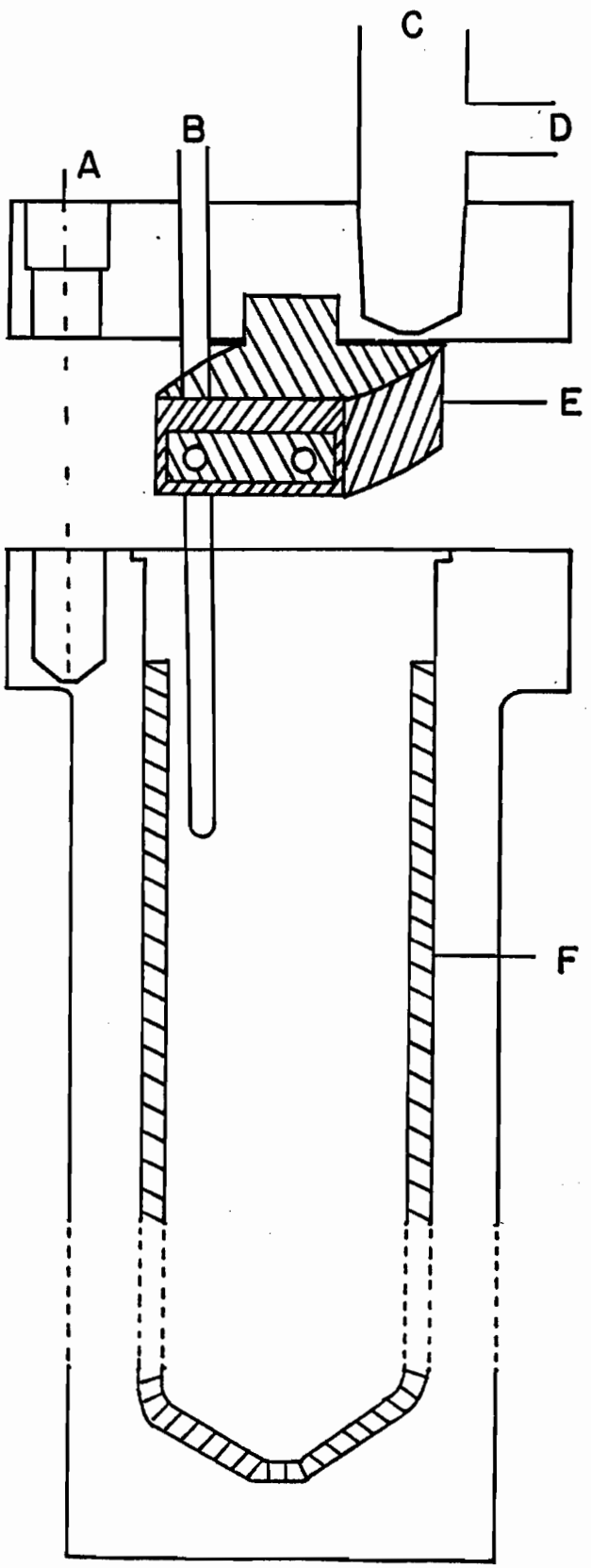

A Allen cap screws
B thermocouple well
C to pressure gauge
D to blow-out safety valve
E Teflon film hanger
F Teflon lining

Figure 5: Schematic representation of the hydrolysis pressure autoclave.

called 600EW-f-I. Further hydrolyses were conducted at lower pressure (1.5 MPa) and resultant films will be called 600EW-f-II.

For experimental techniques which required dry samples, the following procedure was used. Films were initially weighted down between sheets of absorbant paper for 24 hours at room temperature. They were subsequently kept at atmospheric conditions of temperature, pressure and humidity. A few samples of 600EW-f were dried at 100°C under reduced pressure for 5 days and subsequently kept at ambient conditions.

2.1.3 Determination of Extent of Reaction

Conversion of the ester precursor to the ionomer was verified by FTIR through the measurement of the intensity of the symmetric and asymmetric carbonyl salt stretching vibrations at 1400 and 1575 cm^{-1}, respectively. Since the absolute value of absorbance intensity is dependent on film thickness, the values used were normalized with respect to the weaker of the two ether CO stretching vibrations, which appears at 1171 cm^{-1}. For I_x signifying the absorbance intensity at x cm^{-1}, a value of 0.85 and 1.25 for I_{1400}/I_{1171} and I_{1577}/I_{1171}, respectively, was the minimum acceptable for this study. This value indicated approximately 85 % conversion of the ester groups to salt groups. In other words, ionic carboxylate salt groups formed 17 % of all the pendant groups for the 600EW material at 85 % conversion.

The extent of reaction was also verified by NMR for dilute solutions of 0.45 % ionomer in deuterated DMSO. Since it was not always possible to dissolve the ionomer, this method could not be used in all cases.

2.2 GENERAL CHARACTERIZATION

2.2.1 Viscosity and Density

Viscosity of the ester precursor materials in chloroform was measured in an Ubbelohde viscometer at 30.0 $\pm$ 0.2°C. Reduced viscosity values obtained for five solutions were plotted as a function of concentration and extrapolated to zero concentration to determine the intrinsic viscosity.

Density of the 600EW ester, which does not absorb water, was determined by the hydrostatic weighting method (Snell, 1966). By using the following relation,

$$d_o = \frac{m}{(w - w_o)/d_W} + d_A$$

where
d_o = density of sample
m = initial weight of dry polymer
w = total weight after sample immersion
w_o = weight of water + container
d_W = density of water at 20°C (0.9982 g/cc)
d_A = density of air at 20°C (0.00129 g/cc)

the density was determined in de-ionized water on an analytical balance. The value used for the hydrated weight was an average of 10 measurements.

2.2.2 Thermal Stability

Thermo-gravimetric analyses were conducted under reduced pressure using a quartz-spring apparatus at heating rates of ca. 5°/minute. Alternatively, isothermal tests of thermal stability were also performed as follows. Samples were placed in test tubes and kept under continuous suction from a vacuum pump. The test tubes were placed in an asbestos-insulated aluminum block which could be heated on a hot-plate. The temperature was raised to the desired value and the samples kept at that temperature for intervals of ca. 12 hours. The samples were weighed at the end of each interval, the total experimental time spanning 3 days.

2.2.3 Differential Scanning Calorimetry

A Perkin Elmer DSC-2 equipped with a thermal analysis data station was used for all measurements. Samples were analyzed in the form of films at a scan rate of 20°/minute. Unless otherwise specified, second runs were obtained after quenching at 320°/minute.

2.2.4 Scanning Electron Microscopy and X-Ray Diffraction

Electron micrographs were obtained on an ISI model SX-30 instrument operating at 15 kV. The wide angle X-ray diffraction (WAXD) patterns were obtained on a Phillips PW 1730 X-ray generator with CuKα incident radiation at 40 kV and 35 mA. The photographs were analyzed with a Joyce microdensitometer.

2.2.5 Nuclear Magnetic Resonance (NMR) and Fourier Transform Infrared (FTIR) Spectroscopy

NMR spectra were obtained for 0.45 % solutions of polymer on a Varian T-60 instrument. Infrared data were obtained on a Nicolet 7199 FTIR instrument. Samples were in the form of thin films of ca. 30 micrometers in thickness.

2.2.6 Contact Angle

The shape of a drop of distilled water on freshly prepared thin film samples of 600EW ester and ionomer material was photographed after 30, 60, 90 and 150 seconds. The same measurements were made on Nafion and its precursor. The latter film samples were previously boiled in dilute nitric acid to ensure a clean surface. The contact angle, i.e. that angle enclosing the liquid, was measured with a protractor to a precision of $\pm$ 2° of arc.

2.3 VISCOELASTIC PROPERTIES

2.3.1 Torsion Pendulum and Vibrating Reed

Dynamic mechanical behaviour was studied by an inverted free vibration torsion pendulum operating at ca. 1 Hz and a vibrating reed spectrometer at higher frequencies. The torsion pendulum is essentially the same instrument which has been described earlier (Cayrol, 1972), modified by the addition of an automated data acquisition program based on a PDP-11 minicomputer (Bazuin, 1984). The vibrating reed

spectrometer was also described previously (Williams, 1978). It was updated by interfacing with a microcomputer for data acquisition and calculations (Besso, 1983). Details of this interface are given in Appendix II. For these experiments only, samples were compression molded at 290°C for 15 minutes at a load of 14 MPa. The experiments were always conducted during a heating run. Heating rates were always below 1°/minute.

2.3.2 Glass Transition

Glass transition temperatures (T_g) were measured by torsion pendulum and by DSC. In the torsion pendulum runs, the highest temperature peak of the loss tangent *vs.* temperature curve was taken as the T_g.

2.3.3 Tensile Tests

Stress-strain measurements were performed on an Instron floor model 1122. The instrument was modified by the construction of two temperature-controlled chambers. The first can be described as a bath which allowed testing under water or in aqueous solution at temperatures ranging from 25 to 90°C. The second is a three-zone tube furnace which permits testing in air at temperatures ranging from 25 to 500°C. In both cases, the temperature was controlled to $\pm$ 0.2°C. Details of the apparatus are described in Appendix III.

In the first mode, experiments were performed at 80°C in de-ionized water, in dilute (0.1 *M* or 5.6%) and

in 20% aqueous KOH solution. Film samples were allowed to reach equilibrium prior to testing. In the second mode, samples were tested at 25, 100, 200 and 280°C. A constant elongation rate of 2 mm/minute was used in all cases. The results obtained are an average of 2-5 runs.

Dry film samples were cut by hand with the use of a sharp knife blade. The overall specimen length was ca. 5.0 cm and the reduced gage length (g.l.) was 2.5 cm. Typical specimen width was 0.5 cm and thickness was 0.0150 cm as measured by a dead weight micrometer.

The tensile (Young's) modulus was calculated from the slope of the initial linear portion of the force-elongation curve. The following relations were used:

$$\text{Stress (MPa)} = \frac{\text{force}}{\text{cross-sectional area}} = \frac{\text{g-f} \times 981 \times 10^{-7}}{\text{width} \times \text{thickness}}$$

$$\text{Strain (\%)} = \frac{100 \times \text{c.p.t.}}{\text{g.l.} \times \text{m.r.}}$$

$$E\ (\text{MPa}) = \frac{\text{stress}}{\text{strain}} = \frac{\text{g-f} \times 981 \times \text{m.r.} \times \text{g.l.} \times 10^{-7}}{\text{width} \times \text{thickness} \times \text{c.p.t.}}$$

where sample dimensions are in centimeters

g-f = grams - force

m.r. = magnification ratio accounting for different crosshead and recorder speeds

c.p.t. = chart paper travel, in cms

981 = acceleration factor in cm sec^{-2}

10^{-7} = conversion factor from dyn cm^{-2} to MPa

Errors influencing the final calculated value originated chiefly from the measurement of initial sample dimensions and from that of centimeters of chart paper travel. Uncertainties in width, thickness and distance of chart paper travel were 0.05 cm, 5 micrometers and 0.5 cm, respectively. For experiments run in water or solution, the difficulty of specifying sample thickness greatly increased the uncertainty of the numbers obtained. For values of modulus calculated for dry experiments, an error of 13 % can be expected. For wet experiments, the error more than doubles to a possible maximum of 30 %. Systematic errors were considered insignificant relative to the magnitude of the indeterminate error detailed above.

2.3.4 Stress Relaxation

The instrument previously described (Navratil, 1972) was updated and partly rebuilt to include an improved temperature control module based on a SYM microcomputer. The five-zone furnace now consists of a Variac-controlled 500 W main heater and of five 100 W auxiliary band heaters. The usable temperature range was extended to 600^{o}C, with a precision of 0.1^{o}C. The entire stress relaxometer assembly is described in Appendix IV. The commented program for temperature control is given in Appendix V.

Film samples were tested in tension only. The strain applied was usually less than 2 %. It was verified that this was well within the region of linear viscoelastic

response by testing the sample at strains of up to 3 %.

Treatment of the stress relaxation data was greatly facilitated by a computer program recently written by L. Gauthier.

2.4 PRECISION OF RESULTS

The precision of the experimental results reported in this study will be expressed in the form of relative precision. This indicates the uncertainty in terms of a fraction of the value of the result and is obtained by using the following relation:

$$\% \text{ relative precision} = \sigma_{n-1} \; / \; \bar{x}$$

where σ_{n-1} = standard deviation with population parameter taken to be n-1

$\bar{x}$ = sample mean value

3. RESULTS

3.1 CHARACTERIZATION

3.1.1 Precursor Viscosity and Density

The intrinsic viscosities determined for the ester precursors of 800EW, 600EW and 400EW materials ranged from 0.75 to 1.06 dl/g and are given in Table 2. The 600EW ester film was found to have a density of 1.38 g/cc (σ_{n-1} = 0.113).

Table 2 Intrinsic viscosities for ester precursor polymers in $CHCl_3$ at 30°C

	800EW	600EW	400EW
batch 1	0.79	0.744	0.635
batch 2		1.055	

3.1.2 NMR and FTIR

As stated earlier, both methods were used to monitor the extent of conversion from the ethyl ester precursor to the ionomer. In the NMR spectra, the resonance peak situated at δ = 1.56 ppm in the precursor (due to the 3 protons of the methyl group) disappeared on complete conversion to the ionomer.

The infrared absorption spectrum of 600EW ester is shown in Figure 6. The high frequency region only shows peaks due to aromatic carbon-hydrogen stretching absorption

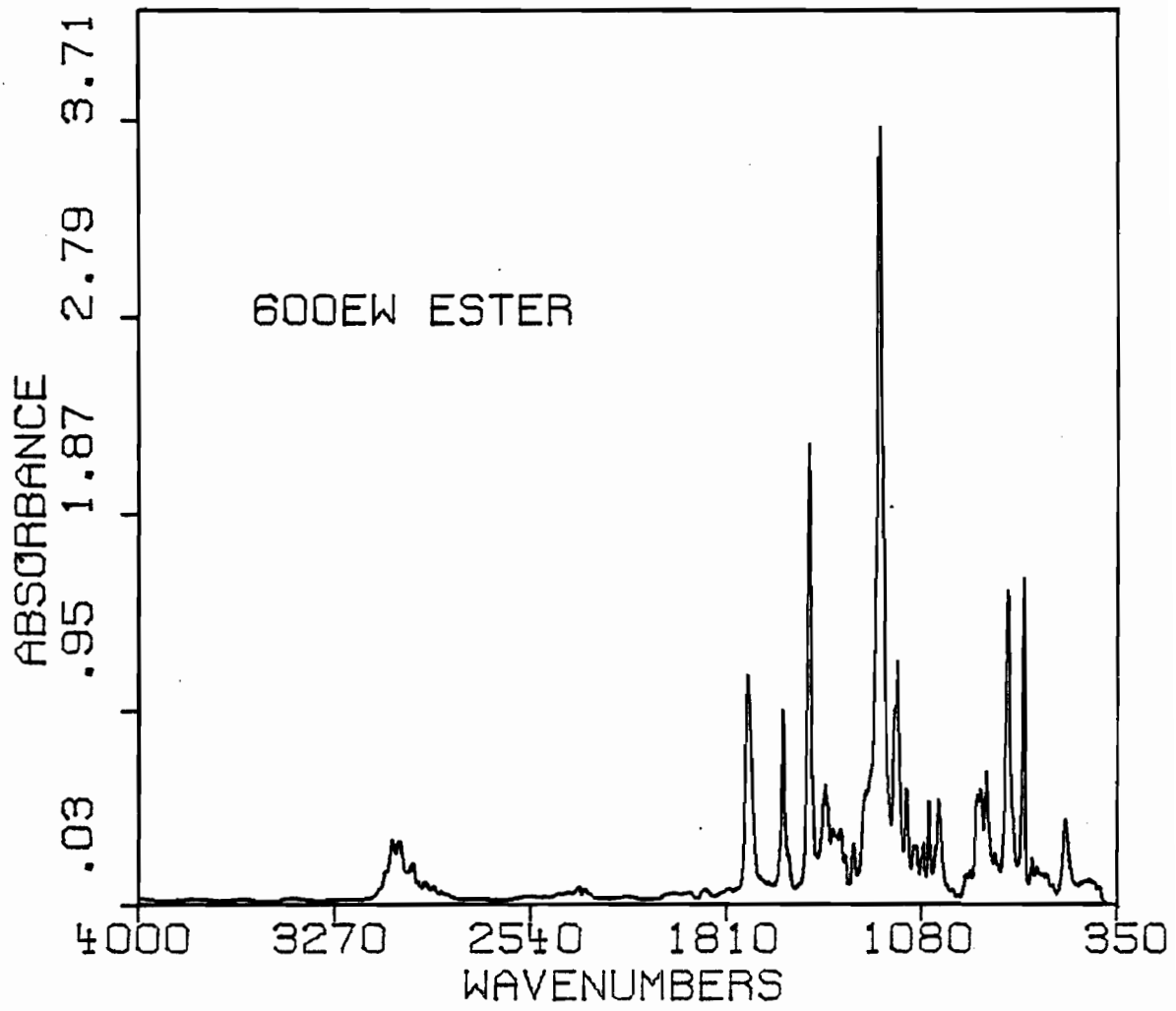

Figure 6: FTIR spectrum of 600EW ester

(2800 to 3200 cm^{-1}) and does not change on conversion to the ionomer. The region of particular interest is that between 1000 and 2000 cm^{-1}. Spectra for 600EW ester and 600EW-f in this frequency interval are shown in Figure 7. The spectrum for 600EW-p is identical to that of 600EW-f. The assignments of the peaks of interest are given in Table 3.

Table 3 Absorbance peak assignments in the infrared spectra of 600EW ester and ionomer (Ø = C_6H_4)

Frequency (cm^{-1})	Due to	Assignment
1600	aromatic ether backbone	C==C in plane vibration
1230	--Ø-O-Ø--	stronger Ø-O-Ø stretch
1171		weaker Ø-O-Ø stretch
1732	ester --$COOC_2H_5$	antisymmetric C==O vibration
1136		antisymmetric and symmetric C-O-C vibration
1050		
1577	ionomer --COOK	antisymmetric and symmetric stretching of COO^-
1400		

The absorbance peaks ascribed to the aromatic ether stretching vibration remain constant in both ester and ionomer. The ester group vibrations evident at 1732, 1136 and 1050 cm^{-1} (indicated by arrows in Fig. 7) are not seen in the ionomer. In the latter, two new peaks appear at 1577 and 1400 cm^{-1} (also indicated by arrows), reflecting the antisymmetric and symmetric stretching vibrations of the

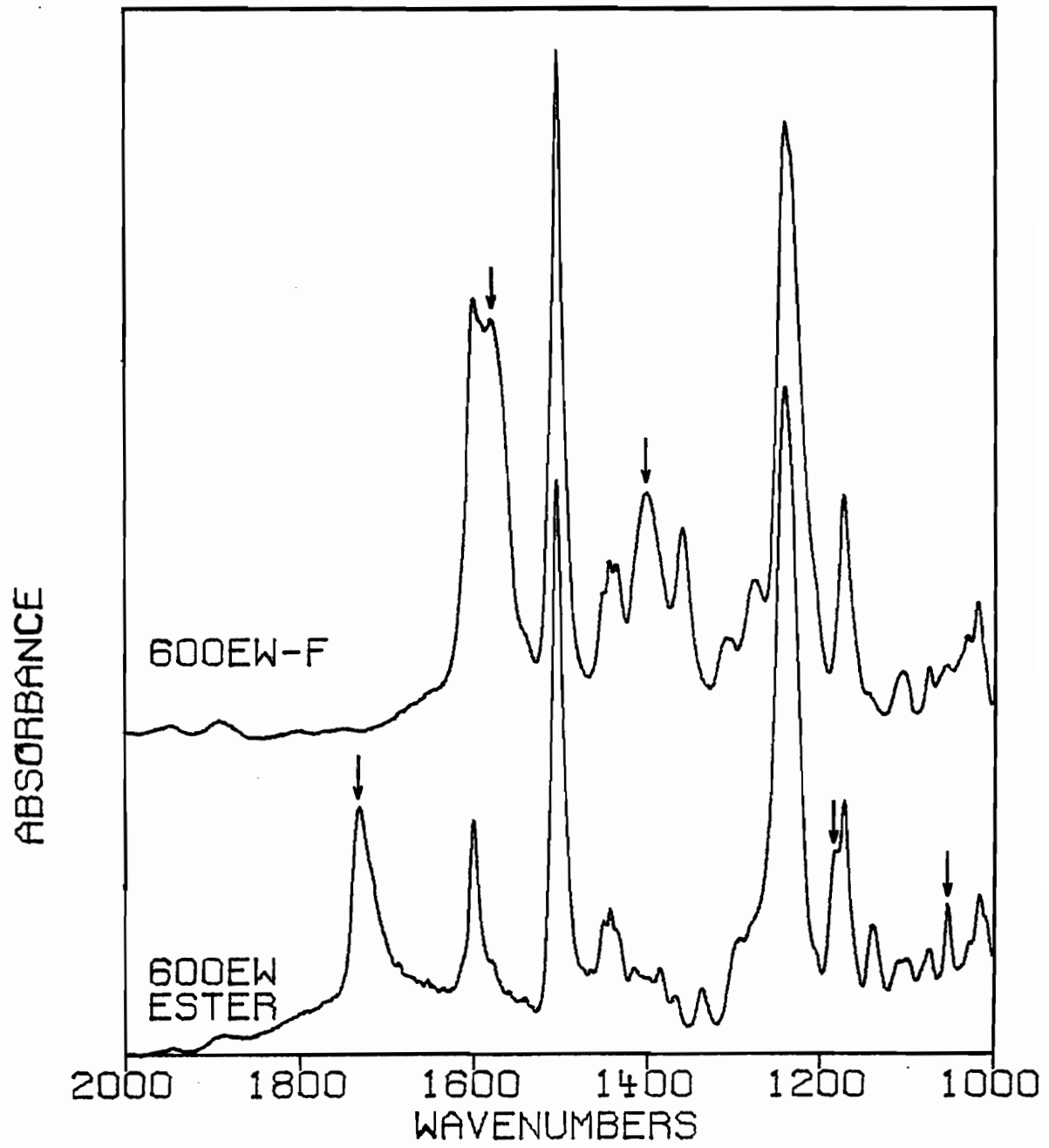

Figure 7: FTIR spectra of 600EW ester and ionomer

carboxylate anion. Typical values of the absorbance intensities of the monitored peaks are shown in Table 4 for several hydrolysis batches of the 600EW ionomer material. It must be noted that the values for percent conversion to the ionomer salt are only a useful approximation. They were arrived at by assigning the relative intensities of the 1400 and 1577 cm^{-1} peaks as 0% for the ester and 100% for samples hydrolyzed until no further increase in these intensities was observed.

Table 4 Relative absorbance intensities of vibrations used for monitoring extent of the hydrolysis reaction

Sample	I_{1400}/I_{1171}	I_{1577}/I_{1171}	% Conversion
600EW-f-I	1.015	1.6	100
600EW-f-II	0.876	1.312	90
E26125	0.947	1.25	90
E26160	0.948	1.54	100
EB695	0.7067	0.6125	60
600EW-p-I	1.115	1.313	100
600EW-p-II	0.85	1.279	88
600EW ester	0.298	0.198	0

Although the 1732 cm^{-1} absorption was absent from the spectra of the powder hydrolyzed ionomers and from those of most of the film-hydrolyzed samples, under some experimental conditions this band reached a minimum absorbance but did not completely disappear. The intensity of the salt carbonyl absorbance bands indicated better than 85% hydrolysis in all cases. This is shown in Figure 8.

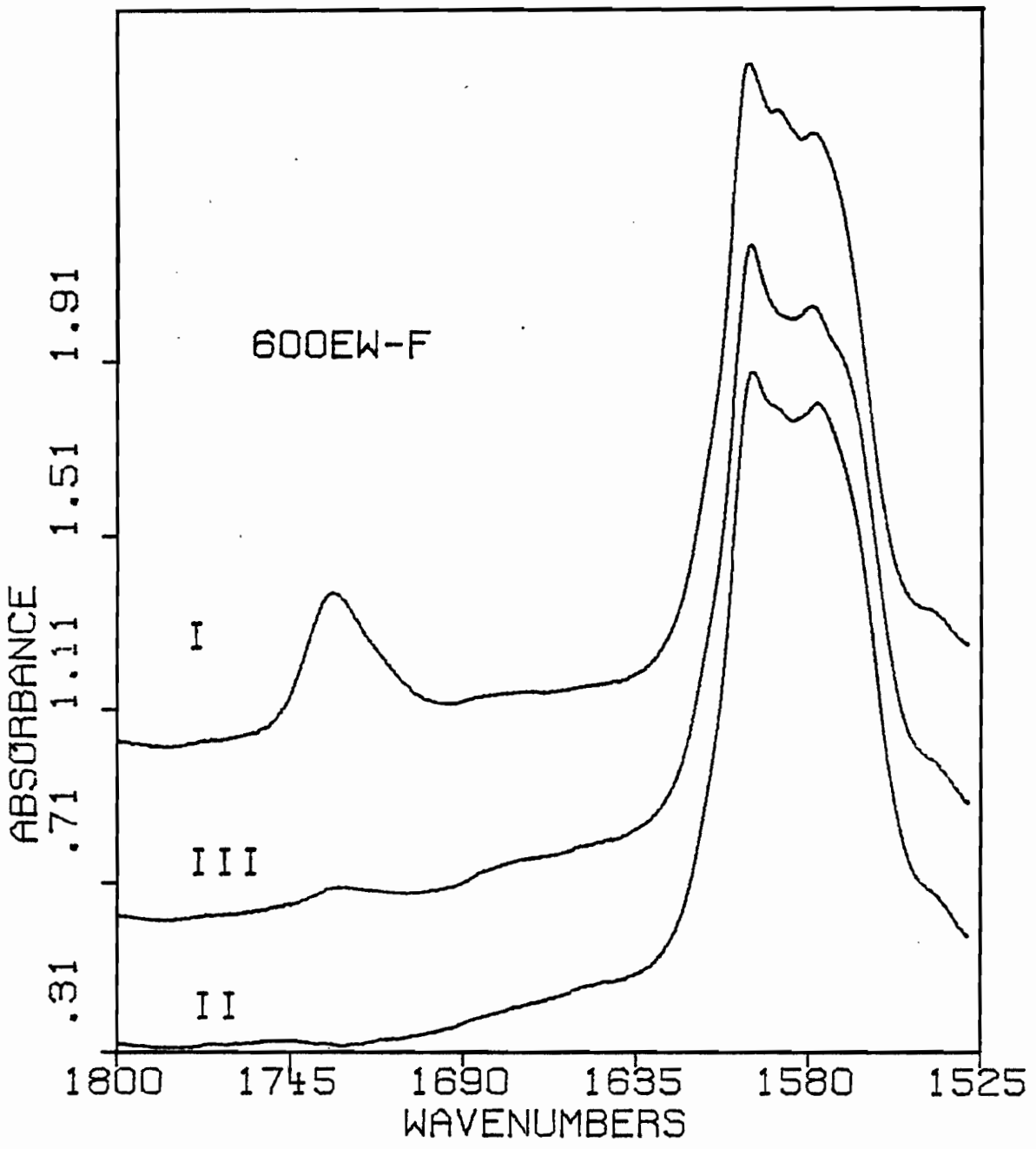

Figure 8: FTIR spectra of 600EW-f showing the effect of crosslinking on the absorbance intensity at 1732 wavenumber for hydrolysis batches I, II and III

The presence of this band has been attributed to the formation of diester crosslinks via a transesterification reaction catalyzed by ethylene glycol. Crosslink formation is also reflected in stress-strain curves and will be treated more extensively in the discussion.

3.1.3 Thermal Stability

Thermogravimetric results for experiments performed using the quartz-spring apparatus are shown in Figure 9 for 600EW ester and 600EW-f. Samples of the 600EW ester and ionomer material show the beginning of weight loss at ca. 400°C. Accurate thermogravimetric analysis of 400EW-f was made impossible by the enormous water content (>200 %) of the initial film sample. The results obtained indicate a stability comparable to that of 600EW materials.

The isothermal stability tests performed on 600EW ester and ionomer yielded the results shown in Figure 10. A significant uncertainty is introduced in these measurements by the fact that the ionomer samples were found to be extremely hygroscopic, absorbing ca. 5 % water in 30 seconds. Thus the initial dry weight used may have been that of a sample containing a significant amount of water.

3.1.4 Differential Scanning Calorimetry

DSC scans of the ester precursors of 400, 600 and 800 equivalent weights appear virtually identical and are

Figure 9: TGA results for 600EW ester and ionomer

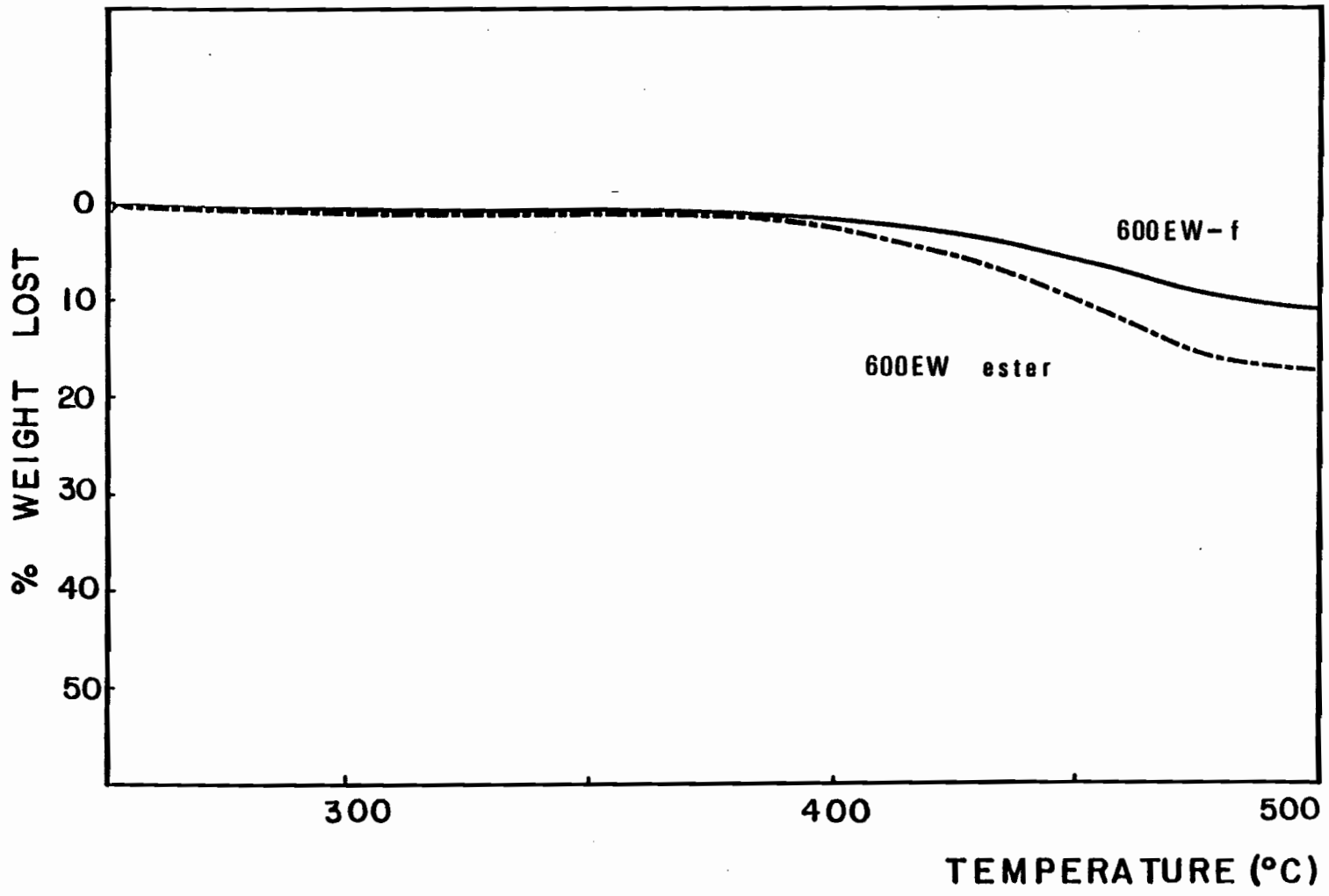
% WEIGHT LOST
0
10
20
30
40
50
600EW-f
600EW ester
300
400
500
TEMPERATURE (°C)

Figure 10: Isothermal stability test results for 600EW ester and ionomer

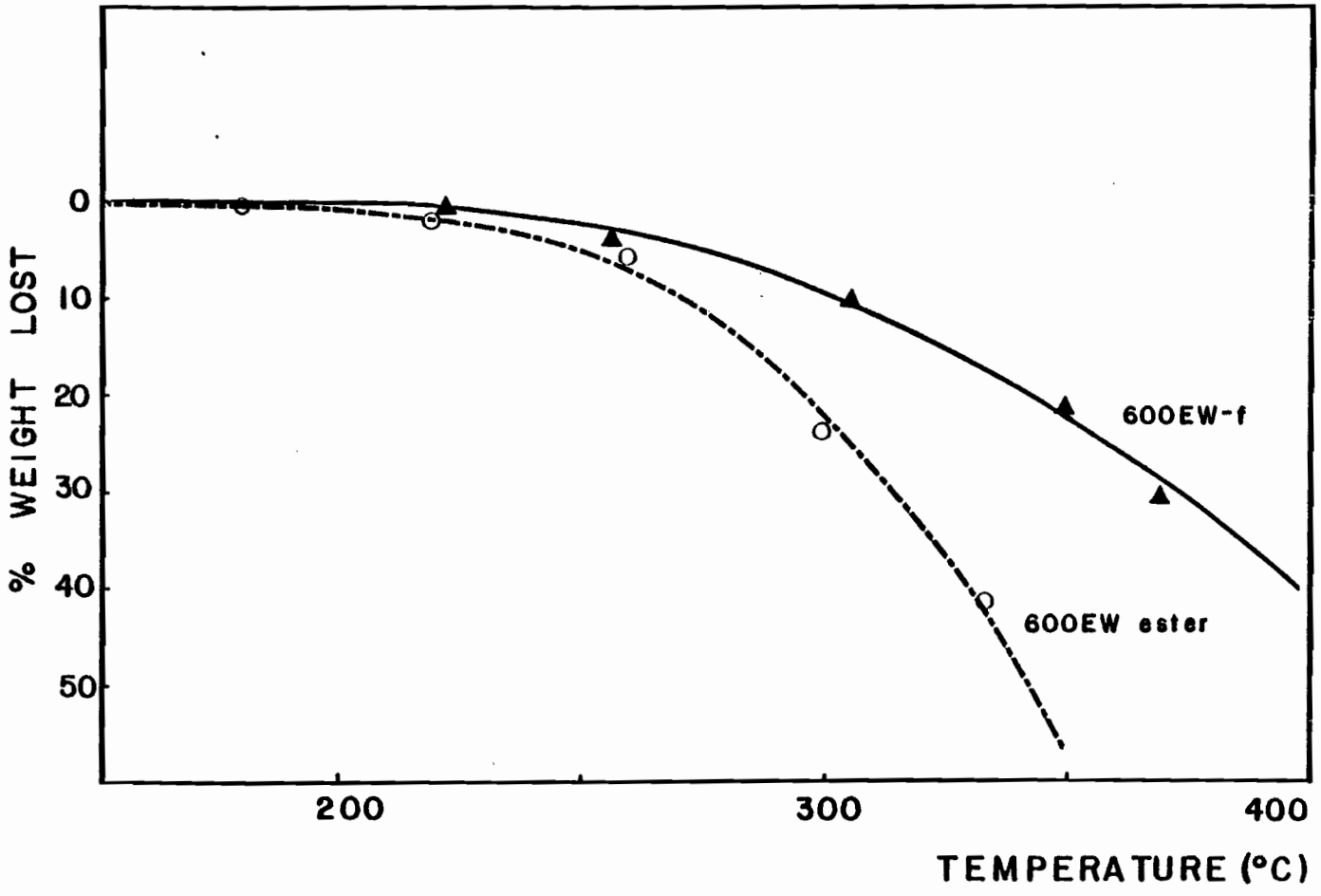
% WEIGHT LOST
0
10
20
30
40
50
200
300
400
TEMPERATURE (°C)
600EW-f
600EW ester

shown in Figure 11. The common features to be noted are the glass transition occurring at ca. 290°C and a large endotherm peaking at 438°C. The heats corresponding to this high-temperature peak increase with increasing ethoxycarbonyl content. This endotherm is due to the decarboxylation reaction which marks the onset of sample degradation. A second heating run no longer shows the high temperature peak. The glass transition persists, but on a much reduced scale.

Ionomer DSC scans are shown in Figure 12. A new transition (shown by arrows) is apparent, relative to the ester curves, at temperatures increasing with ionic content. This is assigned to the ionomer glass transition. The high-temperature endotherm peaking at ca. 500°C for the 600EW ionomer is attributed to the presence of residual ester groups. Comparison with the position of the ester precursor decarboxylation peak indicates that, in the ionomer, this reaction is not only shifted to higher temperature but that the total heat of reaction (area under the peak) is much reduced. This is clearly illustrated in Figure 13, where the behaviour of a partially neutralized sample is compared with that of the ester and the ionomer. This reflects the reduction in the number of ester groups on saponification. A transition at ca. 290°C is also evident for all the ionomer samples, although in each case the total heat of transition is lower than both that of the ionomer glass transition and that of the corresponding transition in the

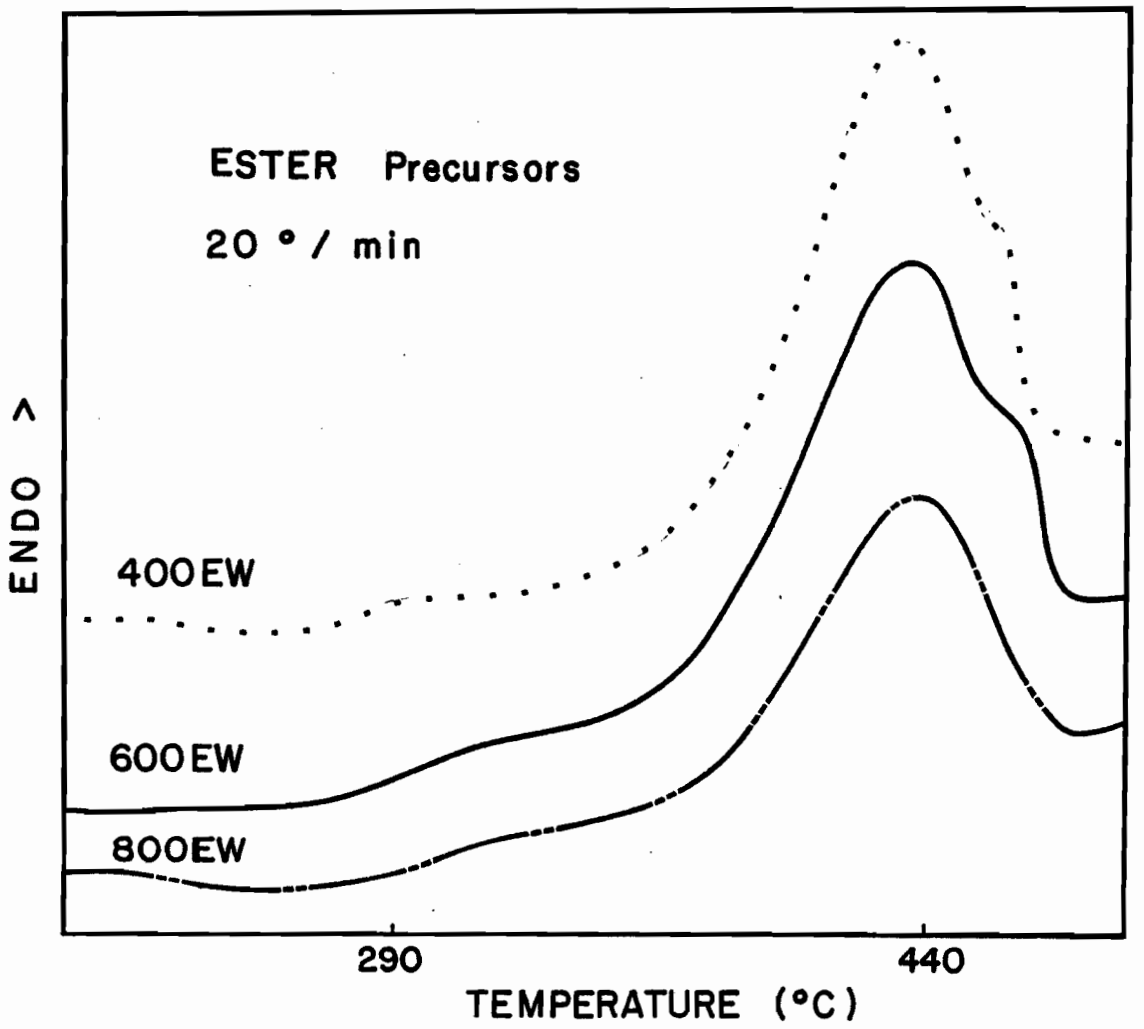

Figure 11: DSC curves for ester precursors of 400, 600 and 800 equivalent weight

Figure 12: DSC curves for ionomers of 1200, 800, 600 and 400 equivalent weight

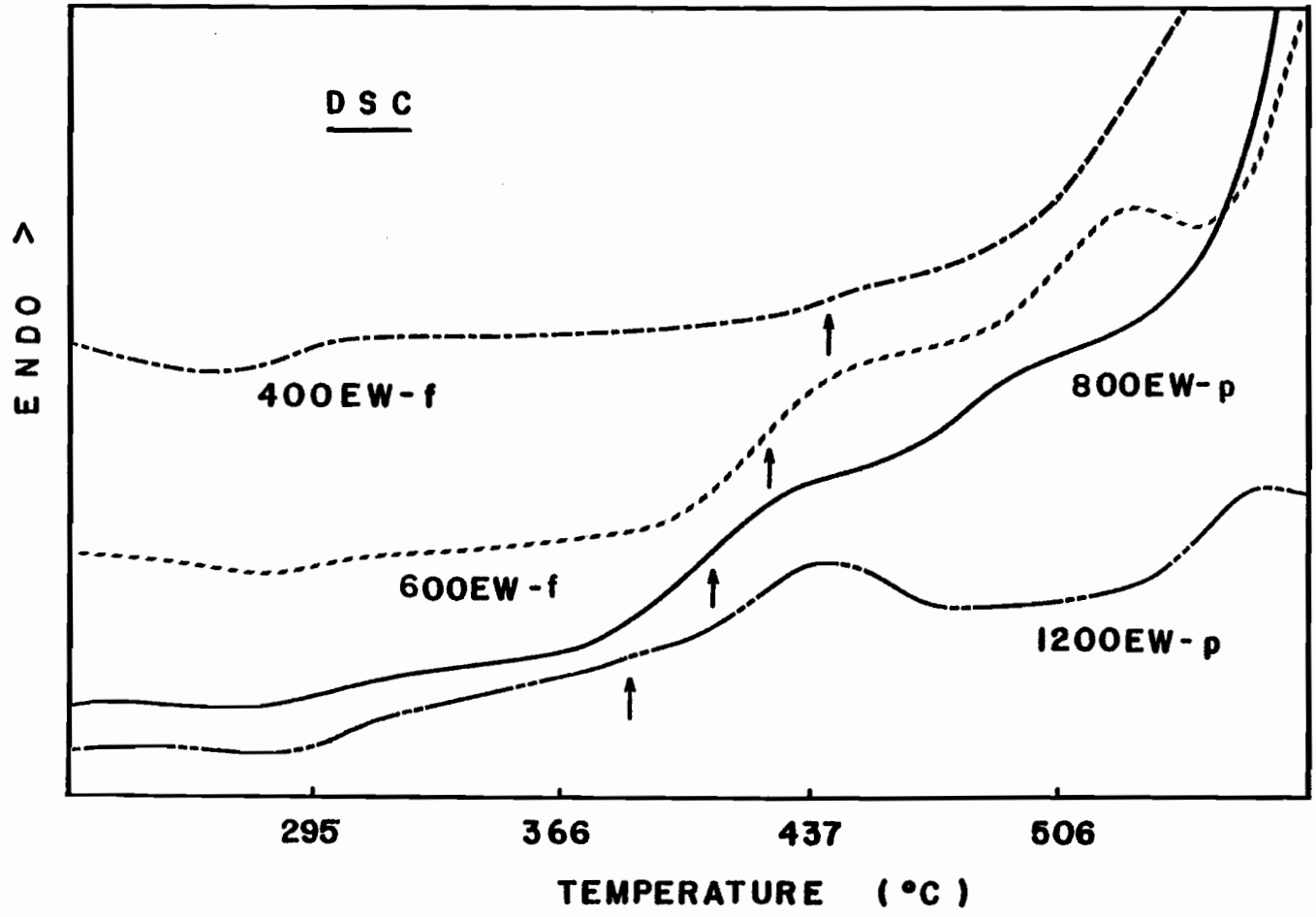
DSC
ENDO >
400EW-f
600EW-f
800EW-p
1200EW-p
295
366
437
506
TEMPERATURE (°C)

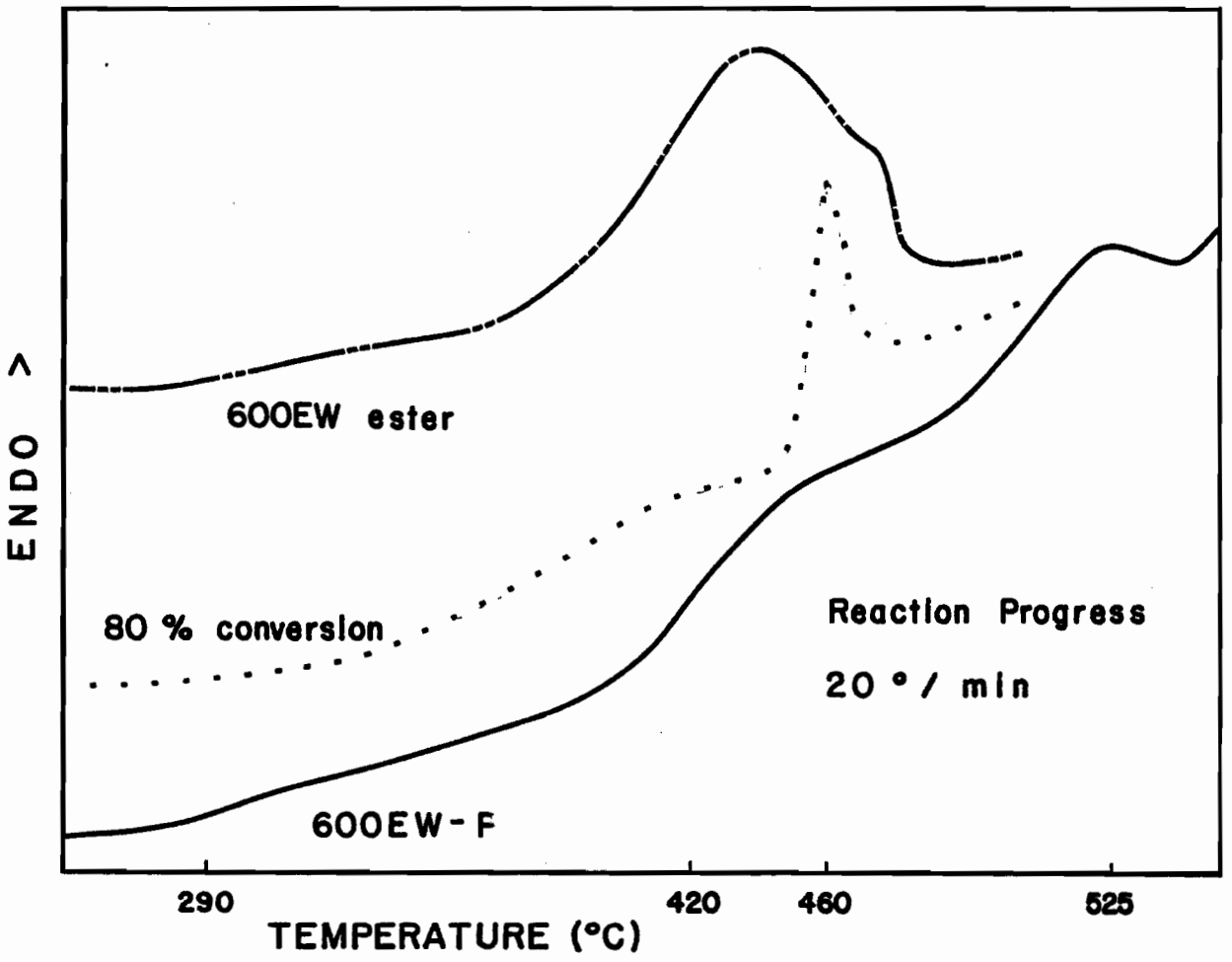

Figure 13: DSC curves for 600EW ester, a partially neutralized 600EW sample and 600EW-f

ester precursor. The DSC transition temperatures are tabulated in Table 5.

Table 5 DSC transition temperatures (°C) obtained at a scan rate of 20 degrees/minute

	1200EW	800EW	600EW		400EW
Batch			1	2	
Precursor					
Glass transition	-	292	288	290	285
Decarbox. peak	-	439	437	438	437
Ionomer					
Low temperature	-	297		292	287
Glass transition	355	405		420	440
High temperature	-	492		525	-

Since both the glass transition and the decarboxylation reaction are rate-dependent phenomena, the effect of varying scan rates was measured for 600EW ester samples cast from chloroform. Although the glass transition could not be clearly measured for all samples, the effect was evident on the shape and temperature of the peak for the high-temperature endotherm (Figure 14). Alternate scan rates used were 40, 10 and 5 degrees/minute.

The effect of solvent used for the initial casting solution was also investigated. The solvents were toluene, xylene and tetrahydrofuran. Results were essentially the same as for chloroform.

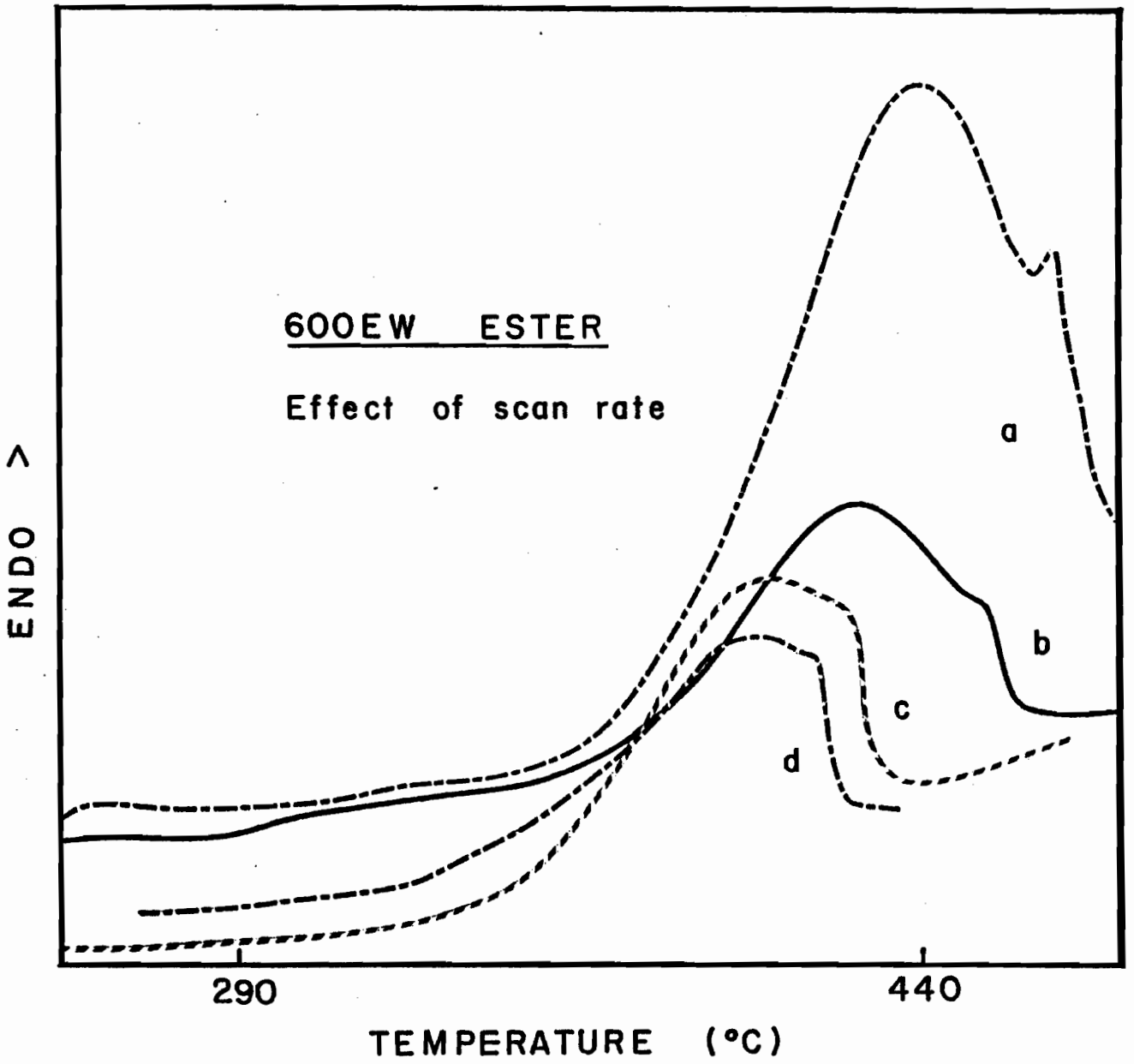

Figure 14: Normalized DSC curves for 600EW ester obtained by heating at different scan rates
a - 40 degrees/minute
b - 20 degrees/minute
c - 10 degrees/minute
d - 5 degrees/minute

3.1.5 Scanning Electron Microscopy

In all cases, micrographs were taken of the film surface and of a cut surface of a film sample. The latter samples were obtained by cutting the film with a very sharp blade. A tensile fracture was also studied. Only the 600EW material was studied by SEM.

3.1.5.1 600EW ester precursor

Micrographs of the 600EW ester precursor were taken for the material directly after casting (as is), following annealing at 205°C, and following a pretreatment in which the material was kept at 195°C and 1.5 MPa in water for five days. The latter treatment was performed to observe the effects of hydrolysis conditions, i.e. temperature and pressure, on the film. No ethylene glycol was used since its effect, if any, is only operative in an alkaline medium. Micrographs are shown in Figures 15 to 17, respectively.

In the untreated sample, holes of 300 to 500 nm in diameter are visible in the surface. The interior displays numerous circular voids of diameters ranging from 1 to 5 micrometers. The annealed ester shows much lower void content in both surface and interior. The holes still visible are much reduced in diameter. The boiled sample gives a picture similar to that of the untreated ester with the difference that the surface pores appear slightly eroded (crater-like) and the fracture appears more brittle.

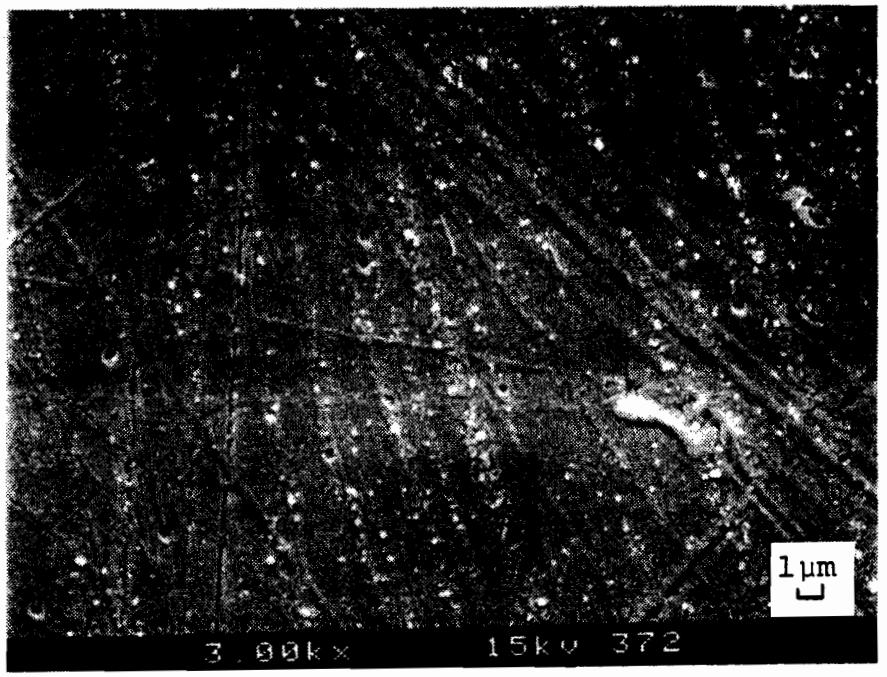

a

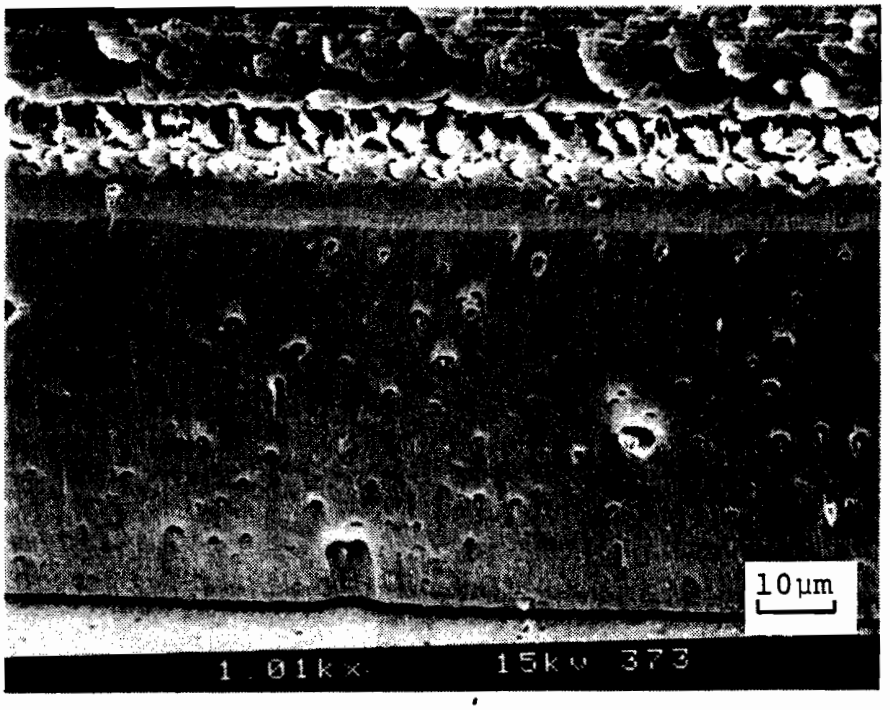

b

Figure 15: SEM photograhs of the surface (a) and cut (b) of an untreated 600EW ester film

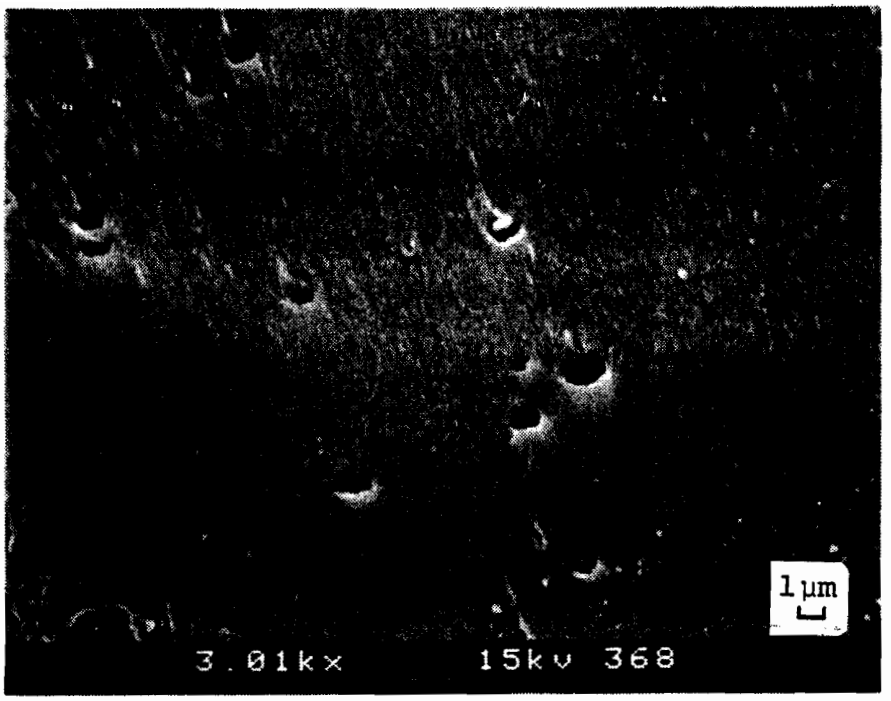

a

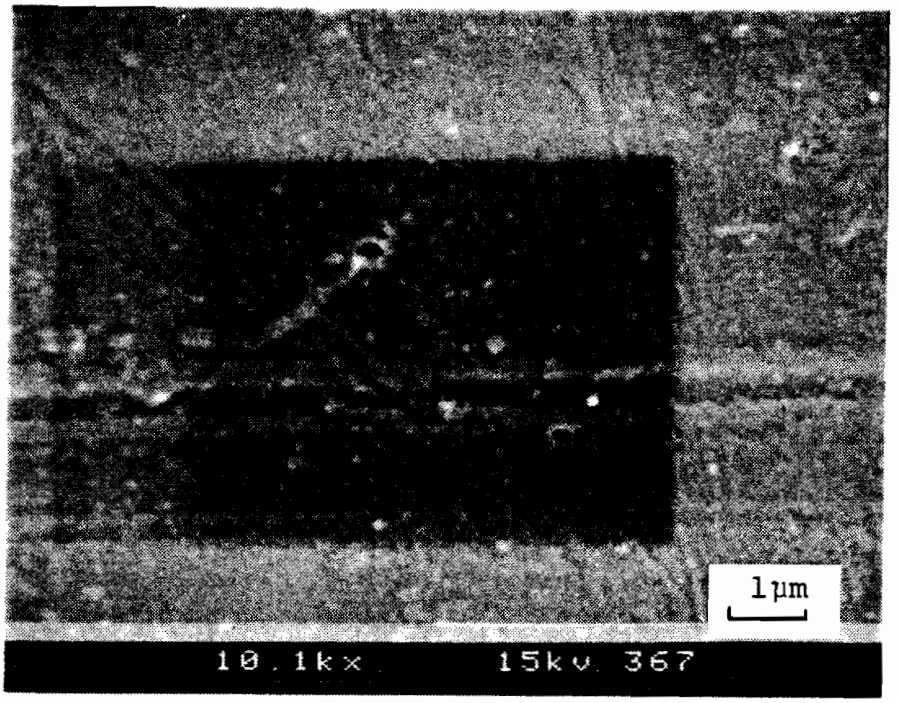

b

Figure 16: SEM photographs of the surface (b) and cut (a) of an annealed 600EW ester film

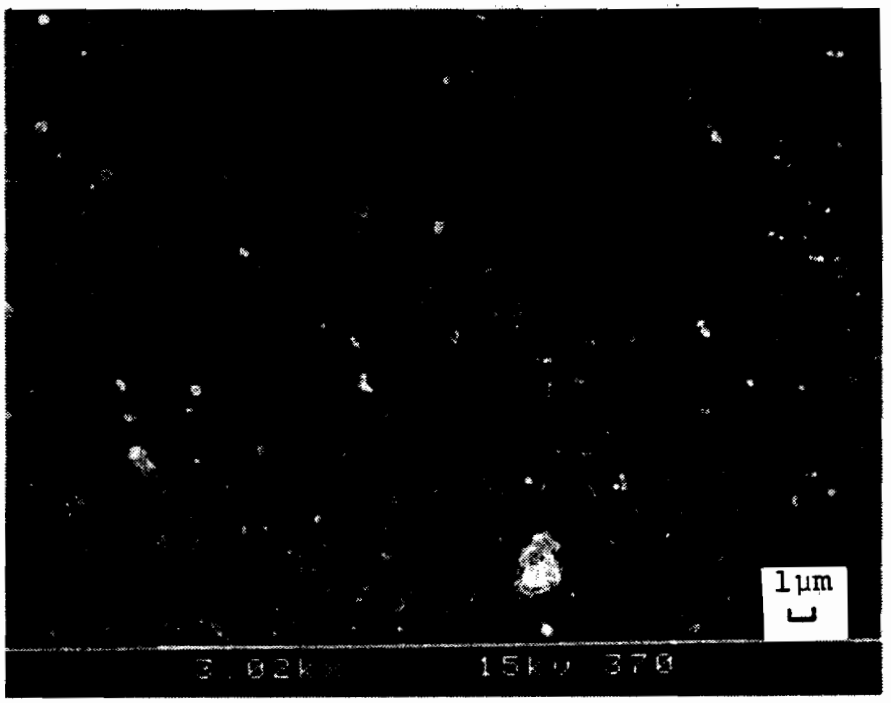

a

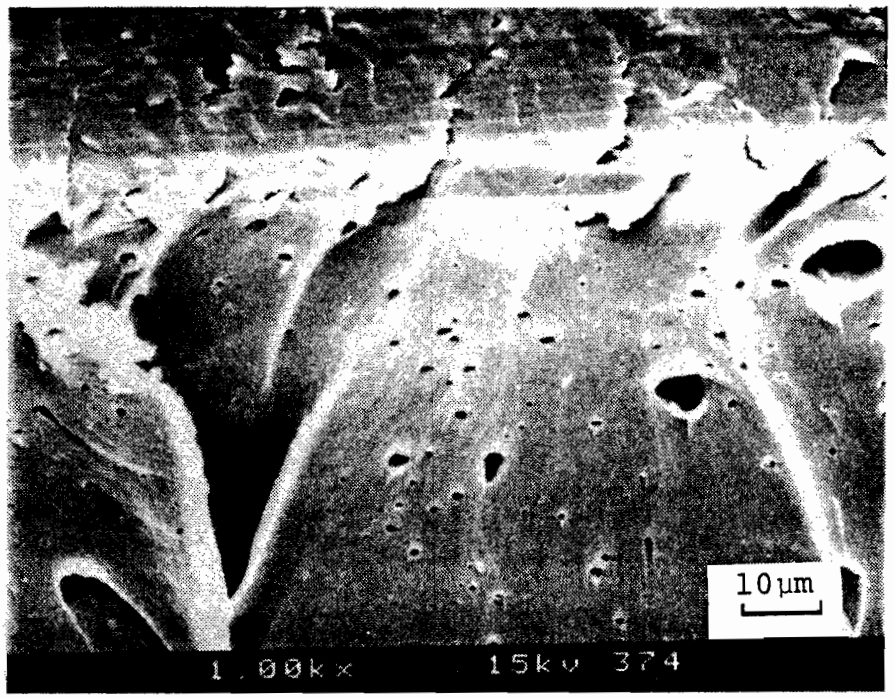

b

Figure 17: SEM photograph of the surface (a) and cut (b) of a 600EW ester film which had been kept in water at 190°C and 225 psi for 5 days

3.1.5.2 600EW ionomer

The micrographs of the surface and cut of a 600EW-f sample are shown in Figure 18. The cut reflects a specimen partially broken into a V-shape so as to illustrate the continuity of the features observed on both sides of the cut. The surface features resemble those of the ester whereas the interior shows slightly larger and more numerous pores.

In Figure 19, the fracture incurred at the end of an Instron tensile test in 20 % KOH (a) is shown along with that obtained by cutting a hydrated sample (b). Comparison of (a) and (b) shows enlarged pores and a more pronounced degree of orientation in the Instron-fractured sample. Small channels lying in a direction roughly perpendicular to the tensile axis are also evident in (a). The fracture is qualitatively more jagged in case (a) than in case (b). The edge features outside of the parentheses-like demarcation lines in (b) are believed to be artifacts due to the knife-cutting method employed. The "parentheses" themselves are not thought to represent a macro-pore, but rather the boundaries of the sample cross-section which was not flattened by the incision.

The effect of drying on the internal film structure was explored by comparing fractures of a sample stored in water continuously, a sample kept at ambient conditions of pressure, temperature and humidity, and one dried at 100°C under reduced pressure. The resultant

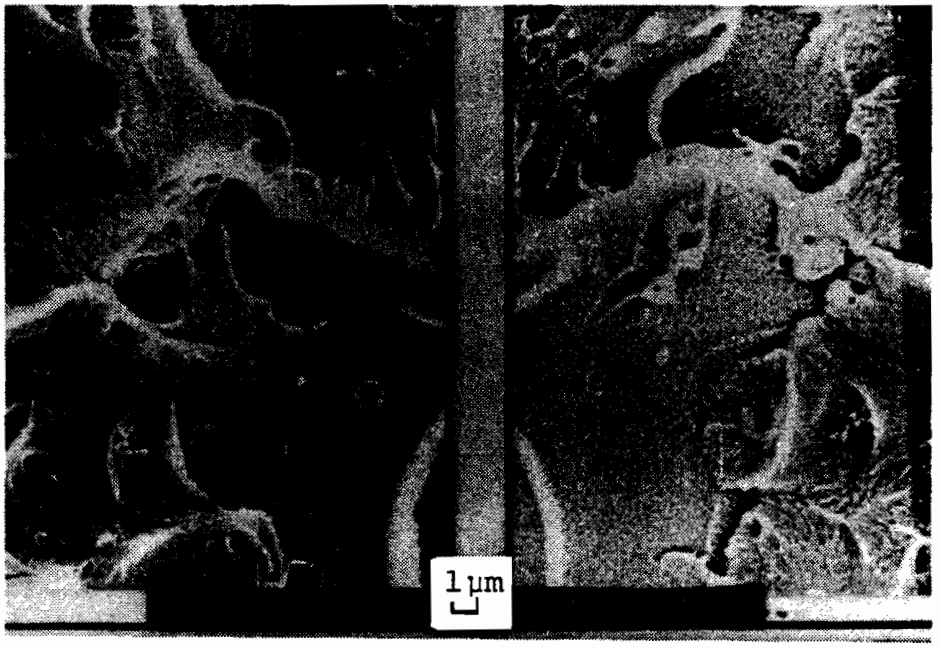

a

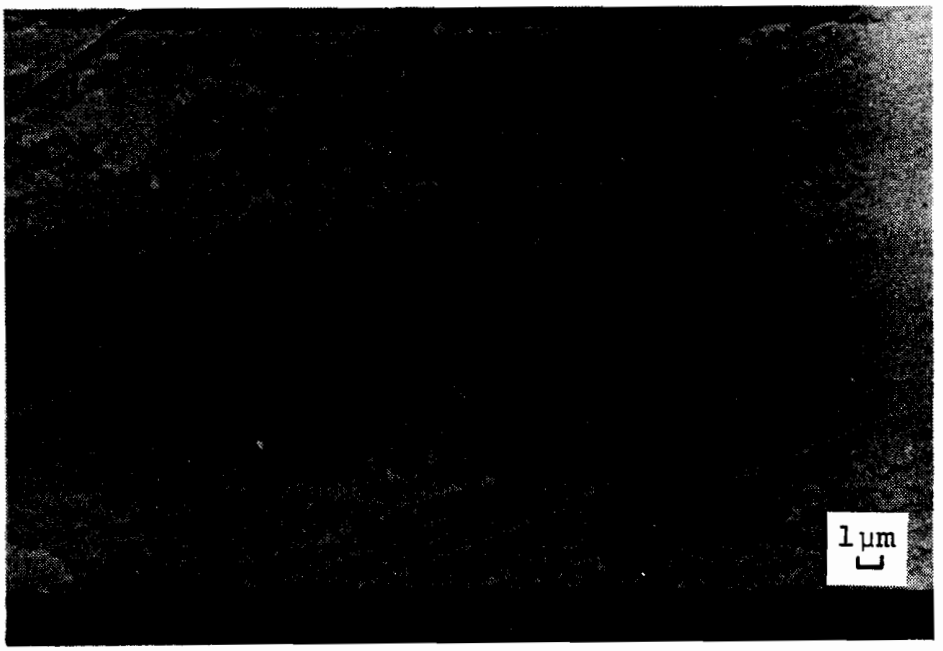

b

Figure 18: SEM photographs of the surface (b) and V-cut (a) of 600EW-f film

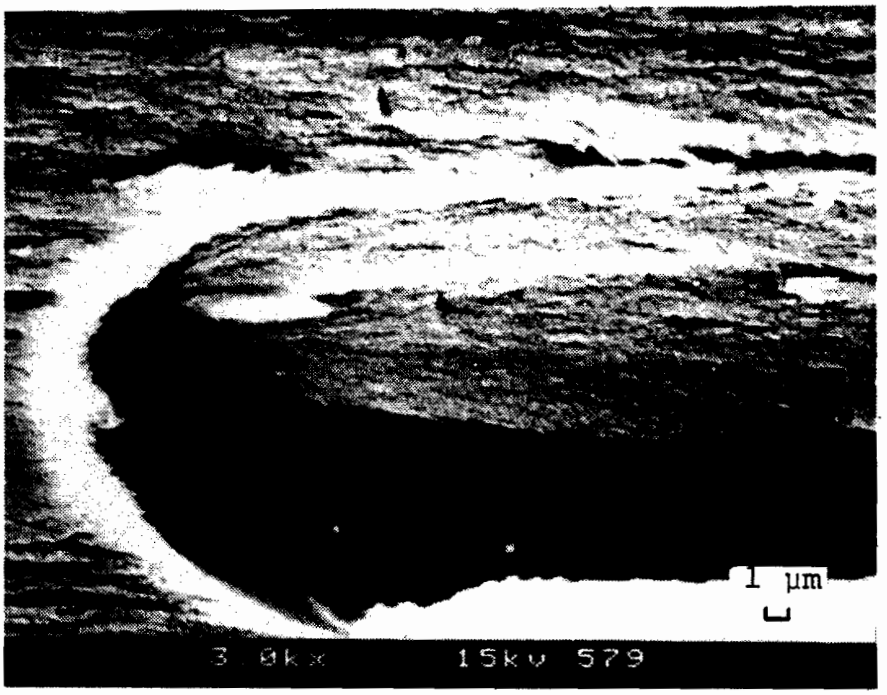

a

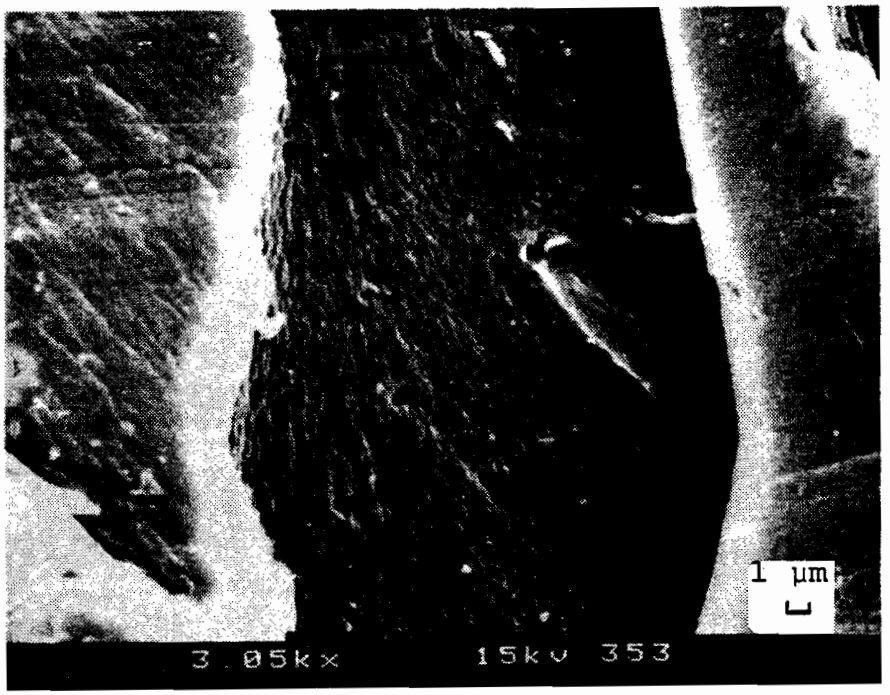

b

Figure 19: SEM photographs of 600EW-f cross-sections obtained by Instron fracture (a) and by sharp blade incision (b)

micrographs are shown in Figure 20 (a), (b) and (c), respectively. The major effect of drying appears to be the appearance of a large number of very small pores (diameters $\leq$ 100 nm), previously masked by water engorgement. The effect on the sample dried *in. vacuo* (c) is even more pronounced. The fractures of the dried material are more brittle and do not show the effect of the blade incision. In the sample dried *in. vacuo.*, channels of *ca.* 800 nm width are visible in the direction roughly perpendicular to the surface.

Micrographs of the powder hydrolyzed 600EW-p show a smooth surface with no pores apparent even at 25 Kx magnification. The fracture of 600EW-p shows very small pores and some discontinuous channels roughly parallel to the cross-sectional cut. This can be seen in Figure 21.

3.1.6 X-Ray Diffraction

The wide angle X-ray diffraction patterns of three 600EW ester samples (unstrained, annealed at 270°C and strained by Instron tensile testing) were obtained. They are shown in Figure 22 in the form of microdensitometer traces across the meridional WAXD pattern. The untreated ester (A) shows a low degree of orientation as indicated by the peak at *ca.* 9°. The peak at about 17° is due to the amorphous halo. Annealing (C) appears to produce no increase in orientation whereas sample straining at 25°C causes a significant increase (B), evidenced by the appearance of complementary diffuse arcs in both the equatorial and

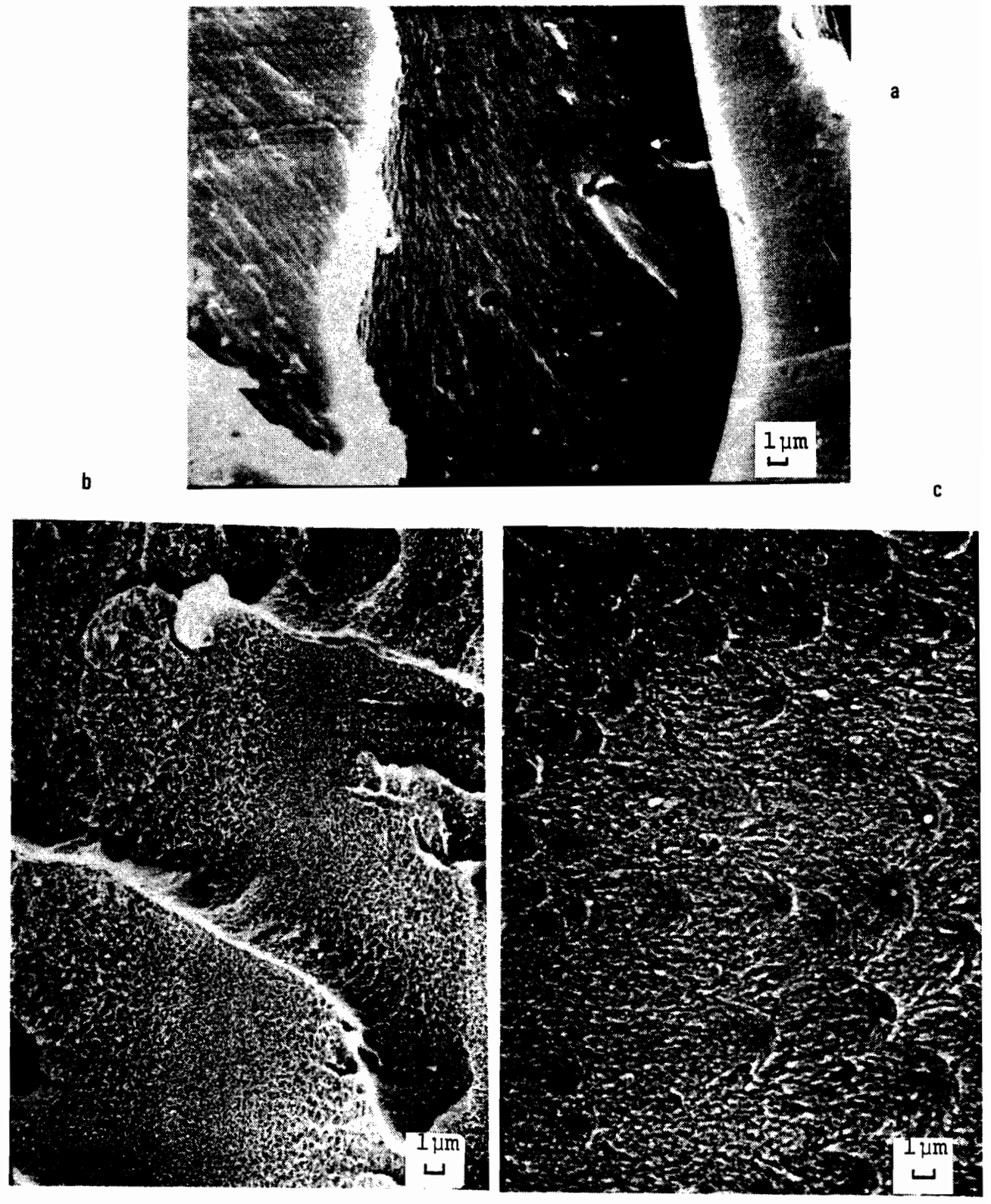

Figure 20: SEM photographs of 600EW-f cuts showing the effects of various pretreatments
a - continuously kept in water
b - kept dry at ambient conditions
c - dried in. vacuo. at 100°C for 5 days

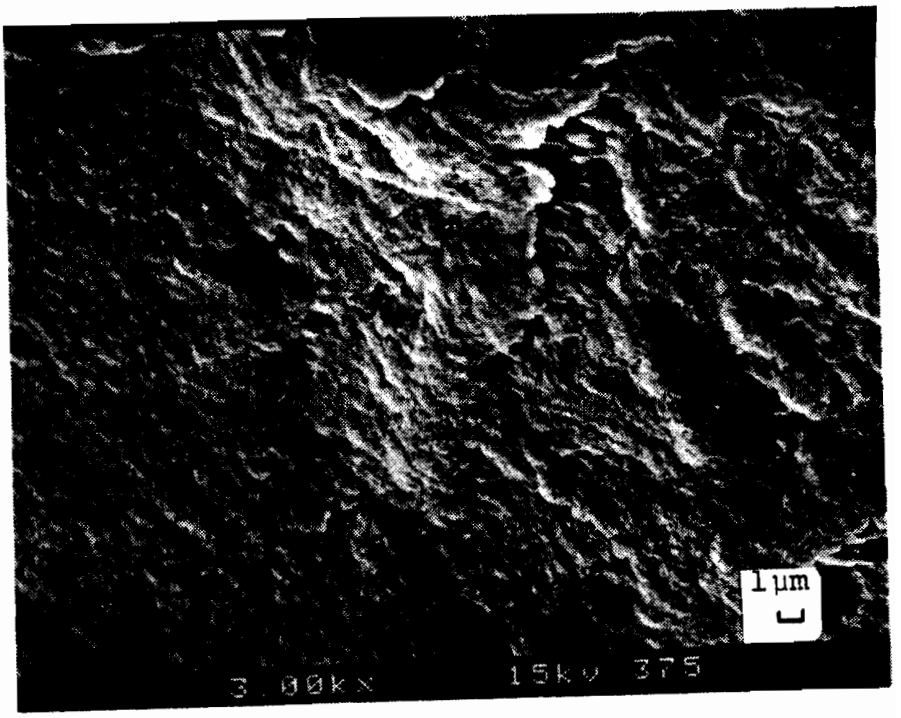

Figure 21: SEM photograph of a cut surface of a powder hydrolyzed 600EW ionomer film cast from DMSO

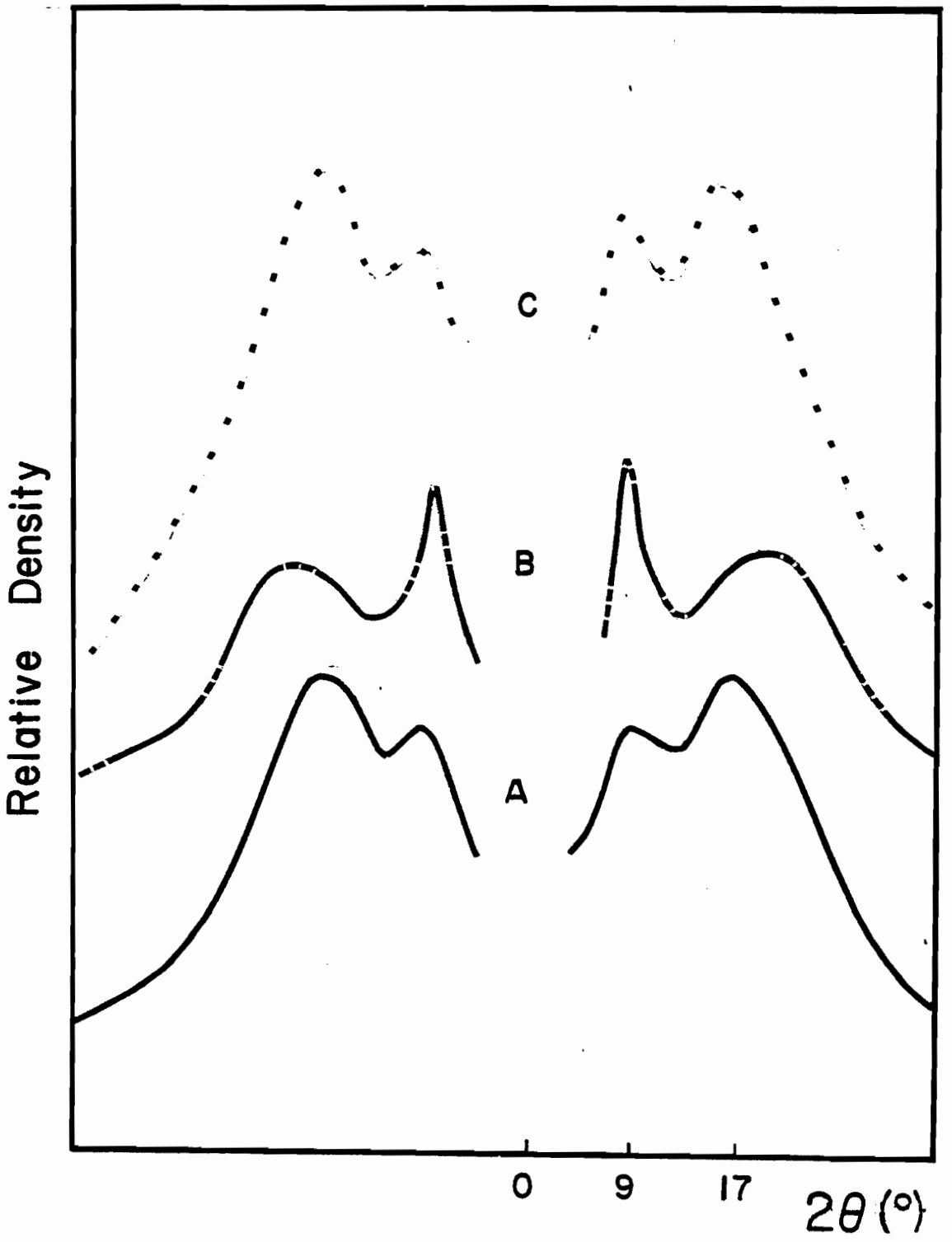

Figure 22: Microdensitometer traces of wide angle X-ray diffraction patterns for 600EW ester ,unstrained (A), strained by 130 % (B) and annealed (C)

meridional directions. This orientation was also observed in the 600EW-f material.

3.1.7 Contact Angle

The results of measurements of contact angle as a function of time for the 600EW ester, 600EW-f as well as Nafion and its precursor are given in Figure 23. Over a period of three minutes, a decrease of ca. 70° is observed for 600EW-f. Nafion shows a rapid decrease followed by a stabilization of the contact angle after ca. 90 seconds. A total reduction of 10° is apparent after three minutes. The 600EW ester shows a continuous decrease in contact angle over time which is comparable to Nafion. The Nafion precursor appears impermeable to water over the period of the experiment.

3.2 VISCOELASTIC PROPERTIES

3.2.1 Torsion Pendulum and Vibrating Reed

The dynamic mechanical spectra of the ester precursors of 400, 600 and 800 equivalent weight (obtained by thetorsion pendulum) show a single broad peak in the loss tangent at low temperature (ca. -100°C), in addition to the glass transition. The three precursors show practically identical behaviour. The behaviour of the storage modulus (G'), loss modulus (G'') and loss tangent (tan δ) as a function of temperature is shown in Figure 24 for the 800EW ester.

A low temperature peak is also observed in the 800EW ionomer, but the glass transition shifts to a higher

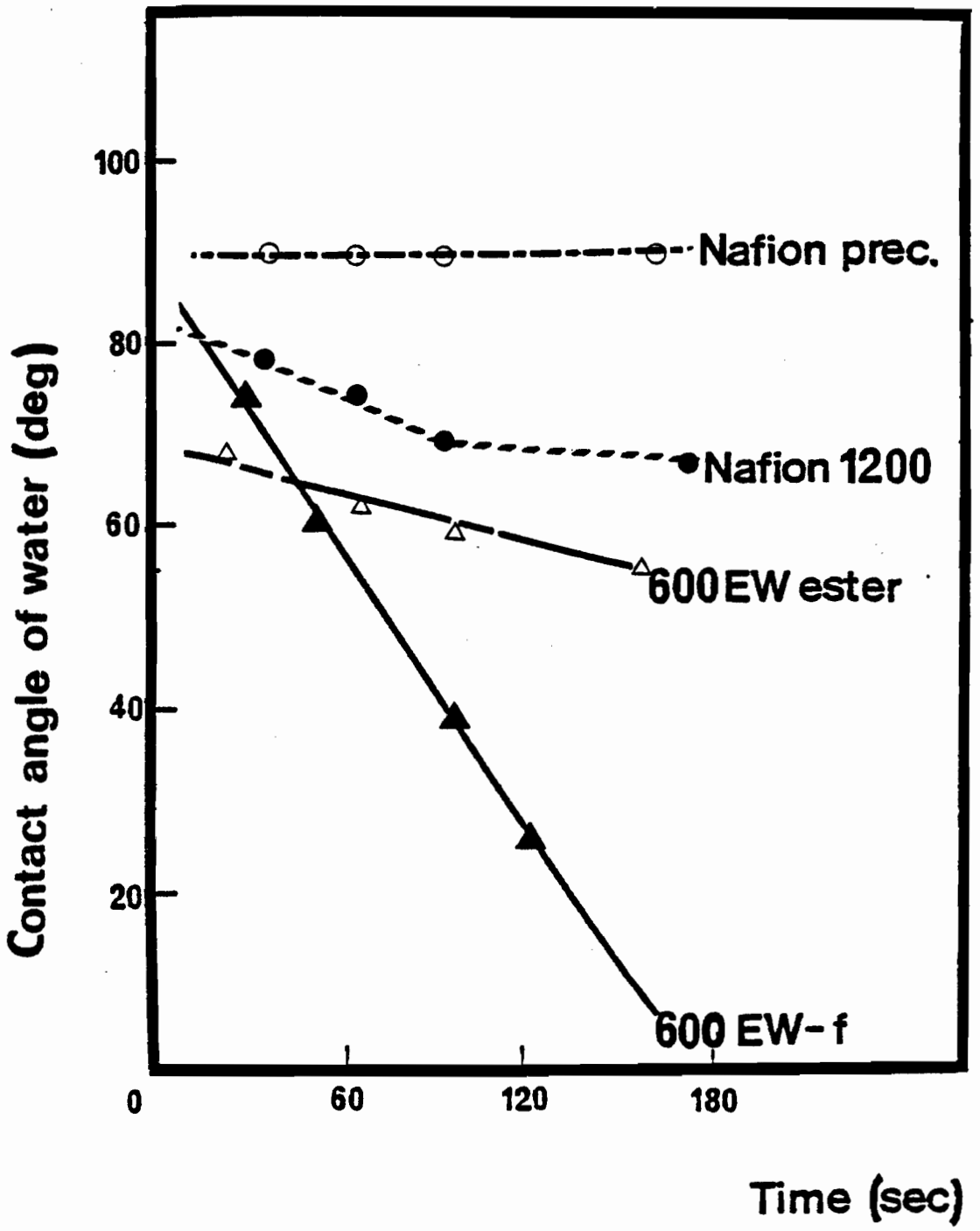

Figure 23: Contact angle of water as a function of time for 600EW materials and for Nafion

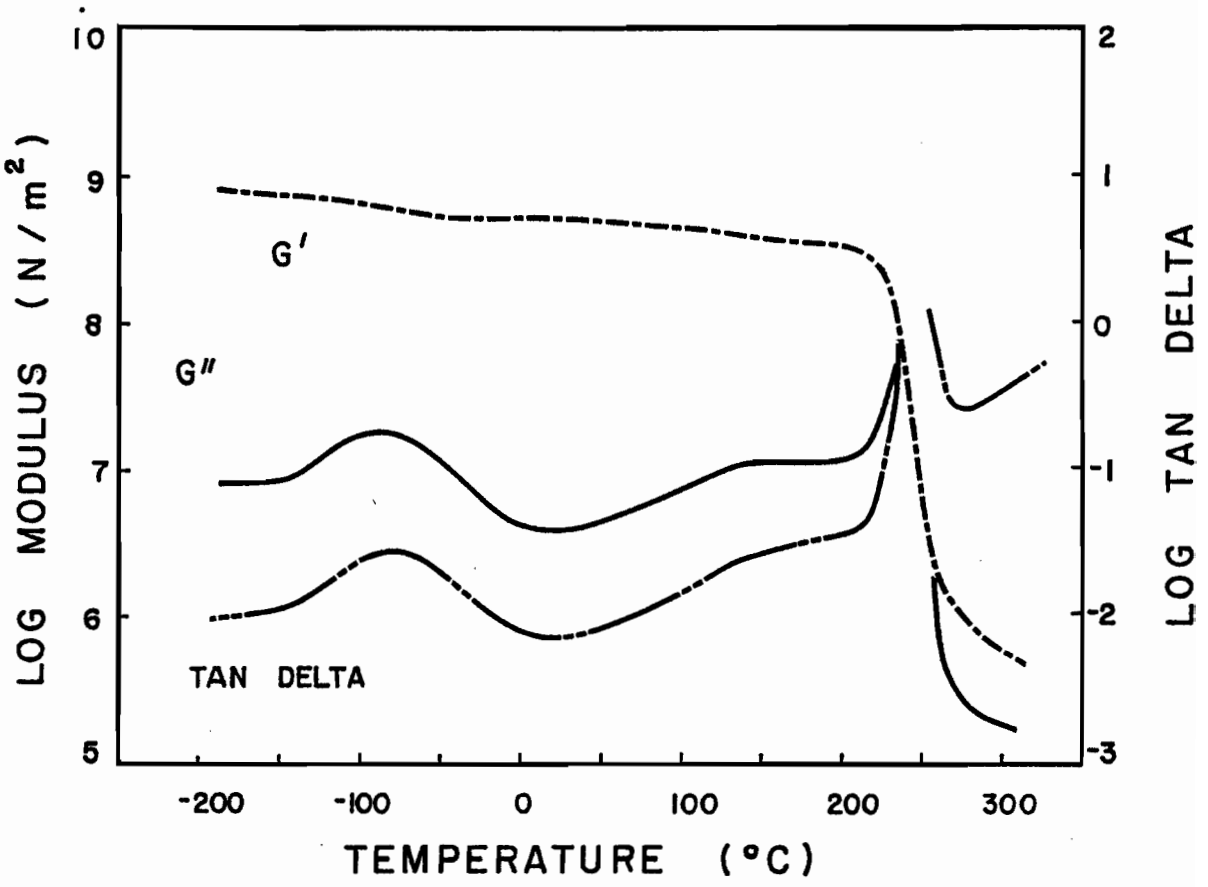

Figure 24: Dynamic mechanical spectra of 800EW ester obtained at ca. 1 Hz (Torsion Pendulum)

temperature, as shown in Figure 25. The loss tangent curves in the glass transition region of the 800EW ester and ionomer are compared in Figure 26. It was not possible to perform the experiment on the 600EW ionomer since the material decomposes at molding temperatures.

The loss tangent curves obtained for the same samples using the vibrating reed show corresponding low temperature transitions at slightly higher temperatures. They are shown in Figure 27 for the ester precursors. An Arrhenius-type plot for the 800EW ionomer indicates an activation energy of ca. 60 kJ/mole for this low temperature transition. For both esters, the activation energy for the motion reflected by that dispersion was slightly higher (70 and 100 kJ/mol for 800 and 600 esters, respectively). The peak temperatures obtained by dynamic mechanical testing are given in Table 6. The testing frequency is shown in brackets.

Table 6 Peak temperatures (^{o}C) for molded samples

	Torsion T_g	Pendulum T_{low}	Vibrating Reed T_{low}
800EW ester	250(0.3)	-85(2.1)	-60(285)
ionomer	330(1.5)	-85(3.1)	-35(491)
600EW ester, batch 1	255(0.3)	-60(2.2)	-
batch 2	235(0.3)	-65(1.8)	-38(212)
400EW ester	243(0.3)	-70(2.8)	-

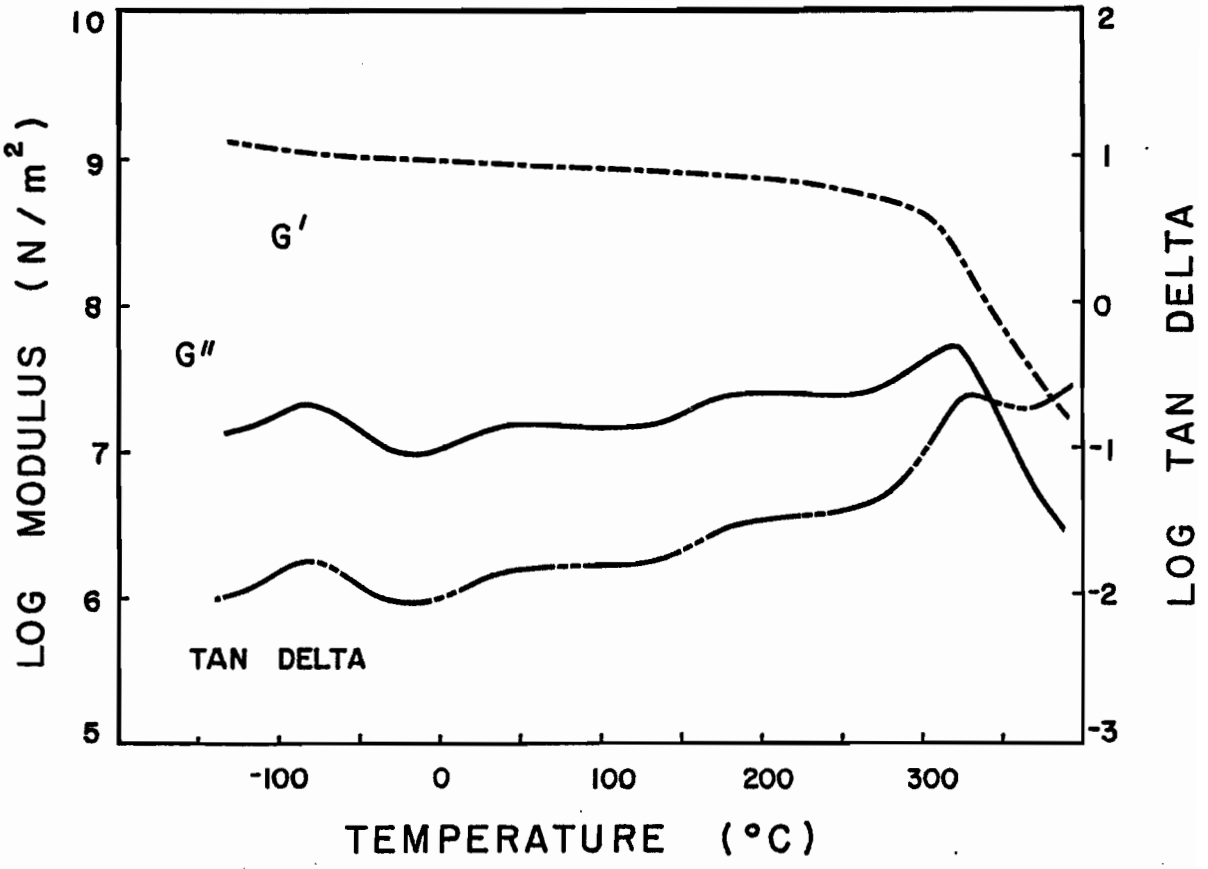

Figure 25: Dynamic mechanical spectra of 800EW ionomer obtained at ca. 1 Hz

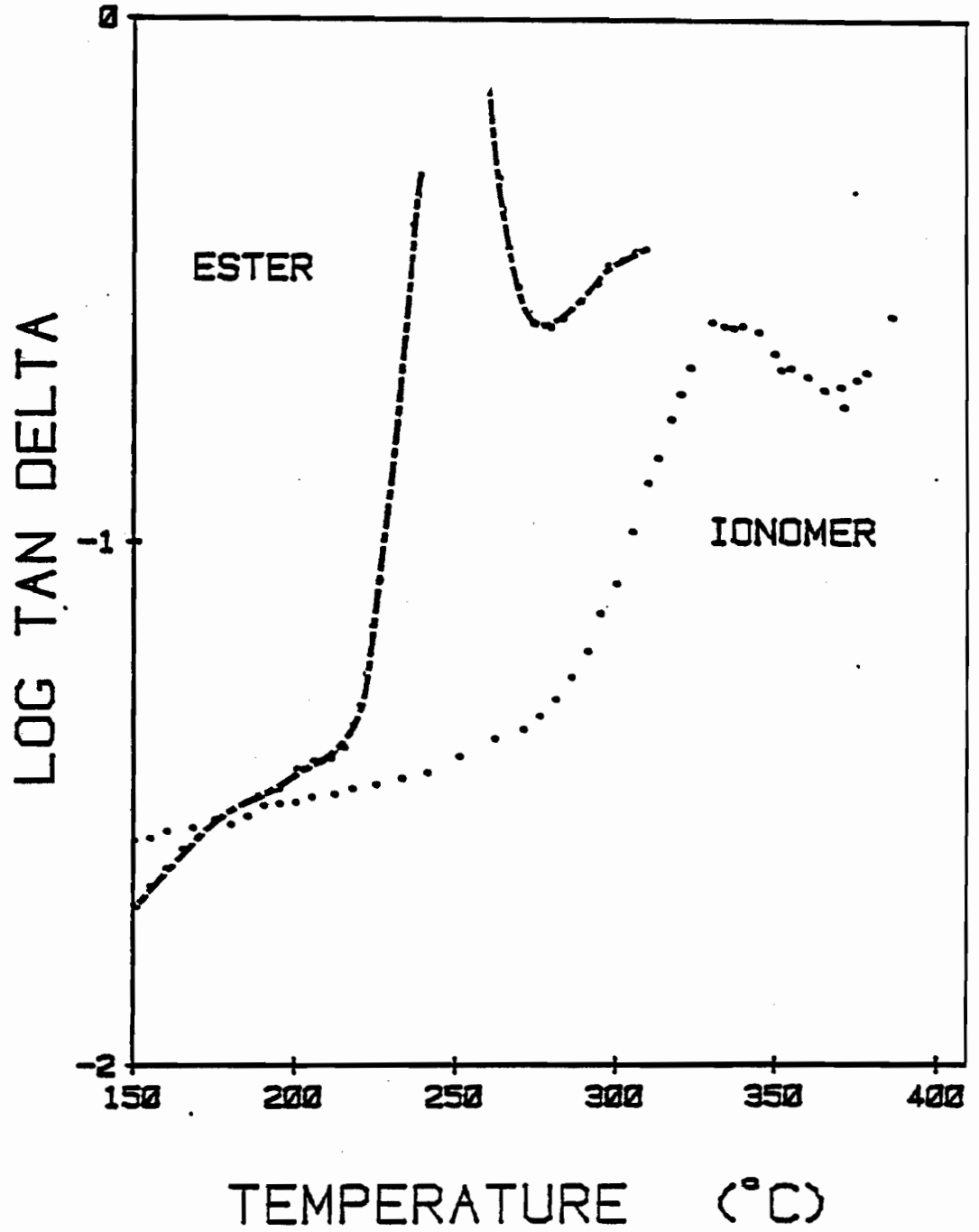

Figure 26: Mechanical loss tangent as a function of temperature for the 800EW precursor and ionomer obtained at ca. 1 Hz

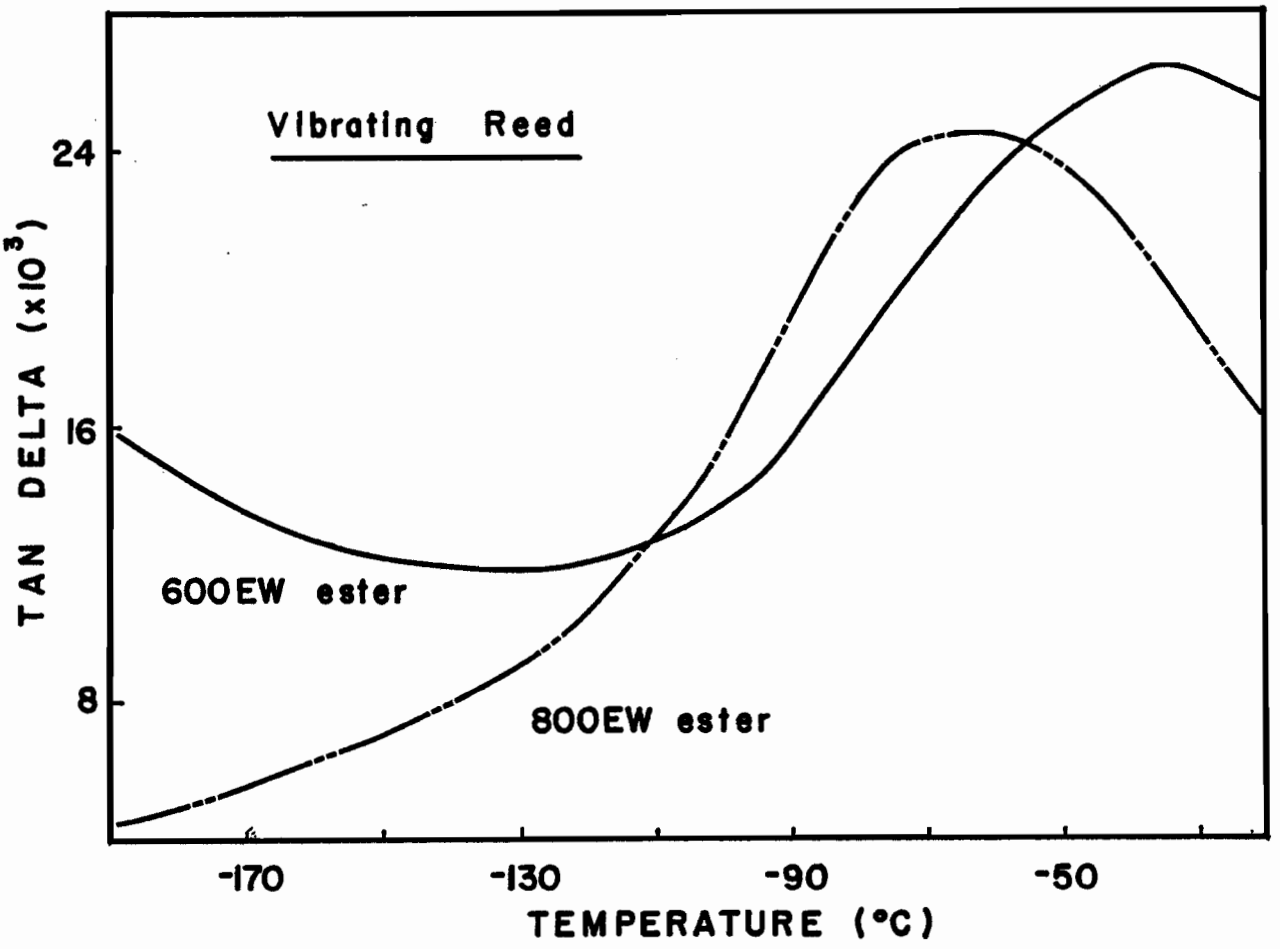

Figure 27: Mechanical loss tangent as a function of temperature for the ester precursors of 600 and 800 equivalent weight obtained at ca. 350 Hz (Vibrating Reed)

3.2.2 Tensile Tests

The stress-strain experiments were primarily conducted on 600EW material. Nafion was studied for comparison.

3.2.2.1 Dry/high temperature experiments

The behaviour of the 600EW ester, a partially neutralized (60 %) 600EW-f sample and Nafion, all in the dry state at 25°C, is shown in Figure 28. The partially neutralized material is seen to be hard and very brittle. Nafion and the 600EW ester appear strong and tough, showing break strains of 180 % and 160 % , respectively. A yield point is observable for the 600EW ester at ca. 10 % elongation.

Stress-strain curves were obtained for dry 600EW ester and ionomer as a function of temperature. For the ester, the modulus decreases steadily with temperature at a rate of ca. 3 MPa/°C. For the ionomer, the modulus increases as the testing temperature increases to 100°C but starts to decrease at higher temperature. Break strain and tensile strength (the latter defined as the maximum stress incurred by the sample) follow the same pattern. The modulus, break strain and tensile strength show a drastic decrease at 290°C, suggesting the occurrence of an anomalous process in the ionomer between 200 and 290°C. The dry 600EW-f is extremely brittle, as can be deduced from the very low values of elongation to break (Figure 29). The results for dry tensile testing are summarized in Table 7. The

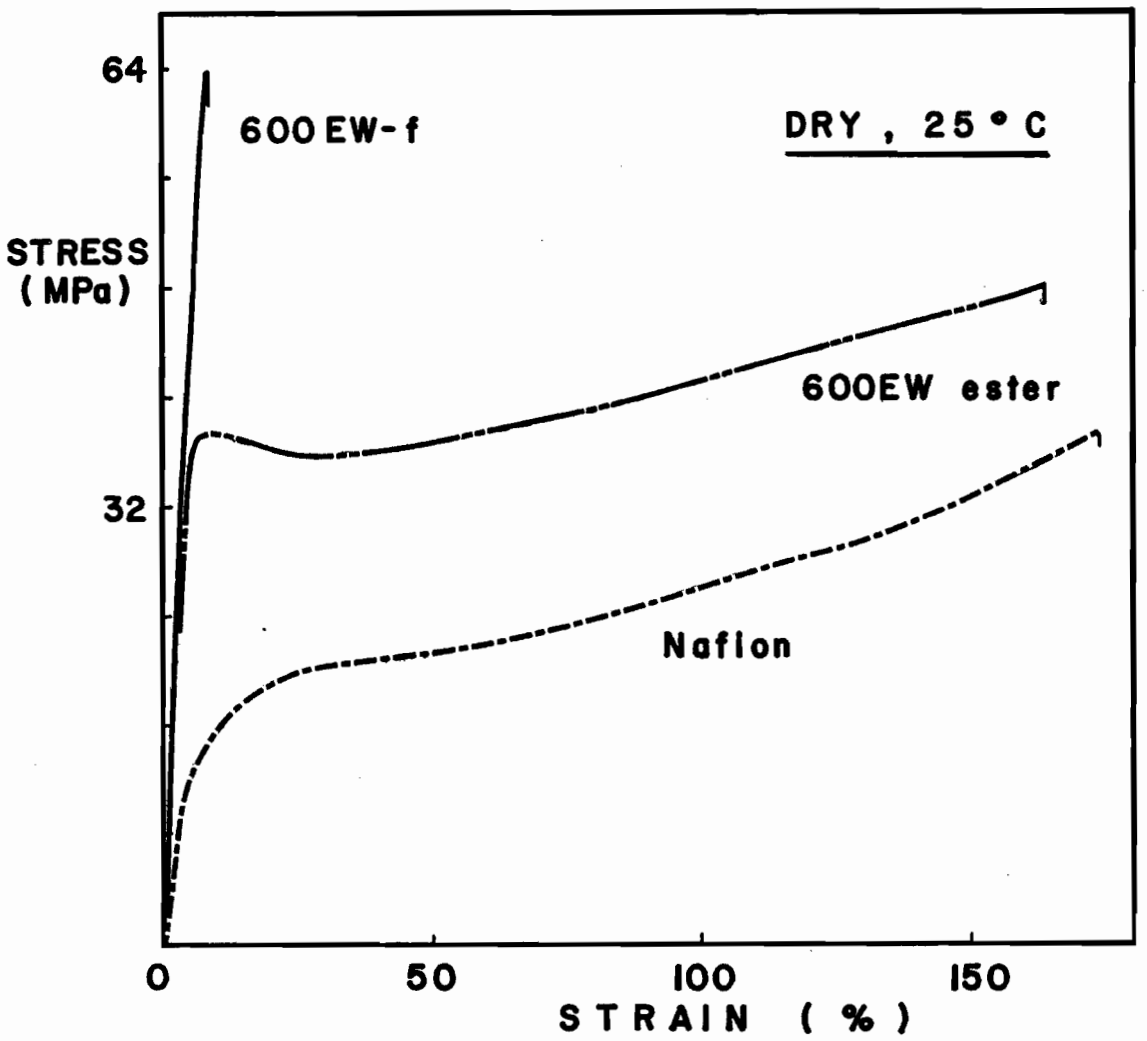

Figure 28: Stress-strain curves obtained in the dry state for Nafion and 600EW aromatic systems

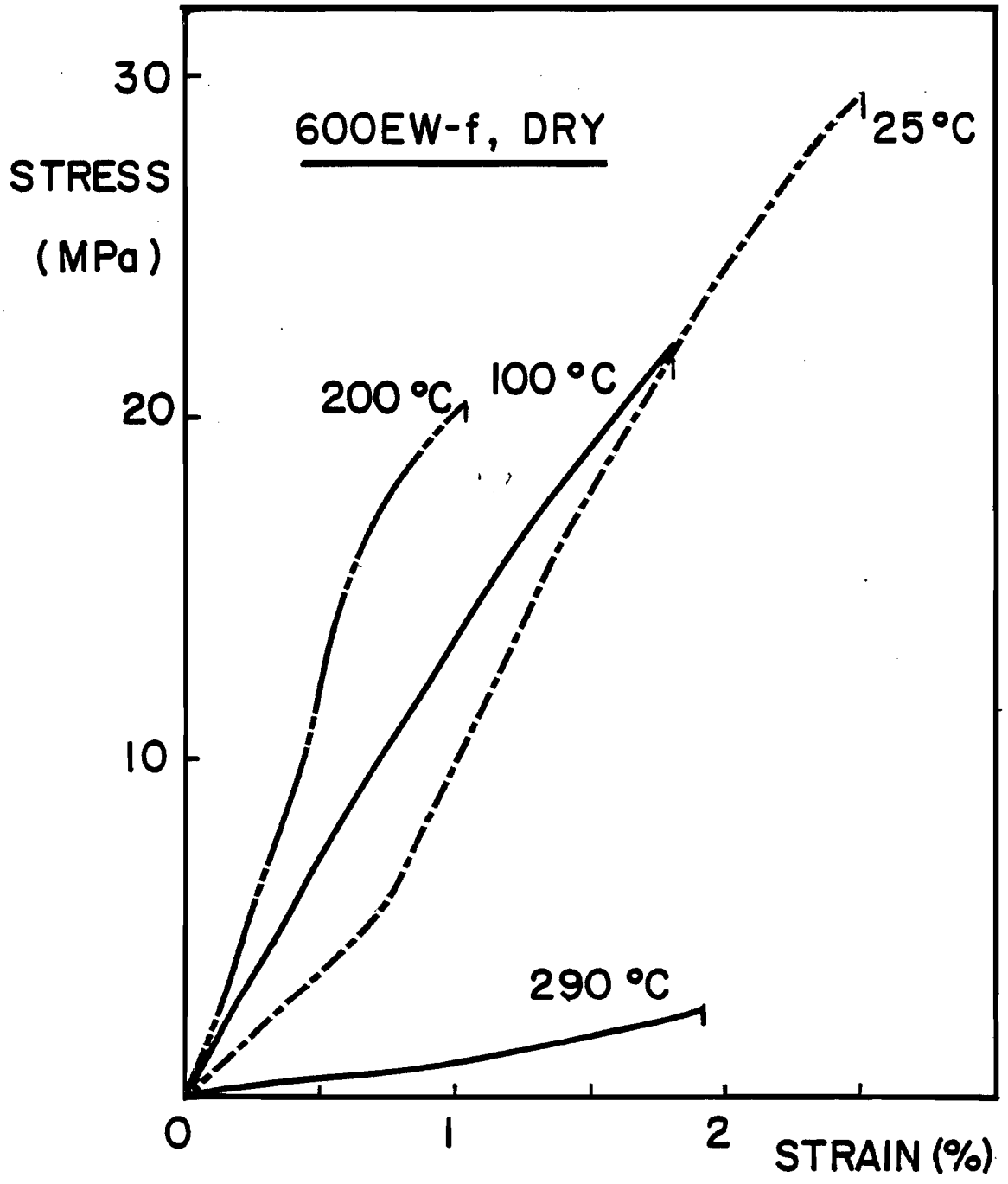

Figure 29: Stress-strain curves as a function of temperature for 600EW-f-II in the dry state

values of percent relative precision are given in brackets immediately following the modulus value.

Table 7 Tensile testing results for the dry state

	Temperature (°C)	Modulus (MPa)	Tensile Strength (MPa)	Break Strain (%)
600EW ester	25	1400 (18)	50	160
	100	1300 (31)	55	158
	200	900 (23)	35	160
	240	750 (10)	18	130
600EW-f-II	25	1600 (3)	27	2.3
	100	1900 (40)	18	1.8
	200	1600 (29)	14	1.0
	290	150 (32)	4	1.9
Nafion precursor	25	12 (2)	11	600
Nafion 1200	25	260 (23)	35	210

3.2.2.2 Experiments in water/solution

The effects of several variables, pertaining to sample history, influence the results and were individually tested. These variables are listed below.

a. hydrolysis conditions - under some conditions, film hydrolyzed samples became crosslinked (c.f. 3.1.2) to varying degrees.

b. period of storage in water - samples were tested over a period of three months.

c. drying conditions - some samples were dried at 100°C under reduced pressure and others were allowed to dry at ambient conditions.

d. storage conditions - in the period between completion of hydrolysis and performance of the tensile test, the samples were stored either in air (ambient conditions) or in de-ionized water.

The effect of these variables on the 600EW ester and Nafion samples was not tested since both of these materials were kept in air (ambient conditions) since preparation. The effects of these variables on 600EW-f were measured in experiments run in KOH solution. The results obtained under water and in dilute KOH solution did not differ significantly for the 600EW material. All the tests conducted in a liquid environment were performed at a temperature of 80°C unless otherwise specified.

The stress-strain curves for the 600EW ester, a partially neutralized sample (ca.70 %) and the 600EW-f ionomer are shown in Figure 30. A yield point occurs at ca. 5 % elongation in the ester, which reaches an elongation to break of 80 % and a modulus of 1500 MPa. As the material is converted to the ionomer, the yield point gradually disappears, elongation to break is reduced and the modulus decreases by about one order of magnitude in the 600EW-f. The tensile strength also decreases in going from the ester to the ionomer.

The effect of varying hydrolysis conditions, with the ensuing crosslinking of the material, is illustrated in

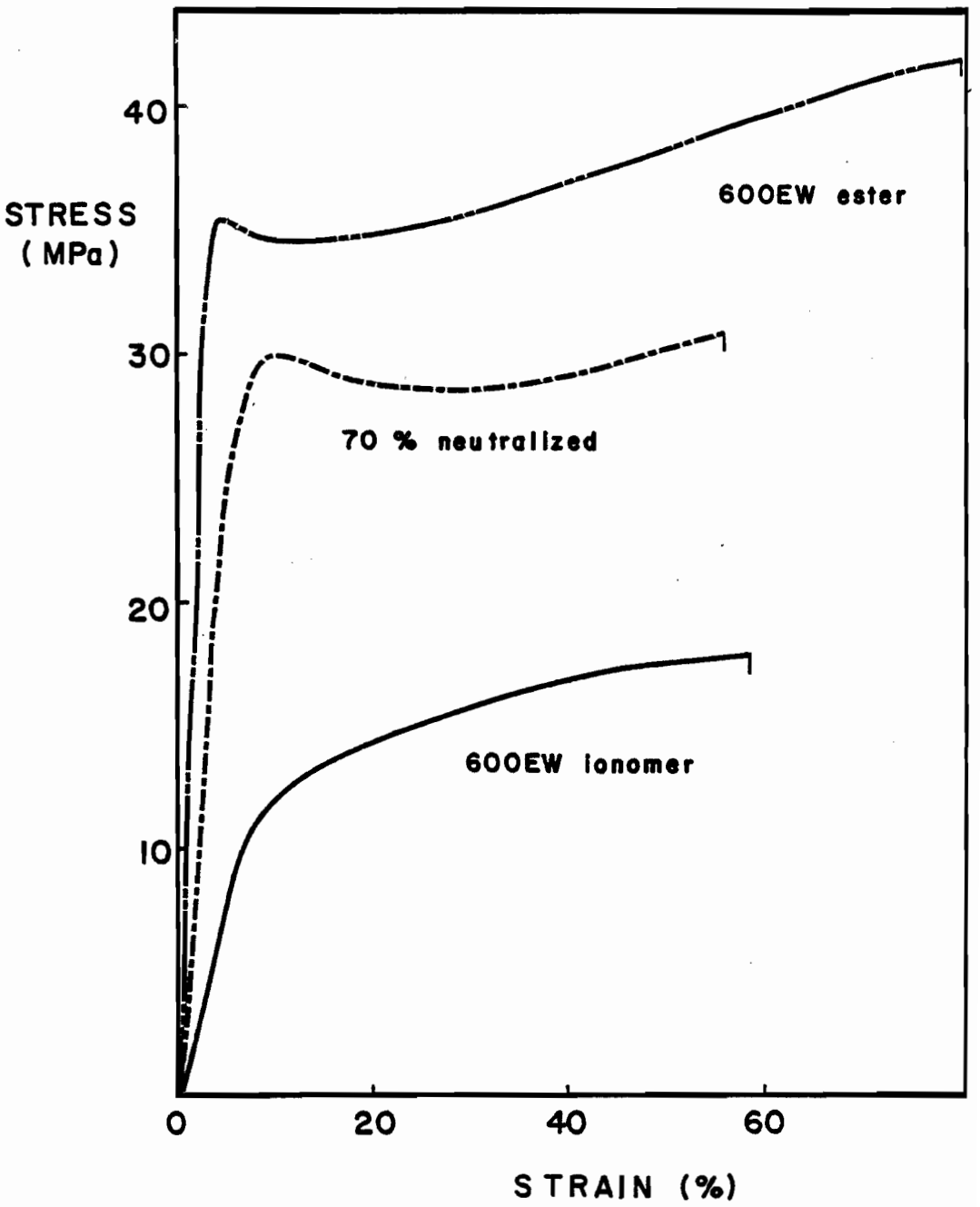

Figure 30: Stress-strain curves as a function of hydrolysis reaction progress in 600EW systems in 0.1M KOH at 80°C

Figure 31. The samples were kept in water continuously since hydrolysis and are probably plasticized to the maximum possible extent. The most striking difference occurs in maximum extension to break, which decreases from ca. 45 % in the crosslinked sample (I) to ca. 20 % in (II) (c.f. section 2.1.2 for nomenclature). Tensile strength is significantly reduced in the case of (II). The moduli for (I) and (II) (300 and 80 MPa, respectively) are consistent with the assumption that I is more crosslinked than II. All subsequent tests were performed on one of these two samples, as specified.

The effect of storage conditions on 600EW-f-II is shown in Figure 32. Sample (a) had been kept dry at ambient conditions whereas (b) and (c) had been continuously kept in water for 2 weeks and 3 months, respectively. Sample (a) was allowed to equilibrate for 8 hours in the solution at temperature prior to testing. Again, the main difference occurs in the extension to break, the highest being observed for the sample stored in the dry state. The modulus and tensile strength differ only slightly for the three samples.

The effect of drying procedure on 600EW-f-I is shown in Figure 33. The results for samples which had been dried in vacuo. at 100°C for 5 days (a) or kept at ambient conditions (b) are compared with those of the sample continuously kept in water (c). The elongation to break decreases steadily with drying but the tensile strength remains approximately constant.

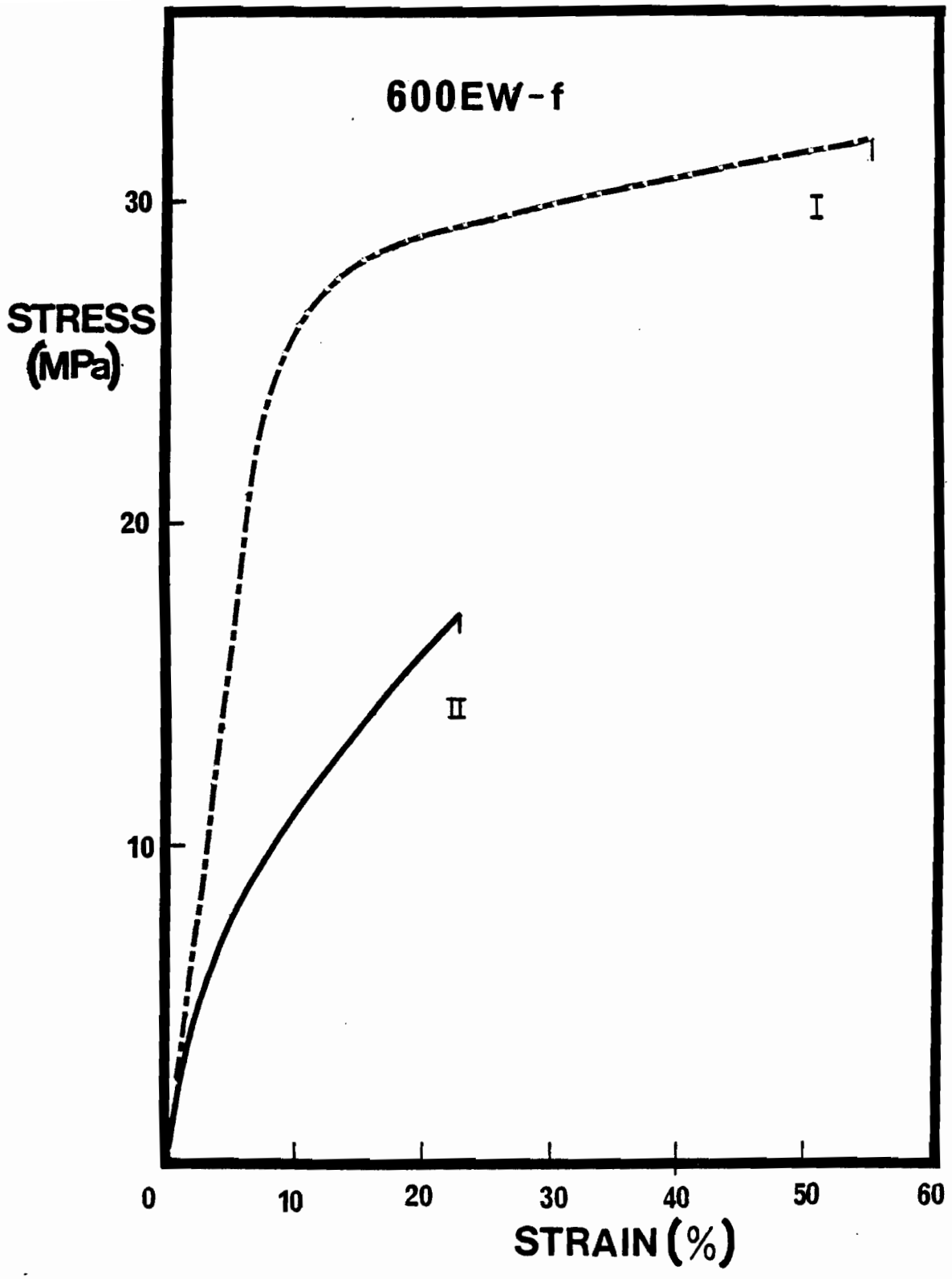

Figure 31: Stress-strain curves for 600EW-f, showing the effect of crosslinking, run in 20 % KOH at 80°C

Figure 32: Stress-strain curves for 600EW-f, showing the effect of storage conditions, run in 20 % KOH at 80^{o}C
a - kept dry at ambient conditions
b - kept in water for two weeks
c - kept in water for three months

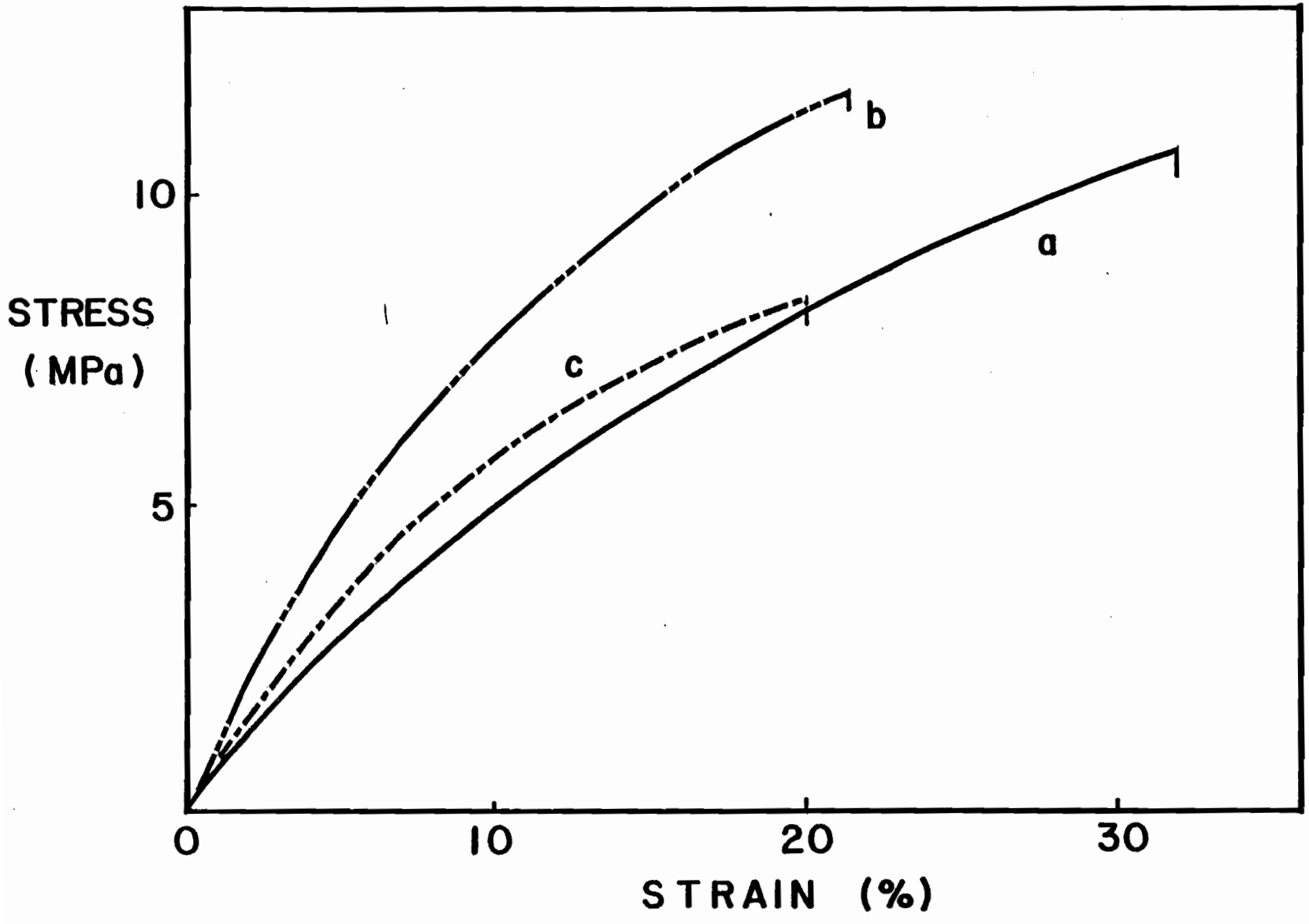
10
5
STRESS
(MPa)
b
a
c
0
10
20
30
STRAIN (%)

Figure 33: Stress-strain curves for 600EW-f, showing the effects of drying pretreatments, run in 0.1 M KOH at 80°C

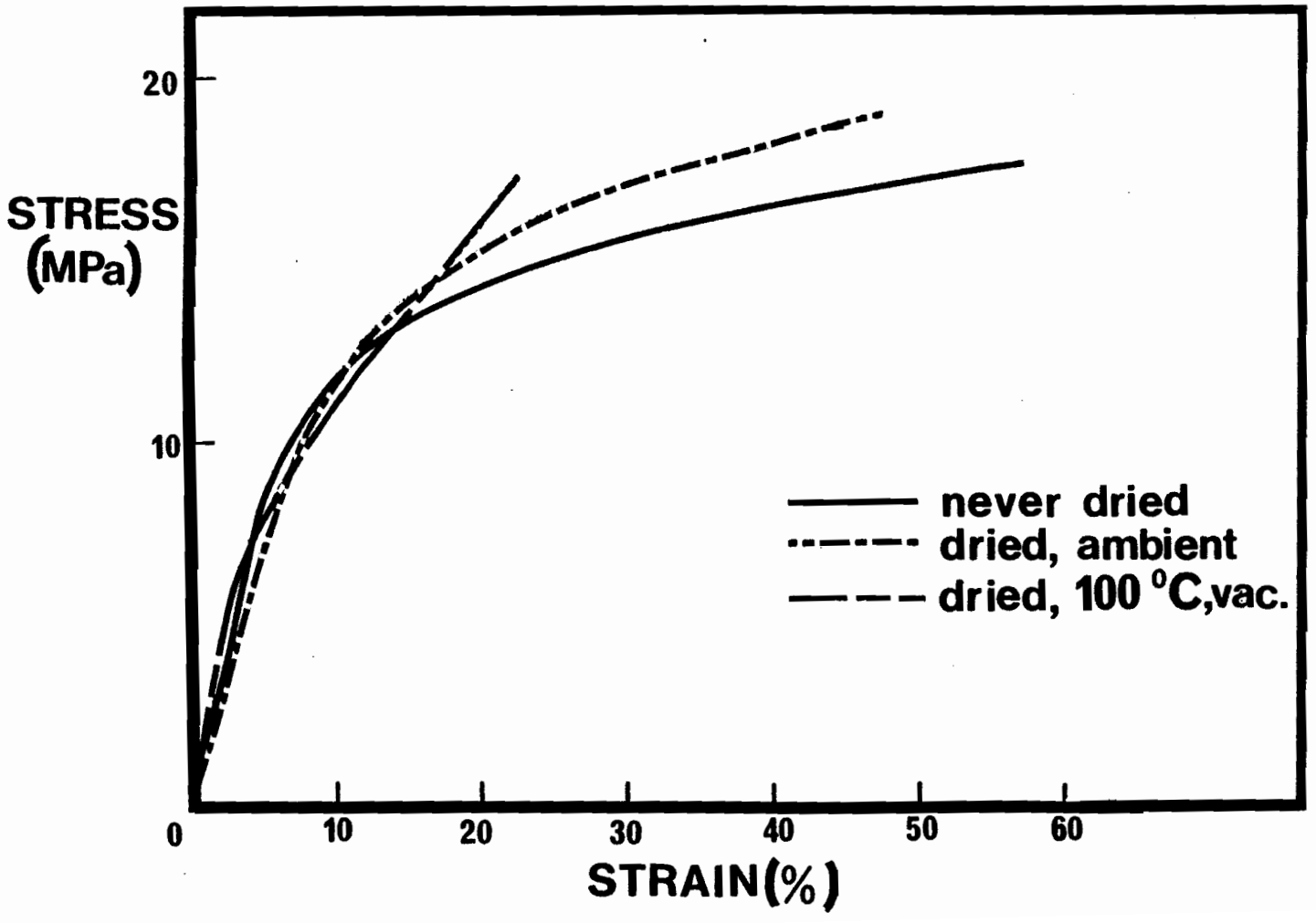
20
10
0
STRESS
(MPa)
10
20
30
40
50
60
STRAIN(%)
never dried
dried, ambient
dried, 100 °C,vac.

The effect of KOH concentration in the testing medium was investigated for the 600EW material and Nafion. When tested in water (0 % KOH), the 600EW ester and ionomer retained the same values (within experimental precision) as those obtained in 20 % KOH for all parameters. Inspection of Figure 34 shows that the stress-strain curves for the 600EW-f remain essentially the same in both environments. By contrast, the values of the parameters obtained in water for Nafion show substantial variation from those obtained in KOH solution. This is shown in Figure 35, which depicts the stress-strain behaviour of Nafion in different testing environments. The results obtained under water and in 20 % KOH solution are summarized in Table 8. Due to the limited amount of sample obtained from each hydrolysis batch, it was not possible to perform all of the various experiments on each batch. This is the reason for the blanks in Table 8.

The behaviour of Nafion and 600EW-f-II (kept dry at ambient conditions since hydrolysis) as a function of temperature in 20 % KOH solution was also investigated. Experiments were performed at 27, 50 and 80^{o}C for both samples. In both cases, the modulus and break strain show a decrease directly proportional to temperature. The two ionomers differed in that Nafion shows an increase in the tensile strength with decreasing temperature whereas the opposite is observed for 600EW-f. The modulus as a function of temperature for these materials is plotted in Figure 36.

Table 8 Tensile testing results in water (W) and 20% KOH. The figures appearing in brackets are the percent relative precision.

Sample	Test Temperature (^{o}C)	Modulus (MPa) W	Modulus (MPa) KOH	Tensile Strength (MPa) W	Tensile Strength (MPa) KOH	Break Strain (%) W	Break Strain (%) KOH
600EW ester	80	1560 (3)	1500 (10)	40	50	79	84
600EW, 70 % conversion	80	620	-	30	-	55	-
600EW-f-I							
continuously hydrated	80	200 (12)	300 (17)	18	18	58	45
kept dry, ambient	80	180 (16)	-	19	-	47	-
dried in. vacuo.,100^{o}C	80	270 (9)	-	17	-	23	-
600EW-f-II							
hydrated 3 days	80	-	79 (12)	-	8	-	20
hydrated 3 months	80	-	86 (17)	-	8	-	13
kept dry, ambient	80	130 (15)	110 (20)	8	11	13	32
	50	-	140 (13)	-	9	-	13
	27	-	170 (23)	-	8	-	9
600EW-p	80	240 (18)	-	14	-	11	-
Nafion precursor	80	4 (0.5)	-	2	-	>328	-
Nafion 1200	80	57 (3)	110 (12)	21	17	395	155
	50	-	180 (4)	-	17	-	120
	27	-	230 (10)	-	20	-	65

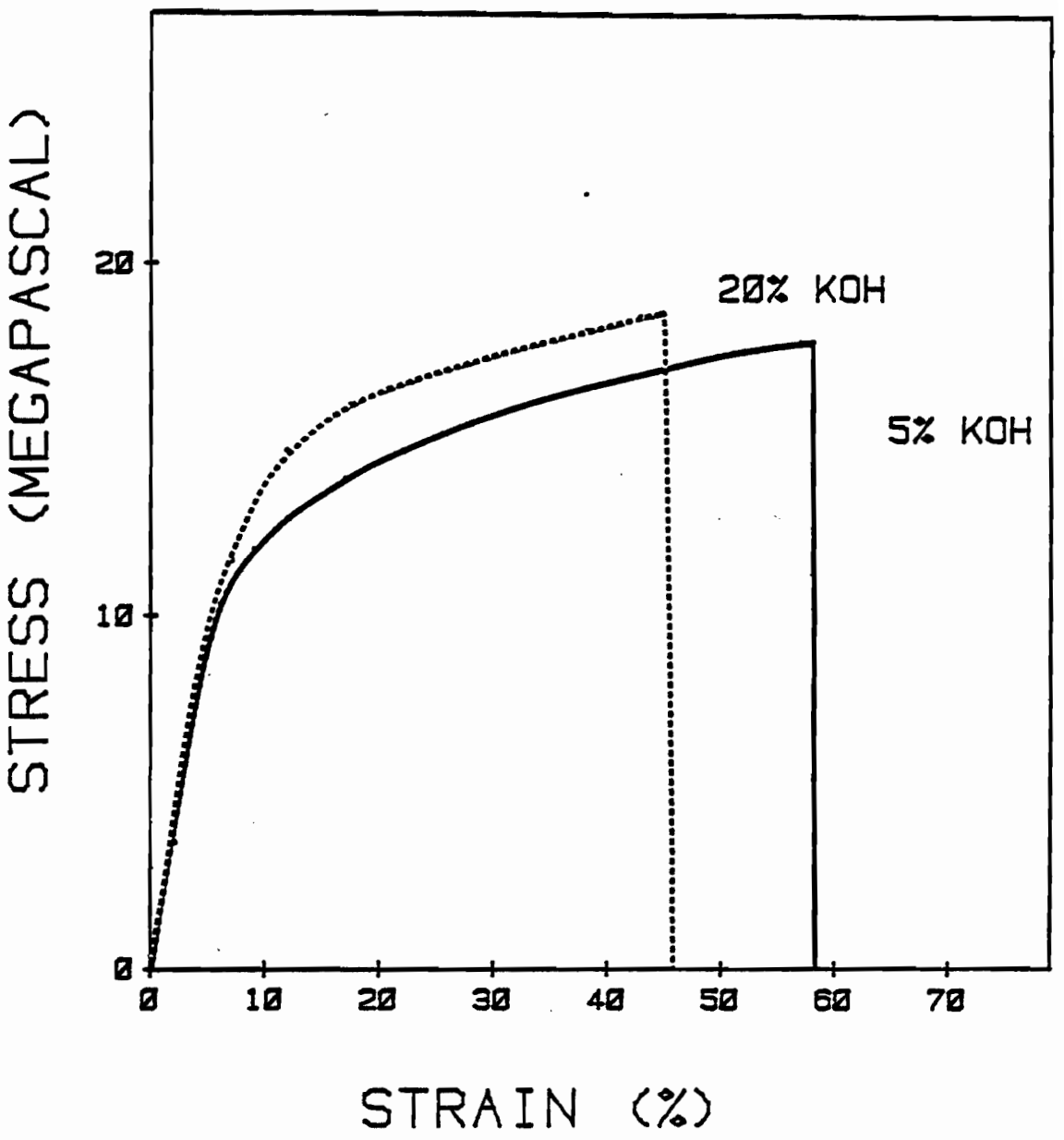

Figure 34: Stress-strain curves for 600EW-f, showing the effect of the concentration of the testing solution at 80°C

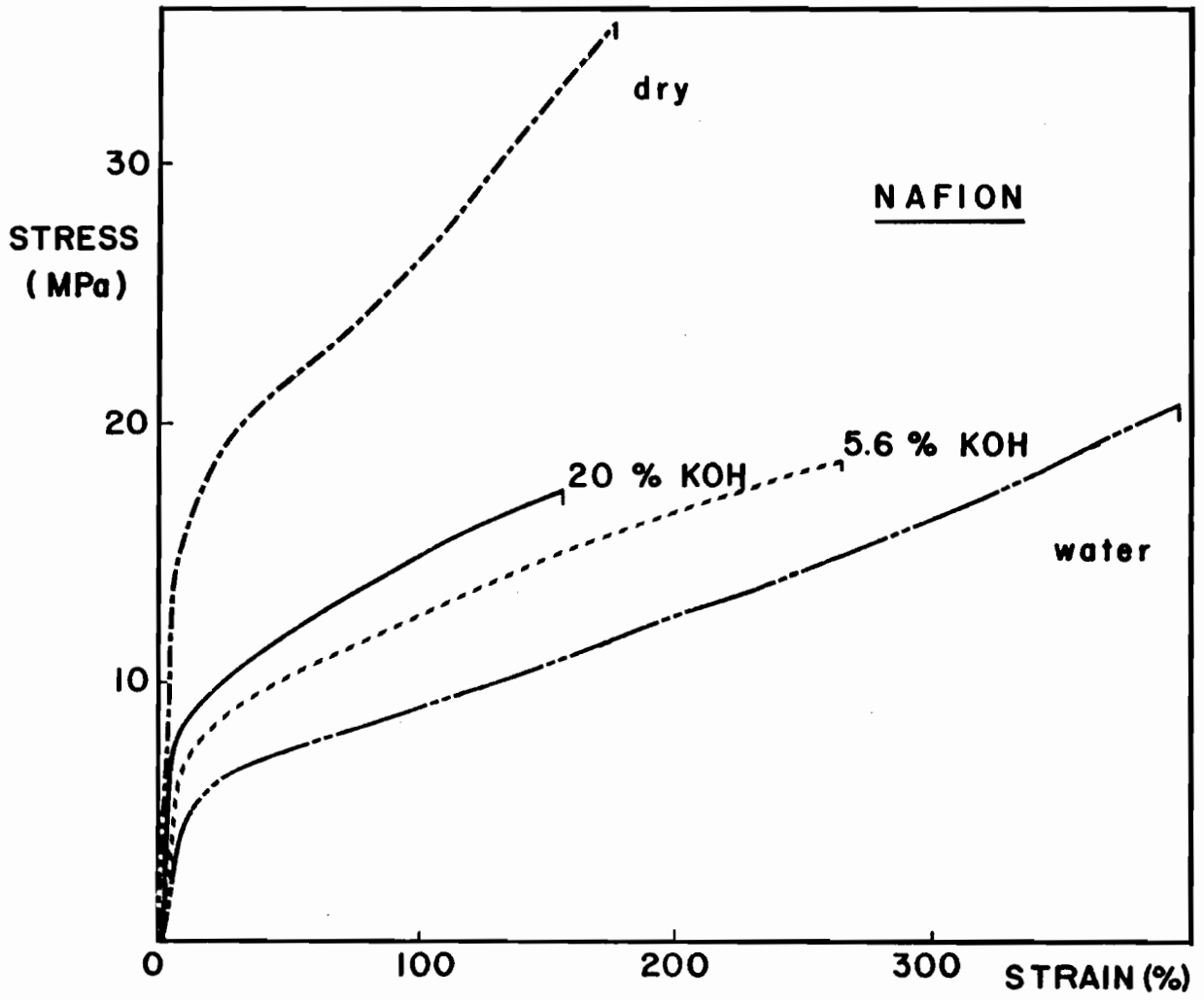

Figure 35: Stress-strain curves for Nafion 1200 in the dry state, in water, in 0.1 M KOH and in 20 % KOH solution at 80°C

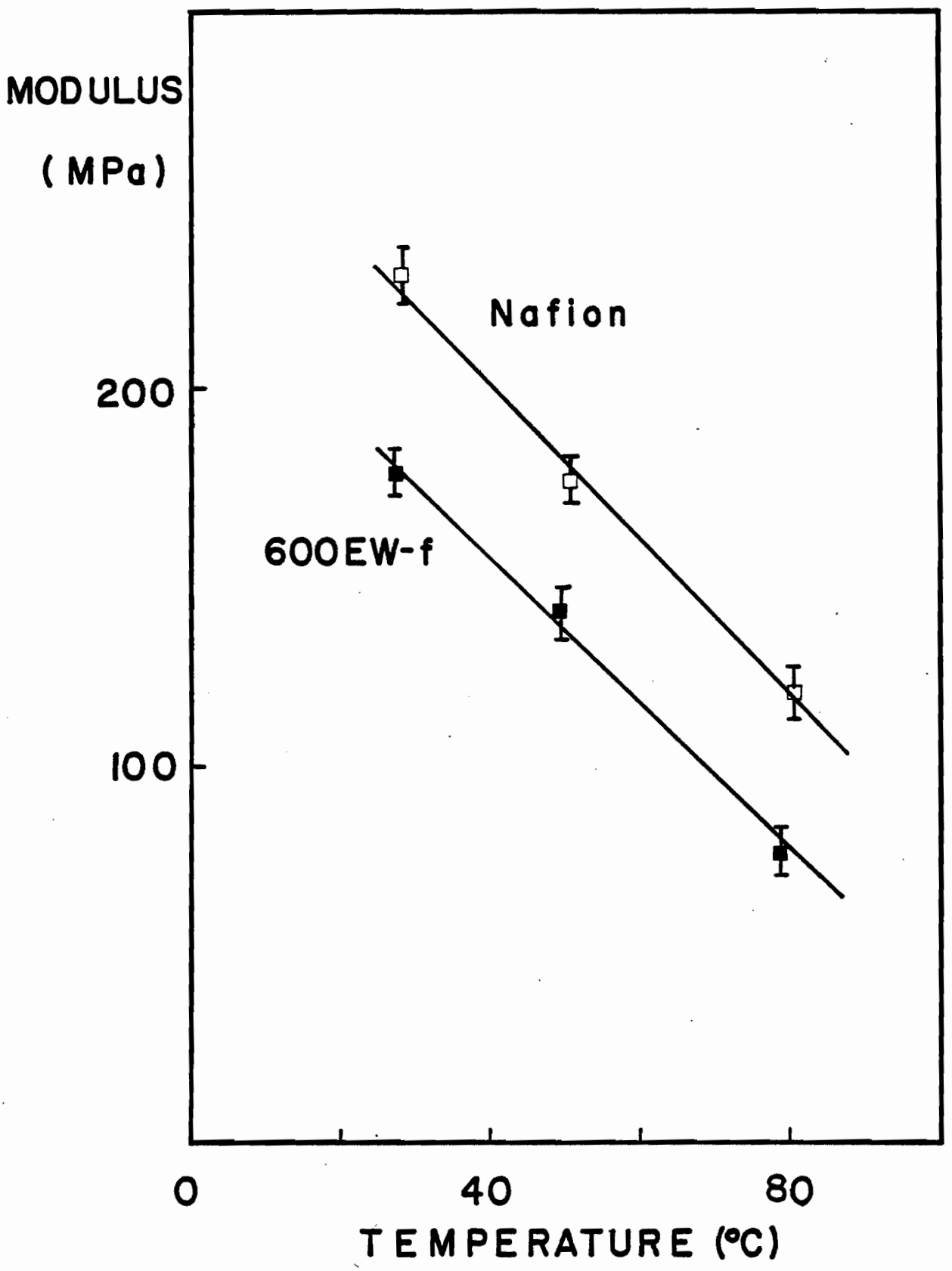

Figure 36: Tensile moduli as a function of temperature for Nafion 1200 and 600EW-f, obtained from stress-strain tests in 20 % KOH at 80°C

3.2.3 Stress Relaxation

Stress relaxation experiments were performed only for the 600EW ester precursor. Due to the extensive degradation which occurred on heating for the prolonged periods of time required to equilibrate at high temperature, it was not possible to study the 600EW ionomer by that method. Prolonged exposure to temperatures above the glass transition also proved to be a problem in the testing of the ester precursor. It was circumvented by the use of fresh samples for the runs at higher temperatures.

The master curve obtained for 600EW ester is shown in Figure 37. Good time-temperature superposition is found, although one of the lower temperature curves required slight vertical shifting in addition to the normal horizontal shifting. The glass transition was used as the reference temperature and the WLF shift factors c_1 and c_2 had values of 7.05 and 44.1^{o}K, respectively. The activation energy calculated for the glass transition was 790 kJ.

Figure 37: Stress relaxation master curve for the 600EW ester precursor film

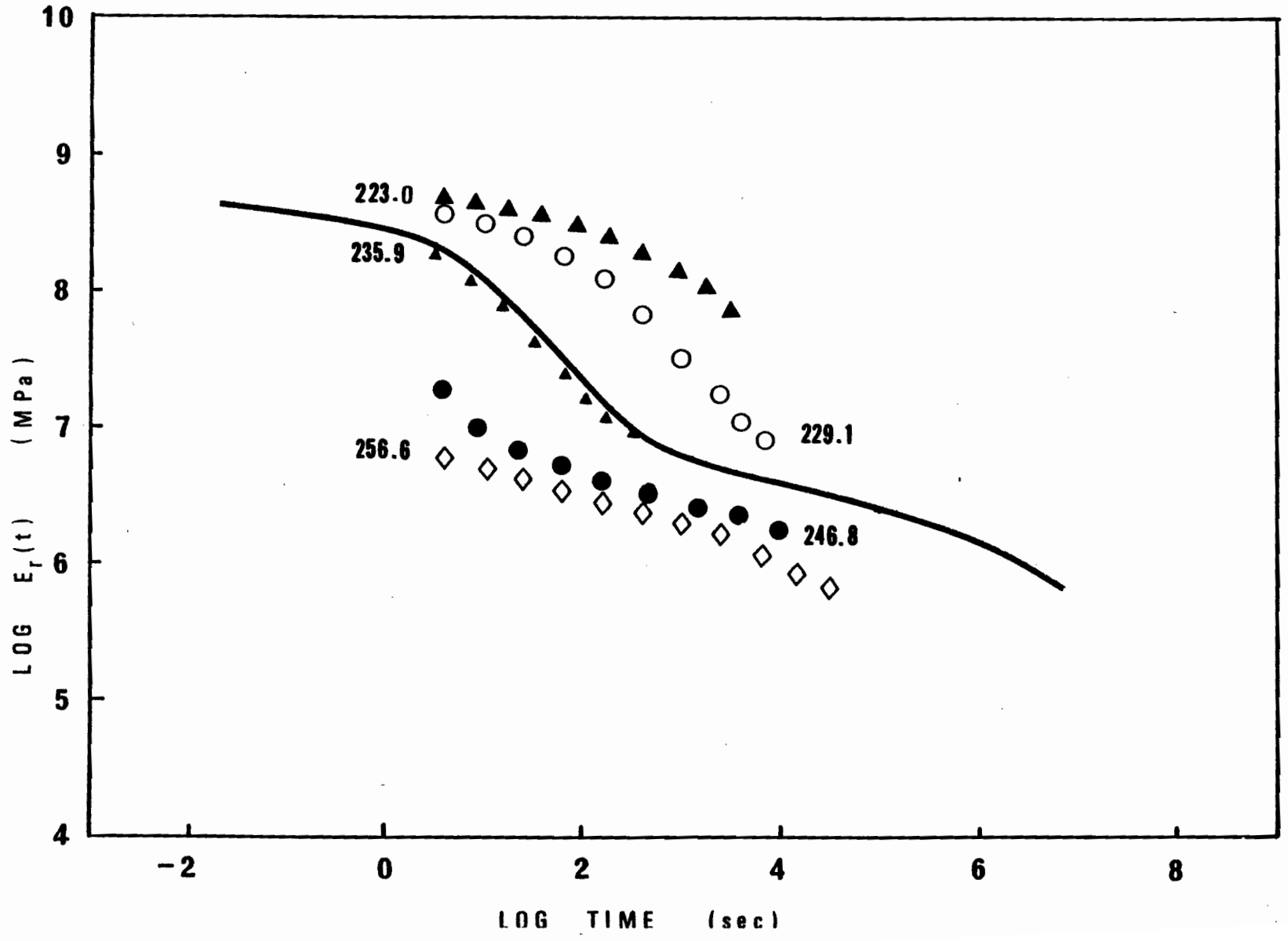
10
9
8
7
6
5
4
LOG $E_r(t)$ (MPa)
−2
0
2
4
6
8
LOG TIME (sec)
223.0
235.9
229.1
256.6
246.8

4. DISCUSSION

4.1 MATERIAL CHARACTERISTICS

The intrinsic viscosity values for the ester precursors suggest a high molecular weight. The density of 1.38 g/cm^3 found for the 600EW ester is lower than that of Nafion 1200 (ca. 1.95 g/cm^3) (Takamatsu and Eisenberg, 1979), probably due to porosity. It is reasonable to assume that the density of the 600EW-f ionomer is close to that of the ester precursor material, since no significant changes in the appearance of the sample cross-section are evident by SEM following the hydrolysis.

4.1.1 Porosity

There are several sources of evidence for the presence of porosity. Those already mentioned are scanning electron microscopy, water contact angles and the preliminary water uptake observations. Other studies, using methods such as low temperature DSC (Besso et. al., 1984) and transport property measurements (Steck et. al., 1984) were performed and they also indicate porosity in the ionomer films.

In the DSC study of hydrated 600EW-f conducted in the subambient temperature range, two endotherms appear near 0^{o}C. They reflect the fusion of the water held within the material. The fact that a double melting peak occurs for the same process suggests two distributions in the size of pores in the sample. The first endotherm peaks at 0^{o}C and

corresponds to the large size porosity observed by SEM. The second one, peaking at -15°C, corresponds to a microporosity not visible by SEM. As to the transport property measurements, conductance results obtained for the 600EW ionomer films were typical of microporous materials. The pores are present in the ester form as seen in Figures 15 to 18. They are merely modified in shape and size by the subsequent hydrolysis process (Figures 19 to 21).

Porosity emerges as an inevitable side-effect of the solution casting method employed to manufacture the ester film. The solubility of 600EW ester in chloroform is fairly good (5-7 %) but not excellent. A proposed mechanism of film formation which is consistent with the features observed is the following.

After casting of the solution on the glass substrate, solvent evaporation causes decreased chain mobility. Typically, a polymer crust forms at the surface and is not redissolved by the underlying solvent. Some solvent escapes through the center, where the skin only forms in later stages, but the bulk of the chloroform must now evaporate through a less direct route. Since chloroform is not an excellent solvent for the system, it is hypothesized that the polymer microphase-separates during the course of solvent evaporation. At this stage, the system could be described as consisting of dense polymeric domains separated by a solution of lower concentration. This solvent-rich phase may lead to the formation of channels. These channels

would be of very restricted continuity since, with more solvent evaporating, the system is getting progressively closer to the glassy state. This is, of course, speculative at best.

The course of events is supported in particular by the SEM results which show few pores in the surface but a much larger number of voids in the sample cross-section. The larger pores of 1 - 5 micrometers in diameter visible in the fracture micrographs are probably caused by the further evaporation of solvent residing in the solvent-rich phase. These channels remain since the system is in the glassy state, when molecular motions can no longer "fill" the space previously occupied by the solvent.

The microvoids created by solvent evaporation from the system in the glassy state are not observed by SEM since these "micropores" are probably of very small dimensions. Diameters of less than 1000 Å would not be visible by SEM as this is close to the resolution limit of the technique. Their presence is strongly indicated by the results of the low temperature DSC and transport studies mentioned earlier.

The 600EW-p material, also cast from a solution but evaporated at high temperature, appears non-porous. Much better solubility is indicated, since a homogeneous film implies continuous redissolution of the surface polymer layer as the lower stratum precipitates out of solution and the film is built from the glass substrate up. Thus the two factors of interest appear to be the quality of the solvent and the temperature, or speed, of evaporation. Variation of

these two parameters leads to a range of film structures. The Nafion film examined by SEM also showed a homogeneous structure, free of large pores.

4.1.2 Orientation

It is well recognized that polymers can have varying amounts and types of directional order. The results of the wide angle X-ray diffraction study indicate that the substituted polyphenylene ether systems, although not crystalline, do possess some degree of orientation. It is useful to recall that although a larger proportion of para links is expected in the backbone, a significant number of ortho linkages exists, thus hindering the formation of crystallites. The essentially amorphous 600EW ester form can be oriented to an appreciable extent, as indicated by the strains of 150 % which are easily obtained. Relatively ordered domains are suggested by the WAXD patterns of the drawn sample. In the as-cast film, only the amorphous halo is clearly observed. Following uniaxial stretching, complementary diffuse arcs appear in both the equatorial and meridional directions, indicating an increase in both inter-chain and single chain orientation (Statton, 1959). Alternatively, it is conceivable that this WAXD peak may be due to the porosity of the film.

4.1.3 Effects of Hydrolysis on Films

Aside from the slight differences observed by SEM

in the number of pores and their size, the hydrolysis conditions did not at first appear to effect changes other than conversion of the ester side groups to their potassium carboxylate salt form. However, variable solubility in DMSO and variable infrared absorption at 1732 cm^{-1} (Figure 8) in the 600EW-f samples suggested the occurrence of cross-linking in the course of the reaction. Theoretically, the completely hydrolyzed ionomer would show the virtual disappearance of this IR band. This was indeed observed for samples hydrolyzed at lower pressure (ca. 1.3 MPa). However, under some experimental conditions (which included higher pressure of the order of 3 MPa), this band reached a minimum absorbance intensity but did not completely disappear. The intensity of the asymmetric carbonyl absorbance of the salt was comparable in all cases.

These observations suggest that crosslinking occurs when hydrolysis takes place under high pressure. Two of the possible mechanisms are the formation of an anhydride crosslink and the formation of an ester crosslink. The first possibility can be readily dismissed because the IR spectra show no evidence of the two bands expected from the vibrational coupling of anhydride carbonyl groups (Pasto and Johnson, 1969). The second possibility, the ester cross-link, may develop via a base-catalyzed transesterification reaction between the polymer and ethylene glycol. This is schematically shown below.

$$R\text{-}CO_2C_2H_5 \underset{KOH}{\overset{C_2H_4(OH)_2\,/\,H_2O}{\rightleftharpoons}} R\text{-}CO_2C_2H_4OH + C_2H_5OH$$

$$R\text{-}CO_2C_2H_5 + R\text{-}CO_2C_2H_4OH \rightleftharpoons R\text{-}CO_2\text{-}C_2H_4\text{-}O_2C\text{-}R + C_2H_5OH$$

$$2\ R\text{-}CO_2C_2H_4OH \rightleftharpoons R\text{-}CO_2\text{-}C_2H_4\text{-}O_2C\text{-}R + C_2H_4(OH)_2$$

where R = polymer chain

Whether or not this crosslink truly occurs is not known, especially in view of the low concentration of ionic units. However, the low concentration of ethylene glycol in the film itself makes the crosslinking reaction (as opposed to a single transesterification) plausible since the presence of the alkoxide ion of ethylene glycol ($C_2H_4O_2H^-$ species) is quite likely. Nevertheless, whatever reaction occurs appears to affect the product significantly. The differences in tensile stress-strain results for 600EW-f I and II (Figure 31) attest to this fact.

4.1.4 Hydrophilicity

The first indication that the films of 600EW-f material are extremely hydrophilic was observed in the course of the isothermal temperature stability testing. As previously discussed, if the weighing was not performed extremely rapidly, or in a hermetic environment, the weight of the ionomer film was observed to increase by as much as 5 % in a period of 30 seconds. An equilibrium water uptake of ca. 15 % was measured after 30 minutes. This value

corresponds to ca. 8 molecules of water per carboxylic acid group in the ionomer film.

The rate of decrease of the contact angle of water over time for 600EW-f stands as graphic evidence of material wettability (Figure 23). The constant negative slope of the curve is explained by the porosity of the film as well as by the hydrophilic character imparted by the presence of ionic groups. The slight decrease of contact angle with time observed for the ester precursor is attributed to porosity.

In the case of Nafion, an inflection point is observed in the rate of contact angle decrease after 90 seconds. This fact, coupled with observation of the development of a visible swelling of the film during the experimental time, suggests a two-step diffusion process in which water initially diffuses at a faster rate, probably to the boundary of the more ionic aggregates. The penetration of these domains then occurs at a slower rate and causes the progressive phase-separation which leads to the swelling observed. Contrary to Nafion, the surface appearance of the aromatic ionomer does not change with time, suggesting the possibility of a gradual flow through the film.

The differences noted confirm the porous structure of 600EW-f and are consistent with the microphase-separated structure of hydrated Nafion. They indicate that the structure of 600EW-f differs markedly from that of Nafion, in that these results do not suggest the presence of large

ionic aggregates. On the other hand, the continuous decrease in contact angle implies a similar change in the surface energy of the material, which could conceivably be due to the migration of ionic groups towards the film surface.

It should be noted, however, that several factors contribute to making results of contact angle measurements ambiguous to interpret. Contact angle does not only depend on the polar groups inherent to the molecular structure of the material, but also on the effects of surface microstructure, on the possible inclusion of hydrophilic impurities and on the solid-vapour interactions as well as the solid-liquid interactions. The results of recent work (Nayar & Adamson,1983; Fortes,1981) strongly suggest that these factors cannot be neglected in treatments of contact angle, such as that based on the Young equation (Adamson, 1976) from which surface energies can be derived.

4.2 GLASS TRANSITION

The only unequivocal statement which can be made about the glass transition temperature of these aromatic systems is that it is indeed quite high. For, although the transitions are easily identified in both torsion pendulum and DSC results, the transition temperatures obtained by the two methods differ by about 50 degrees. Moreover, DSC results indicate two transitions in the ionomers whereas the dynamic mechanical result for 800EW-p shows only one dispersion in the same temperature range. Also contrary to

what may be expected on the grounds that the transitions shift to higher temperatures with increasing measurement frequency, the transition temperatures obtained by DSC are higher than those obtained in the dynamic mechanical experiments. The values referred to are tabulated in Table 9.

Table 9 Glass transition temperatures (°C) for ester precursors and ionomers (values obtained by torsion pendulum for 1200EW are taken from Rigdahl et.al., 1980)

Sample	Torsion Pendulum		D S C	
	Precursor	Ionomer	Precursor	Ionomer
1200EW	257	280	-	355
800EW	250	330	292	405
600EW	255	-	290	420
400EW	243	-	285	440

The apparent inconsistencies can be resolved to a large extent by considering such factors as sample preparation method, rate and frequency of measurement, and period of exposure of the sample to high temperature. These points will be addressed independently and their individual effects on the results will be estimated, where possible.

4.2.1 Effect of Sample Preparation Method

Sample preparation, in the case of the calorimetric experiments, consisted only of solvent evaporation at room temperature to yield a film. Thus, no conditions leading to possible degradation were encountered. In the case of the dynamic mechanical experiments, samples were

molded at ca. 290°C, this temperature having been chosen as a compromise between achievement of a reasonable closeness to the flow region and minimization of degradation processes. Typically, 2-3 hours were necessary to reach molding temperature. It follows that the sample underwent prolonged heating in air prior to being subjected to any experimental procedure. From the generally darker colour of the molded sample, it was deduced that a small amount of degradation took place. Since degradation quite possibly entails some chain scission, it is reasonable to expect that the resultant low molecular weight material would exert a plasticizing effect on the bulk. This, in turn, would logically lead to a decrease in the glass transition temperature observed.

This hypothesis is proven by the results of a DSC study on a solvent-cast film sample which was subjected to a thermal treatment analogous to that of the molded sample. As a result of this treatment, a reduction of ca. 40 degrees was observed in T_g as measured by DSC. This is shown in Figure 38.

Figure 38 : Normalized DSC curves for 600EW ester films.

a - sample which was not heat treated

b - sample which was subjected to a heat treatment analogous to that undergone by a molded sample

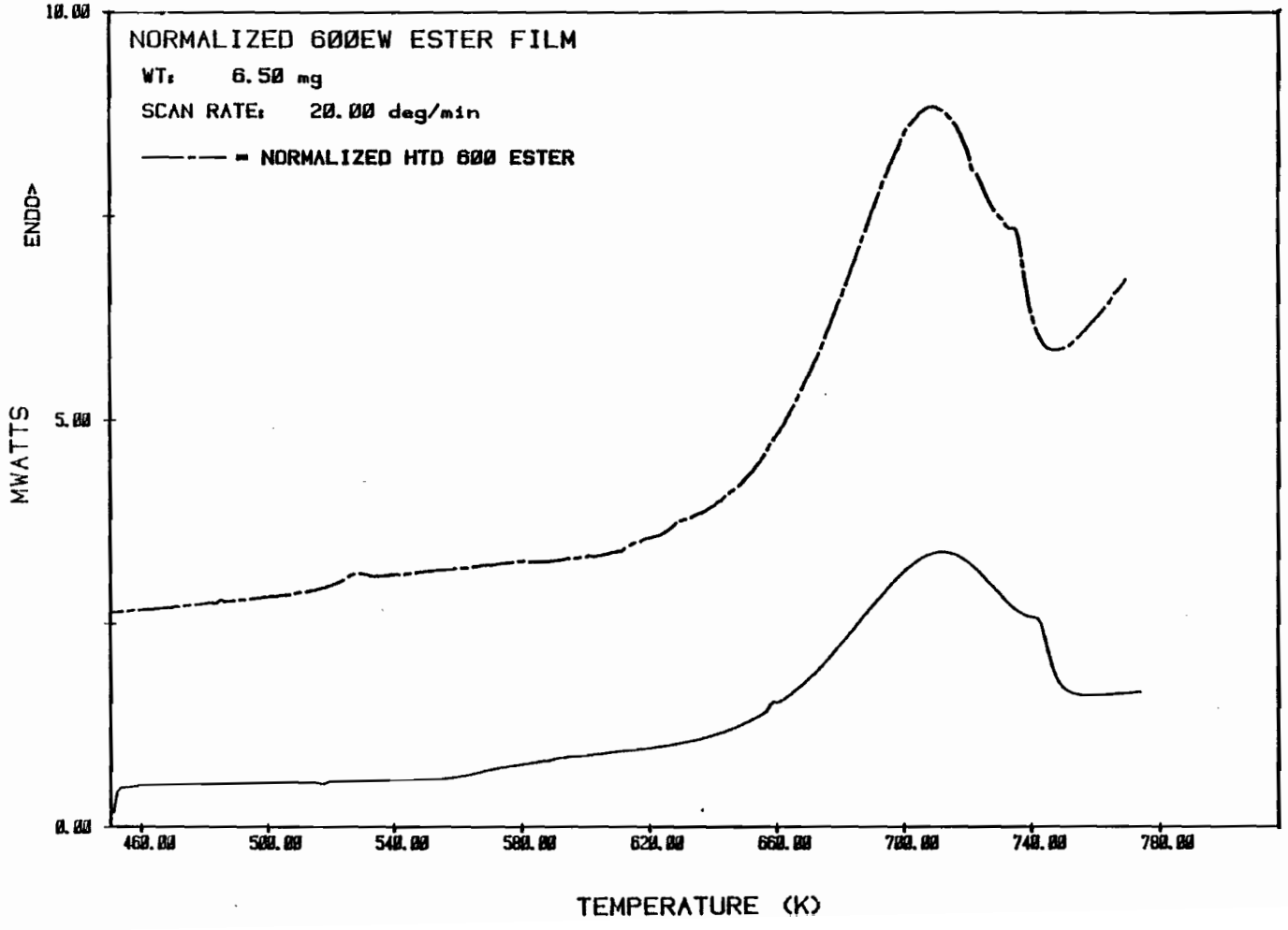
NORMALIZED 600EW ESTER FILM
WT: 6.50 mg
SCAN RATE: 20.00 deg/min
= NORMALIZED HTD 600 ESTER
ENDO>
MWATTS
10.00
5.00
0.00
460.00
500.00
540.00
580.00
620.00
660.00
700.00
740.00
780.00
TEMPERATURE (K)

4.2.2 Effect of Heating Rate and Test Frequency

Heating rate and testing frequency are known to affect the position of the glass transition of polymers. The DSC experiments were usually run at 20 degrees/minute, whereas the heating rate in a torsion pendulum experiment was ca. 0.7 degree/minute. Thus the "static" T_g value obtained by DSC was measured at a much higher heating rate. In the dynamic experiments, the sample was deformed at a frequency of ca. 1 Hz. In an attempt to determine the effect of scan rate on transition temperatures in DSC, the 600EW ester films cast from chloroform were run at 5, 10, 20 and 40 degrees/minute. It can be seen from the resultant curves (Fig. 14) that, unfortunately, the transition at ca. 290 ^{o}C is not evident in all cases. The effect of scan rate is clearly seen on the higher temperature endotherm. However, since it is highly unlikely that the kinetics of the glass transition and the decarboxylation reaction are identical, the effect on the latter cannot reasonably be used to predict that on the measured T_g.

Alternatively, a rough estimate in the change in T_g with rate can be derived by differentiating the WLF equation (Ferry, 1970)

$$d\,T_g \,/\, d \log a_T = c_2 / c_1 = 44/7 = 6^{o}$$

indicating that T_g would change by approximately 6^{o} if the rate (as expressed through log a_T) was changed by a factor of 10 (or 1 on a log scale). This estimate would yield a

glass transition temperature of 280°C, had a rate of 0.6 deg/minute been used.

Although this estimate conveys an approximate value of T_g at best, it does show that the real glass transition would occur at a lower temperature than 290°C, if it had been determined in a standard manner (Kovacs, 1964). Another important factor influencing the measured value of T_g, the sample history, is discussed below.

4.2.3 Effect of Thermal History

The thermal history of the samples used for the calorimetric and dynamic experiments also varies significantly. Not only were the samples used in the latter experiments subjected to molding conditions, they were also kept at higher temperatures during the long period of time required by each run. For, although each individual oscillation is of short duration (e.g. 1 sec, in torsion pendulum), the entire run entails subjecting the sample to elevated temperatures for several hours. Again, this would be conducive to degradation and concomitant lowering of the glass transition temperature.

To summarize, the conditions of the calorimetric tests contribute to raising the apparent glass transition temperature over what it would be at 1 degree/minute whereas those of the dynamic mechanical tests have the opposite effect for these systems. Taken together, the factors discussed in the last three subsections probably explain the

broad differences obtained experimentally. The degradation effect is probably the principal cause of the differences observed. A reasonable conclusion would be that the true glass transition temperature for these materials lies in the range bounded by the DSC result as the upper limit and the torsion pendulum result as the lower limit, the T_g probably being closer to the former.

4.2.4 Effect of Ion Incorporation

As in the case of ionomer systems previously studied, the glass transition temperature of the aromatic ionomers (taken to be the DSC transition at higher temperature) rises with increasing ion content at a rate of 2 - 3 deg/mol % ions. It is noteworthy that the specific heat changes associated with these glass transitions uniformly exceed those associated with the transition at 290°C in the first heating experiment only. After quenching, the second heating run still shows a change in heat capacity at 290°C, but the transition at higher temperature is absent. These facts may indicate that a breakdown of ionic associations occurs at elevated temperature, which is not thermoreversible.

The presence of a single high temperature transition in both the torsion pendulum (for the 800EW ionomer) and DSC results leads to the conclusion that the aromatic ionomers do not contain stable ionic clusters. Rather, since the T_g does increase with ion content, the ionic groups appear to form associations of the

multiplet type. The absence of stable clusters is not surprising in view of the rigidity of the aromatic backbone.

Finally, it is important to point out that despite the differences between T_g's measured by DSC and by torsion pendulum, the results of each method are self-consistent. The above discussion has attempted to elucidate the reasons for the observed discrepancies, but a good understanding of the processes involved is still lacking.

4.3 TRANSITIONS OTHER THAN T_g

4.3.1 High Temperature

As can be seen from inspection of Figure 12, all the ionomers show a transition at ca. 290°C, in addition to the glass transition. Two features render this transition interesting. First, no corresponding dispersion is observed in the mechanical spectrum at that temperature for the 800EW ionomer. Second, this temperature is coincident with the T_g of the ester precursors as determined by DSC. These puzzling observations may be understood if it is recalled that the polymers are synthesized in a manner which may not produce random distribution, possibly due to reactivity differences in the co-monomers. It is entirely possible that large domains of purely phenyl-substituted polymer exist. Thus, in the co-polymer, whether in the ethyl ester or carboxylate salt form, relaxation of these domains may be observed. As to the torsion pendulum result, it is surmised that diffusion

occurs during the slow heating which accompanies a run. The diffusion of the ionic portions of the polymer may act so as to minimize the size of these non-ionic regions. Thus, a potentially uneven distribution of ionic groups resulting from the initial polymerization conditions may well shift to a more homogeneous arrangement. This does not imply chemical bond interchange but rather the breaking and reforming of ionic or electrostatic interactions. This rearrangement may account for the absence of a loss peak at 290°C.

The DSC endotherm which marks the onset of decarboxylation at ca. 400°C in the ester precursor material disappears in the totally neutralized ionomers. In those materials which show the presence of residual ester groups, this reaction is shifted to ca. 500°C and the heat of reaction is much decreased. This is confirmed by TGA, which shows the beginning of weight loss only at 450°C for 600EW-f. Two explanations are possible. The shift of the decarboxylation endotherm to higher temperature may be due to the presence of chemical crosslinks. If it is assumed that the crosslinks consist of a double ester linkage, then it follows that two bonds instead of one have to be broken for decarboxylation to occur. Alternatively, the shift to higher temperature may be related to a steric effect due to ion incorporation. The decarboxylation reaction may simply be hindered by the increasing rigidity of the matrix brought about by Coulombic interactions of the ionic groups.

4.3.2 Low Temperature

The sub-zero temperature transition observed in the dynamic mechanical spectra of the esters of 600 and 800 equivalent weight is a feature common to systems containing the phenylene sub-group in their backbone (Cayrol, 1972; Rigdahl et.al., 1980). Activation energies in the range of 50 to 100 kJ/mole have been reported in the literature. This is in agreement with the results of this work. This relaxation is ascribed to hindered torsional oscillation of backbone phenylene units.

4.4 TENSILE STRESS-STRAIN BEHAVIOUR

4.4.1 600EW ester

The 600EW ester film shows the behaviour typical of a hard, tough material. In the dry state at 25°C, it is characterized by a value of 1400 MPa for the elastic modulus, a break strain of 160 %, a yield strength of 36 MPa and a tensile strength of 50 MPa. The yield point occurs at 10 % strain and is followed by necking and cold-drawing; this is accompanied by strain hardening in the plastic flow region. The resultant chain orientation has been demonstrated by WAXD. It explains the strain hardening which occurs since orientation parallel to the strain axis results in a concomitant increase in the elastic modulus as the molecules approach a fully extended configuration.

The end result of the application of a tensile load to a porous material has many features similar to the

fracture process occurring in a creep experiment. Ductile creep fracture, such as that which occurs in cellulose acetate or cellulose nitrate (Haward, 1942), is characterized by large creep strains accompanied by a progressive whitening of the specimen that indicates the growth of internal voids as the material stretches. This is observed in 600EW ester. It may, at first, appear surprising that a porous, amorphous material should display toughness and ductility. It is known that some materials containing large cracks or notches do not fail. This has been explained (Arridge, 1975) by considering the energy balance maintained between the strain energy used in crack initiation (that is, creation of two new surfaces) and that required for crack propagation. Failure of the material will occur when the energy required to create new surfaces becomes lower than that required for crack propagation. In the case of 600EW ester film, it is proposed that very little energy is required initially for crack initiation because of the flaws which are already present due to the microporosity. A theory treating crack growth in non-crystallizing viscoelastic materials purely as a propagation phenomenon has already been advanced (Greensmith, 1964). Fracture is assumed to occur by the growth of pre-existent flaws and the theoretical predictions of time to break closely agree with experimental data. No energy need be consumed to create new surfaces, since these already exist. Thus the strain energy can be channelled towards the work of cold-drawing. The imbalance of energies defining the rupture condition occurs

on reaching extensions which strain the existing porous infrastructure.

The 600EW ester is already above its brittle-to-ductile transition point at 25°C and shows essentially identical behaviour when tested at temperatures gradually approaching its T_g. Modulus decreases moderately with temperature at a rate of 3 MPa/°C.

The results of testing in water and in KOH solution indicate that the main difference occurs in the break strain and consequently in the energy to break. Both these values are roughly reduced by half for 600EW ester in an aqueous environment. The yield point is still evident, but it now occurs at 5 % strain.

The tensile strength remains constant but the modulus increases slightly to 1500 MPa. The drastic reduction in break strain which occurs when the material has absorbed an equilibrium amount of water is possibly due to the environmental stress-cracking effect observed in many systems.

4.4.2 600EW ionomer

The 600EW ionomer film is an extremely brittle material in the dry state. Break strains of the order of 2 % indicate very low energy to break. Although the material has an elastic modulus of 1600 MPa at 25°C, it is mechanically weak. The modulus value increases to 1900 MPa at a testing temperature of 100°C, this probably being due

to the loss of any residual water in the ionomer film. Increasing the testing temperature to 200°C shows a progressive decrease in tensile strength and in modulus. Beyond that temperature, both of these values decrease dramatically. This is believed to reflect a degradation of the material due to prolonged exposure to high temperature. The dry 600EW-f remains below its brittle-to-ductile transition temperature in all cases.

The mechanical properties of the ionomer improve considerably in an aqueous environment. The water-plasticized material, which had previously been dried and kept under ambient conditions of pressure and humidity, has a modulus of 170 MPa at 27°C in 20 % KOH. This value is lower than that of the ester precursor by an order of magnitude, a fact due to the plasticization of the ionomer film. Increasing the testing temperature to 80°C causes a drop in modulus but a threefold increase in elongation to break. The tensile strength remains approximately constant at 10 MPa. There is no evidence of cold-drawing. The plasticized ionomer has clearly become ductile and the stress-strain curve displays the characteristics of rubber-like elasticity, the ionic interactions providing the effective crosslinks which give rise to a stress-bearing molecular network.

The arguments invoked in discussing reasons for the ductility observed in the porous 600EW ester precursor are also applicable in the case of the equally porous ionomer. Two opposing considerations must be kept

in mind. First, since crack propagation is now carried out in the presence of a plasticizer, the stress needed to propagate the crack is decreased by the greater ability of the polymer to become oriented. Second, the pseudo-crosslinks resulting from ionic associations contribute to an increase in stiffness and therefore to the stress necessary for rupture to occur. However, the cations become free to move in the water swollen sample, thus weakening existing multiplets and their crosslinking effect. This occurrence is energetically favoured by the strong hydrogen bonding between water and the carboxylate ions, an interaction which was found to be significantly enhanced by the presence of K^+ ion (Levy et.al., 1982). Since the hydrated ionomer is ductile, the latter effect appears to override the stiffening influence of the pseudo-crosslinks due to the ionic interactions.

4.4.3 Nafion 1200

The tensile stress-strain behaviour of Nafion (Figure 35) in the dry state is that of a tough material. However, neither yield nor necking is observed as the material stretches uniformly throughout its length. The sudden upturn of the stress-strain curve at ca. 50 % strain is probably due to crystallization induced by molecular orientation. The dry film reaches a break strain of 200 % and has modulus and tensile strength values of 260 and 35 MPa, respectively. A pure aqueous environment causes a

virtual doubling in extension to break and a significant decrease in tensile strength, both results easily understood as an effect of water plasticization. Results obtained in increasing concentration of KOH in the testing medium show a decrease in break strain coupled with an increase in modulus consistent with the findings of previous studies. Energy to break is decreased dramatically in going from a water environment to a 20 % KOH solution. The results confirm that Nafion is plasticized to a much greater extent in water than in KOH solution, due to the establishment of an osmotic equilibrium which would tend to decrease the amount of water in the membrane when it is placed in salt solution of increasing concentration.

As in the case of the aromatic ionomer, the effect of increasing testing temperature in 20 % KOH is an increase in the break strain and a reduction in the modulus. Unlike 600EW-f, Nafion appears to be well above its brittle-to-ductile transition temperature in all the cases studied.

The important physical difference existing between the Nafion ionomer and 600EW-f is that Nafion is non-porous whereas porosity is a major structural feature of the aromatic ionomer obtained by the present method. This fact makes it very difficult to compare directly such sample properties as the tensile strength or the energy to break. Comparison of the moduli is valid since this parameter truly reflects a material property which is independent of the defects existing in any given sample. The 600EW-f ionomer is much more rigid than Nafion in the dry state, as might be

expected from its aromatic, highly substituted backbone. In aqueous 20 % KOH environment, the moduli of the two systems become comparable at ca. 200 MPa at 25°C. This drop in modulus for the aromatic ionomer film has been explained as an effect of plasticization and suggests that the equilibria present in the Nafion ionomer, due to the osmotic effect which tends to decrease the amount of water in the film, are not operative in this case.

However, comparison of the "dry" and "wet" moduli (in 20 % KOH) for Nafion at 25°C shows that they are quite similar (within experimental precision), at 260 and 230 MPa, respectively. Since the hydrophilicity of Nafion is well established, this fact suggests that the plasticizing effect of water is superceded by another structural feature of the system. It is known (Kyu and Eisenberg, 1982) that the Nafions are characterized by a microphase-separated structure where ionic aggregates form the nucleus of hydrophilic domains interspersed in the non-ionic perfluoroethylenic matrix. The virtually constant value of the modulus in the dry state and in concentrated KOH solution implies that the ionic interactions are the major determinants of sample stiffness in both cases. Further, this suggests that the sample immersed in the aqueous alkaline medium contains very little water.

By the same token, the values of the modulus of the aromatic ionomer strongly suggest that the ionic interactions do not play as important a role as in the

Nafion systems. This is a further indication that although the ionic groups may be associated to some extent, they do not form strong aggregates or clusters.

4.5 STRESS RELAXATION

The 600EW ester behaves like an amorphous polymer of high molecular weight. Not surprisingly, time-temperature superposition is applicable over the temperature and modulus range studied. Inspection of Figure 37 shows the stress relaxation to occur in the two stages typical of high polymers. The first stage reflects the short range motion of chain segments between entanglement points whereas the second stage indicates that of the longer-range rearrangements requiring more concerted movement and thus longer times. The two relaxation stages are separated by an inflection point occurring at a log E value of 6.7 MPa, which is related to the average spacing between entanglements. These function as pseudo-crosslinks which briefly suppress the long-range configurational rearrangements.

The log E level at which this flattening occurs is interesting in that it is more than an order of magnitude higher than that which is normally encountered in other non-ionic materials such as PMMA and PS. However, it is comparable to the corresponding values observed for Nafion-H and Nafion-K (Yeo and Eisenberg, 1977). A high degree of chain entanglement may be one of the reasons for this high E value, but it is probably not the only one. These entanglements do not appear to be effective as crosslinks since the

modulus drop at T_g occurs over a relatively narrow time range of about four decades. The effect of backbone rigidity and high molecular weight is clearly displayed by the high terminal log E values for both relaxation stages, since the modulus generally shows a drop in systems of lower molecular weight at comparable times. It was not possible to extend the master curve to longer time periods due to limitations imposed by the degradation occurring after prolonged exposure to high temperature.

4.6 HIGH TEMPERATURE PHENOMENA

The 600EW ester and ionomer materials were found to undergo substantial modifications as a result of heat treatment. Although TGA results show no weight loss at temperatures below 350°C, both materials show evidence of degradation following prolonged exposure to elevated temperature. The evidence comes from DSC, FTIR and a stress-strain study performed on systematically heat-treated samples. The DSC evidence was previously presented in the section discussing the glass transition (see 4.2.1). The infrared results will be discussed below.

In the case of 600EW ester, a comparison of the infrared spectra of a solution-cast sample and of a film sample that was compression-molded at 290°C is shown in Figure 39. As described previously, the molded sample was exposed to T > 250°C for a minimum of one hour under a pressure of 14 MPa. Inspection of Figure 39 shows that two

Figure 39: FTIR spectra of 600EW ester films prepared by compression-molding and casting from solution

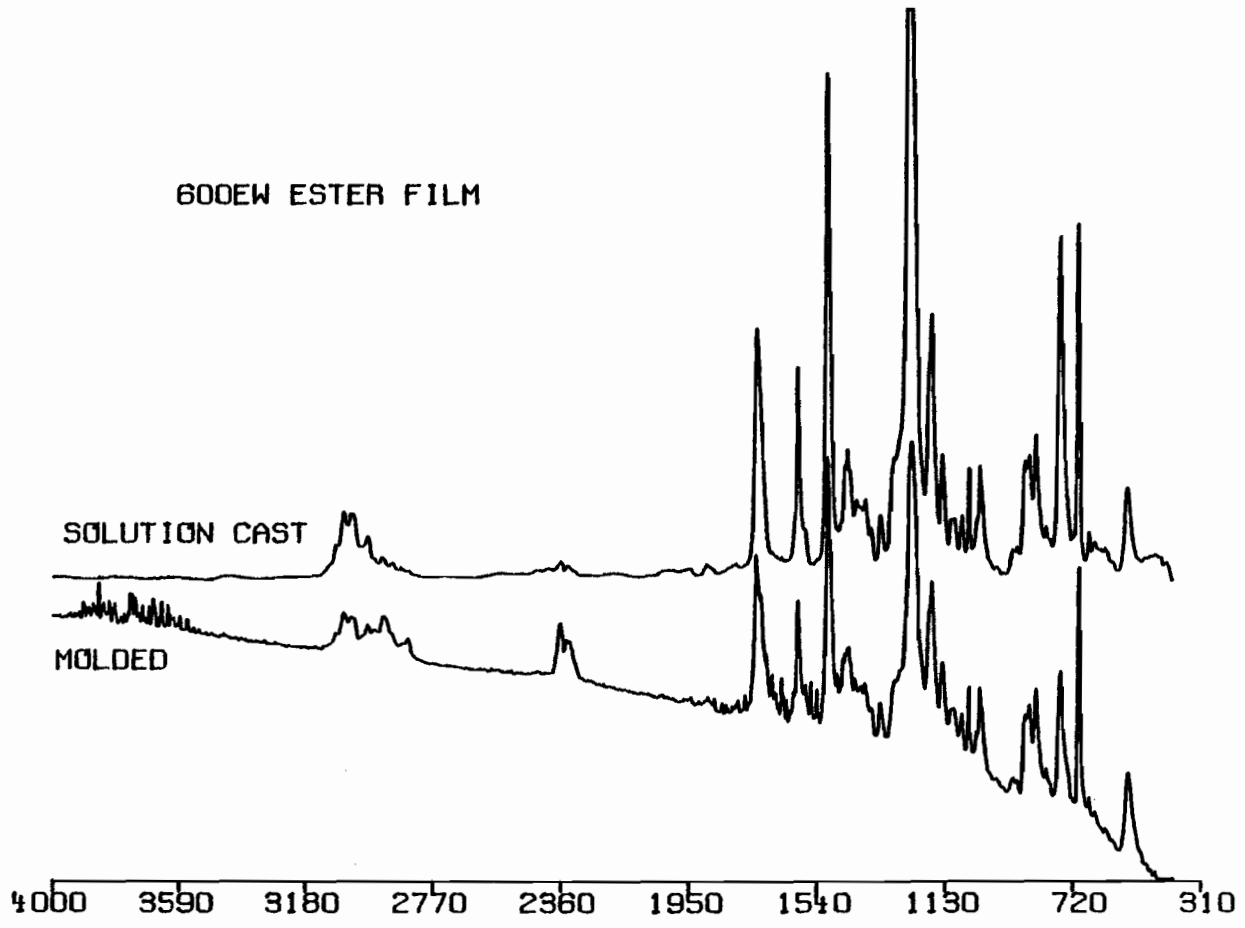
600EW ESTER FILM
SOLUTION CAST
MOLDED
4000
3590
3180
2770
2360
1950
1540
1130
720
310

regions of infrared absorption were especially affected by the molding pretreatment. The first is the aromatic carbon-hydrogen stretching absorption region near 3030 cm^{-1}, where the IR absorption spreads to a much wider range in the molded sample. The other is the carbonyl stretching absorption region near 1730 cm^{-1}, where shoulders appear on the main absorption peak in the molded sample. Although a detailed analysis of the new absorption bands appearing in the molded sample is beyond the scope of this work, it is clear that significant bonding changes have occurred. There is no evidence of the presence of anhydride groups, but the formation of quinones via the oxidation of terminal phenolic groups (Morrison and Boyd, 1972) is a strong possibility supported by the spectrum of the molded sample.

The infrared spectra of 600EW-f-II having undergone 2 hours of exposure to 290°C under N_2 or in air are shown in Figure 40. These indicate a substantial decrease in the absorption intensity of the salt carbonyl bands at 1577 and 1400 cm^{-1} and a new absorption occurring at ca. 1740 cm^{-1}. These changes clearly indicate a substantial reduction in ionic content and thus in ionomeric character. The reduction of the quantity of atmospheric oxygen available during the heating process may have an effect on the rate but does not prevent degradation.

The results obtained thus far lead to the conclusion that exposure of 600EW material to temperatures above 250°C for periods exceeding one hour (to choose some

Figure 40: FTIR spectra of 600EW-f ionomer untreated and heat-treated in air and in N_2

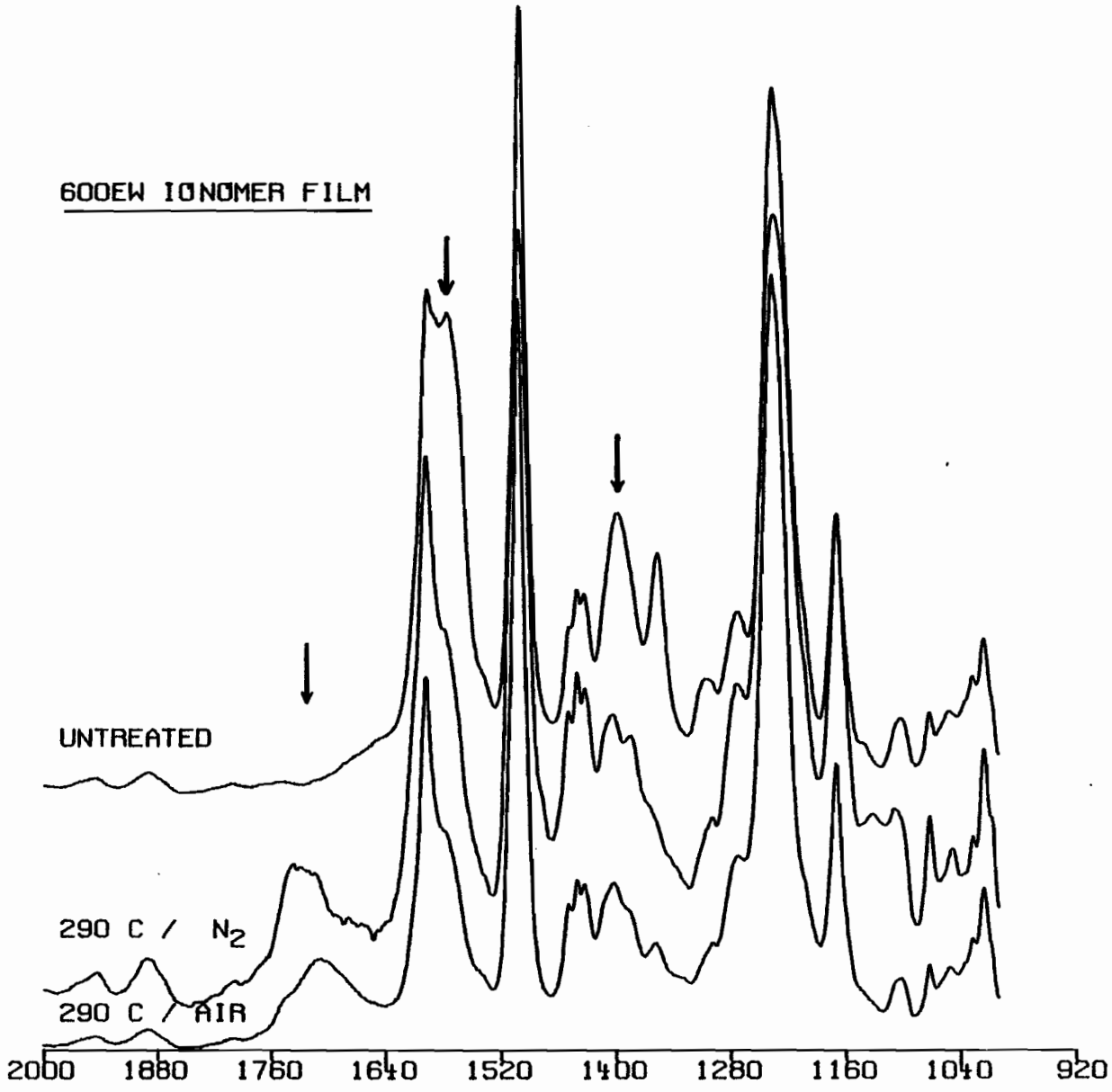
600EW IONOMER FILM
UNTREATED
290 C / N_2
290 C / AIR
2000
1880
1760
1640
1520
1400
1280
1160
1040
920

reasonable arbitrary numbers) causes irreversible changes in their chemical structure. These materials could be described as thermoplastics below 250°C and as thermosets above that temperature. Material properties start to change above that temperature, albeit slowly, in a way which makes it extremely difficult to draw clear-cut conclusions from the results of test methods such as torsion pendulum and high temperature relaxation techniques. It is evident that a complete description of transitions and relaxations requires the use of samples of well-defined thermal histories and the application of various experimental techniques at comparable experimental conditions. Thermal analysis such as DSC emerges as one of the applicable methods for investigating these systems at high temperature because the experimental time scale allows observation of molecular processes with only minimal degradation. Dielectric measurements and variable temperature infrared spectroscopy may prove to be suitable tools for the study of these materials.

5. CONTRIBUTIONS TO ORIGINAL KNOWLEDGE AND SUGGESTIONS FOR FUTURE WORK

5.1 Contributions to Original Knowledge

The study described has achieved its primary goal of exploring the mechanical properties of a new group of semi-rigid polymers based on the stable aromatic ether backbone. The ester precursor and ionomer films both show good mechanical stability up to temperatures of about 250°C in the dry state. Both also show excellent stability in concentrated alkaline environment, a feature of importance in the possible application of the ionomer as a separator in electrolytic processes.

This ionomer system showed unusual features in that it could neither be molded nor readily dissolved in simple solvents. Previous work on the aromatic materials of 1200EW had been performed using molded samples, but ionomers of higher ion content could be studied only in the form of films. Furthermore, thick homogeneous (or pore-free) films cast from DMSO could not be made and it was necessary to obtain the ionomer through hydrolysis of the non-ionic precursor film. These features make this system comparable, in difficulty of handling, to the perfluorinated ionomer materials (Nafion, Flemion) which are produced by only three companies in the world. Because of these limitations, a number of techniques in polymer physical chemistry could not be used.

Despite these difficulties, it was possible to study the material by a range of alternate methods. Differential scanning calorimetry showed the appearance of a transition at higher temperature which is thought to reflect the presence of ionic aggregates. Wide-angle X-ray diffraction showed that the material had a very low level of crystallinity but that it could be oriented. Water contact angle measurements and scanning electron microscopy were used to explore the structures of both the surface and the interior of the aromatic films. Stress-strain testing (in water and in alkaline solution) showed that the non-ionic precursor has a yield point both in air and in solution. A new adaptation to the standard stress-strain tester was constructed and used to obtain the results in water and in solution at temperatures ranging from 20 to 90°C. The ionomer film was shown to retain good mechanical properties in 20 % KOH at 80°C.

It was shown that ion aggregation occurs in the aromatic ionomers of higher ion content, but that large structures such as clusters are not formed in these bulky, semi-rigid systems. The ionic groups were found to contribute to interesting surface effects, as well as to good wettability. With the exception of wettability, the properties of the ionomer, appear to derive more from the relative rigidity of the aromatic ether backbone than from the incorporation of potassium neutralized carboxylate side groups. However, the salt groups impart to these ionomer films the capacity to function in alkaline media as separators which

allow ion transport (Eisenberg et.al., 1984; Steck et. al., 1984).

Other possible applications for the ionomer are in ion-exchange resins and in reverse osmosis, in the form of an asymmetric membrane. The making of asymmetric membranes has been explored in a preliminary fashion and presents no difficulty, the spongy material showing reasonable underwater stress-strain behaviour characterized by a break strain of ca. 30 % and tensile strength of the order of 6 MPa.

The ester precursor material emerges as a tough material, with a potential for orientation which could be exploited to produce very strong fibers. It could thus be considered as a potential candidate for service in extreme and unusual conditions. These range from applications in the reinforcement of elastomeric systems such as transport belts, to functioning as a stiffening element in rigid thermoplastic or thermosetting materials such as propeller and compressor blades, or to application in solar sailing.

5.2 Suggestions for Future Work

Many questions concerning this novel system remain unanswered. The structure of the hydrated ionomer membrane could be further elucidated by the use of infrared spectroscopy. A more controlled study of the changes incurred by the film surface on contact with water could lead to an understanding of the unusual contact angle results reported in this work.

A dynamic mechanical investigation of the ionomer material in film form, such as could be conducted on a suitably modified torsion pendulum, would also be indicated. In this manner, the DSC results pointing to multiplets only could be corroborated. A study of the effects of orientation in the ester and ionomer films would also be of interest, the oriented ionomer membrane being obtained by hydrolysis of the previously drawn precursor film.

It would be equally interesting to investigate the effect of the mobility of the ionic group on the structure of the ionic aggregates in these rigid systems. This could be done by the positioning of the ionic group at the end of an aliphatic side chain rather than directly on the aromatic backbone.

REFERENCES

Adamson, A.W. "Physical Chemistry of Surfaces", Wiley, 1982

Andrews, E.H. "Fracture in Polymers", Oliver and Boyd, 1968

Arnold, C. J. Polym. Sci., Macromol. Rev., 14, 265 (1979)

Arridge, R.G.C. "Mechanics of Polymers", Oxford Univ. Press,1975

Bazuin, C.G., Ph.D. Thesis, McGill University, Montreal,1984

Besso, E. J. Appl. Polym. Sci., 28, 1545 (1983)

Besso, E.; Eisenberg, A.; Legras, R.; Gupta, R.; Harris, F.W.; Steck, A.E.; Yeager, H.L. submitted to J. Appl. Polym. Sci., 1984

Bouda, V. Polymer Bulletin, 7, 639 (1982)

Casper, M.S., Ed. "Hydrogen Manufacture by Electrolysis, Thermal Decomposition and Unusual Techniques", Noyes Data Corporation, 1978

Cayrol, B., Ph.D. Thesis, McGill University, Montreal, 1972

Davidenkov, N.N.; Wittman, F. Phys. Tech. Inst. (USSR), 4, 300 (1937)

Eisenberg, A. and Yeager, H.L., Eds. "Perfluorinated Ionomer Membranes", ACS Symposium Series, No. 180, 1982

Eisenberg, A. Macromolecules, 3, 147 (1970)

Eisenberg, A.; Besso, E.; Harris, F.W.; Gupta, R.; Yeager, H.L.; Steck, A.E. in Vandenberg, E., 1984

Ferry, J.D. "Viscoelastic Properties of Polymers", p.311, Wiley, 1970

Fortes, M.A. "Physicochem. Aspects Polym. Surf.", Proc. Int. Symp., 1, 107, Plenum, 1983

Frazer, A.H. "High Temperature Resistant Polymers", Wiley, 1978

Giuffre, L.; Modica, G.; Spaziante, P.M. "Sulfonated Polyphenylene Sulfide: A New Diaphragm for Electrolytic Cells", paper presented at the IEA workshop on the electrolytic production of H_2, London, 1981

Greensmith, H.W. J. Appl. Polym. Sci., 8, 1113 (1964)

Grot, W.G.F. Chem. Ing. Technol., 50, 299 (1978)

Harrar, J.E.; Sherry, R.J. Anal. Chem., 47, 601 (1975)

Harris, F.W. et.al., Technical Report AFML-TR-76-9, March 1976

Harris, F.W. et.al., Technical Report AFML-TR-78-98, p.22, July 1978

Harris, F.W.; Reinhardt, B.A.; Case, R.D. Polym. Prepr., Am. Chem. Soc., Div. of Polym. Chem., 19(2), 394 (1978)

Haward, R.N. Trans. Faraday Soc., 38, 394 (1942)

Hay, A.S., Sherian,P., Cowan,A.C., Erhardt,P.F., Haaf,W.R. and Theberge,J.E., Encyclopedia of Polymer Science, 10, 92, Interscience, 1969

Jang, B.Z.; Uhlmann, D.R.; Vander Sande, J.B. Proc. of the 186th National meeting of the ACS Div. of Polymeric Materials Science and Engineering, 49, 129 (1983)

Kovacs, A. Adv. Polymer Sci., 3, 394 (1964)

Kyu, T.; Eisenberg, A. in Eisenberg and Yeager, 1982, p.79

Levy, L.; Muzzi, M.; Hurwitz, H.D. J. Chem. Soc., Faraday Trans. 1, 78, 1001 (1982)

MacKnight, W.J.; Earnest, T.R.,Jr. J. Polym. Sci., Macromol. Rev., 16, 41 (1981)

Mark, H.F. in "J. Appl. Polym. Sci.: Applied Polymer Symposia", B. Ranby and J.F. Rabek, Eds., Vol. 35, 13, Wiley, 1979

Matsushige, K.; Radcliffe, S.V.; Baer, E. J. Appl. Polym. Sci., 20, 1853 (1976)

Morrison, R.T. and Boyd, R.N. "Organic Chemistry", Allyn and Bacon, 1972

Mukamal, H.; Harris, F.W.; Stille, J.K. J. Polym. Sci. A-1, 5, 2721 (1967)

Navratil, M., Ph.D. Thesis, McGill University, Montreal,1972

Nayar, B.C.; Adamson, A.W. "Physicochem. Aspects Polym. Surf.", Proc. Int. Symp., 2, 613, Plenum, 1983

Nuttall, L.J.; Titterington, W.A., paper presented at the Conference on the Electrolytic Production of Hydrogen, London, 1975

Orowan, E. Rept. Prog. Phys., 12, 185 (1948)

Pasto, D.J. and Johnson, C.R. "Organic Structure Determination", Prentice-Hall, 1969

Renaud, R.; Leroy, R.L. Int. J. Hydrogen Energy, 7, No. 2, 155 (1982)

Rigdahl, M.; Reinhardt, A.B.; Harris, F.W.; Eisenberg, A. Macromolecules, 14, 851 (1980)

Snell, F.D. and Hilton, C.L., Eds., Encyclopedia of Ind. Chem. Anal., Vol 1, General Techniques, Interscience, 552, 1966

Steck, A.E., Ph.D. Thesis, University of Calgary, 1983

Steck, A.E.; Yeager, H.L.; Harris, F.W.; Gupta, R.K.; Eisenberg, A.; Besso, E. submitted to J. Appl. Polym. Sci. , 1984

Takamatsu ; Eisenberg, A. J. Appl. Polym. Sci., 24, 2221 (1979)

Vandenberg, E., Ed. "Contemporary Topics in Polymer Science", Vol. 5, Plenum, 1984

Vaughan, D.J. Du Pont Innovation, 4(3), 10 (1973)

Vincent, P.I. Polymer, 1, 425 (1960)

Williams, J.R., Ph.D. Thesis, McGill University, Montreal, 1978

Williams, M.L.; Landel, R.F.; Ferry, J.D. J. Am. Chem. Soc., 77, 3701 (1955)

Wrasidlo, W. Macromolecules, 4, 642 (1971)

Yeo, S.C.; Eisenberg, A. J. Appl. Polym. Sci., 21, 875 (1977)

APPENDIX I

SYNTHESIS OF AROMATIC IONOMER PRECURSORS

The following appendix is taken from a previous publication (Eisenberg et. al., 1984). It is the work of R. Gupta and F.W. Harris.

I.1 Monomers

The syntheses of the biscyclopentadienones 1a and 1b were carried out by the following routes:

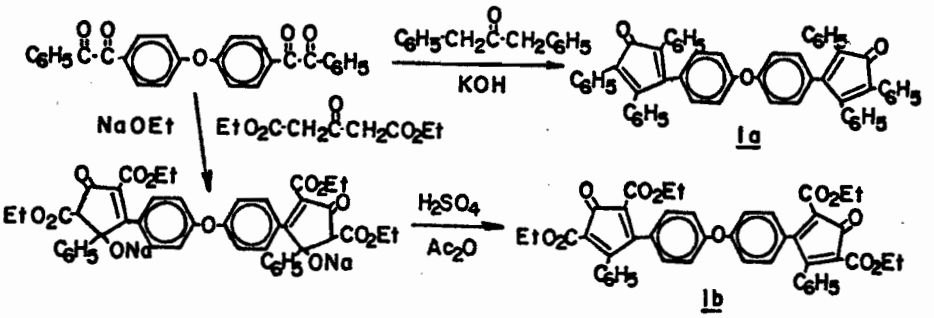

Chromatography of the dark purple 1a and the bright orange 1b on neutral alumina and silica gel, respectively, afforded monomer grade materials.

4-4'-Diethynyldiphenyl ether 2 was prepared from 4-4'-diacetyldiphenyl ether via the following synthetic route:

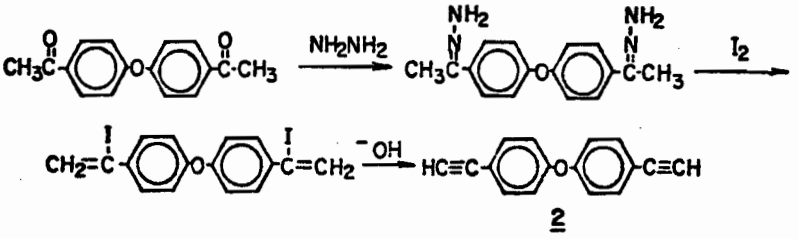

The white monomer was sublimed twice immediately prior to its polymerization.

I.2 Polymers

Monomers 1a and 1b were copolymerized with 2 in molar ratios of 70:30:100, and 40:60:100 to produce polymers 3a, 3b and 3c, respectively. Although the Diels-Alder reaction produces both meta and para catenation along the backbone, only para catenation has been depicted. The polymerizations were carried out in chlorobenzene (20% solids w/w) contained in sealed polymerization tubes. The

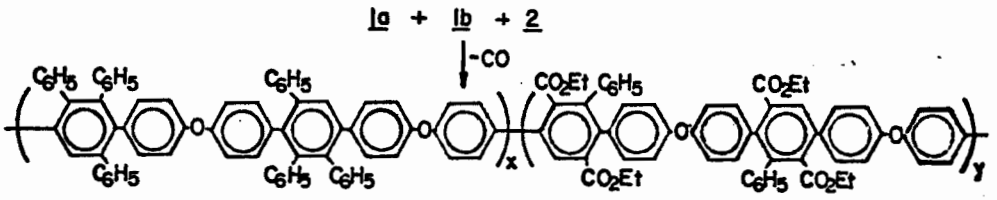

3a	x = 0.7	y = 0.3	EW = 800
b	x = 0.6	y = 0.4	EW = 600
c	x = 0.4	y = 0.6	EW = 400

tubes were heated at 110°C for 18 hours and then at 210°C for 24 hours. Polymerizations were also conducted in a 300-ml, stirred, Parr pressure reactor using an identical heating cycle. In these runs, the carbon monoxide evolved during the polymerization was allowed to escape from the reactor. The off-white, fibrous polymers were isolated by precipitation in ethanol. The ionomer precursors are readily soluble in chlorinated hydrocarbon solvents.

APPENDIX II

VIBRATING REED / AIM-65 INTERFACE

VIBRATING REED / AIM-65 INTERFACE

The vibrating reed experiment makes use of the flexural wave resonance of a viscoelastic cantilever to obtain its dynamic mechanical parameters in the sonic frequency range (100 Hz to 10 kHz). The sample undergoes forced vibration due to an applied sinusoidal excitation near its resonance frequency. The loss tangent, as a measure of the energy dissipated by the material due to its non-elastic (viscous) component, is obtained for a range of temperatures. The vibrating reed was described in detail by Nolle (1948). The theoretical basis of the experiment was treated by Horio and Onogi (1951).

The experimental data collected at each temperature consists of an array of driving frequencies and the corresponding amplitudes of reed vibration. The resonance frequency, which yields a maximum in vibration amplitude (V_{max}), as well as the frequencies at half width ($V_{max}/2$) must be extracted from the array. The dynamic mechanical parameters describing the material can be calculated using these values.

II.1 Hardware

The Rockwell AIM-65 is a computer based on the 6502 (8-bit) microprocessor. The standard AIM-65 components are listed in Table II.1. The 6502 can address an additional 40K bytes of random access memory (RAM), read-

Table II.1 AIM-65 complete standard package of hardware and software

---

HARDWARE

Full-size keyboard
20 column thermal printer
20 character display
2 cassette interfaces
1 20 mA loop teletype interface
1 6522 Versatile Interface Adapter (VIA) incorporating

- 16 individually configurable I/O lines
- 4 handshake (control) lines
- 1 16-bit timer / counter
- 1 16-bit timer

SOFTWARE

8 K Byte Monitor / Editor (ROM)
8 K Byte Microsoft BASIC (ROM)
4 K Byte Assembler (ROM)
4 K Byte read/write memory (RAM)

Table II.2 Equipment used in the Vibrating Reed interface

Component	Manufacturer
AIM-65 computer with 4K RAM, 4K Assembler and 8K BASIC options	Rockwell International Corp. Microelectronic Devices P.O.Box 3669, Anaheim CA
Little Buffered Mother 4-slot motherboard with 4K RAM	Seawell Marketing Inc. 315 N.W. 85th Seattle WA 98117
16 / 8K memory board used as 8K board	Seawell Marketing Inc.
ADC 363KD 16 channel, 12-bit ADC	Analog Devices Ltd. P.O.Box 280 Norwood MA 02062
AD536A rms-to-dc converter	Analog Devices Ltd.
TL081 BIFET operational amplifier	Texas Instruments
Cassette recorder TC-215	Sony Corporation
Power supply for AIM-65/Motherboard	Sorenson Prods., Raytheon Co. South Norwalk CT
Power supply for ADC circuitry	Analog Devices Ltd.

only memory (ROM) or input/output (I/O), thus allowing for easy system expansion. The basic system was expanded to 16K of RAM through the addition of a motherboard. The equipment used in the vibrating reed interface is listed in Table II.2.

Where necessary, the analog data available for input was first converted to direct current (dc), amplified, then digitized. Digitization denotes the breaking up of the analog values into n segments. A 12-bit (n=12) analog to digital converter (ADC) of the successive approximation type was used. This type of ADC has a conversion time which is independent of the input voltage and converts at high speed. A 12-bit conversion is performed in 25 microseconds with a maximum error of $\pm$ 0.012 %. A block diagram of the AIM-65/vibrating reed assembly is shown in Figure II-1.

The data are input to the computer through a parallel interface to memory-addressed I/O ports. These ports are located on the 6522 VIA described in Table II.1.

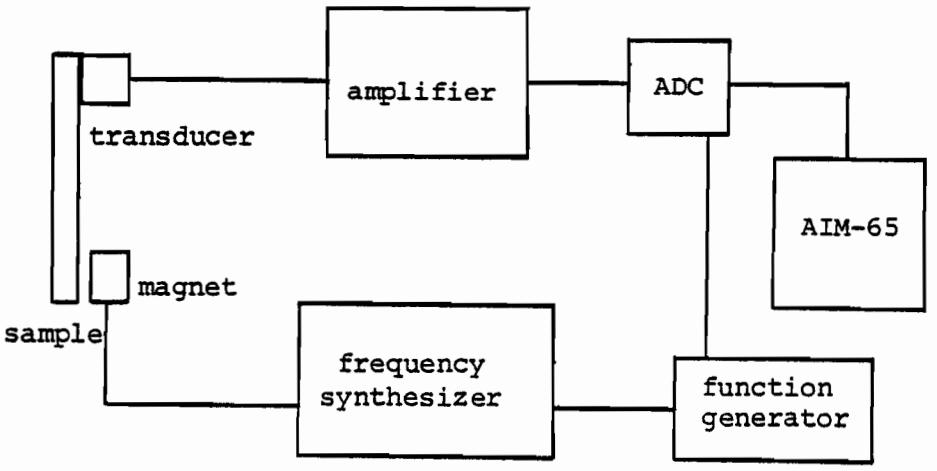

Figure II-1: Block diagram of AIM-65/vibrating reed assembly

Figure II-2 shows the detailed electronic connections between the two-chip analog-to-digital converter (AD363KD) and the AIM-65 Versatile Interface Adapter (VIA 6522). The function of the two handshake lines is to synchronize signal throughput. The channel select line chooses the source of the input signal. This is either the frequency, input through the function generator, or the amplified reed vibration, input from a high gain amplifier.

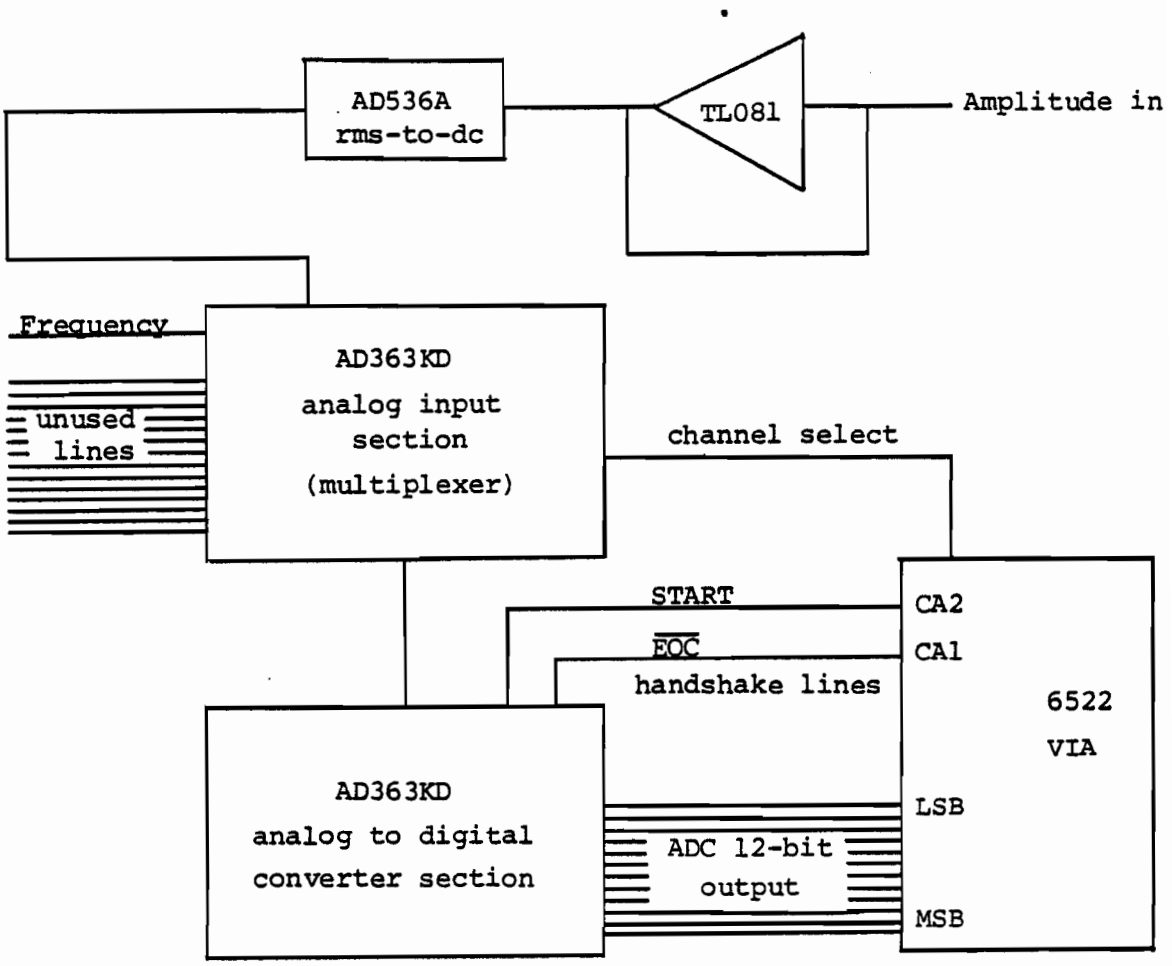

Figure II-2: Schematic of the electronic connections of the AIM-65/vibrating reed interface

Figure II-3 shows the detailed electronic connections of the additional amplifier stage designed to raise the reed vibration signal to the optimal voltage levels needed for efficient use of the ADC input range. This is necessary because the signal output by the reed vibration at certain temperatures and frequencies is of the order of a few millivolts only. The feedback loop of the operational amplifier (TL081) incorporates a multiplexer (DG508, Siliconix) which was included for the following purpose. By connecting feedback resistors of different strength at each output, the amplifier gain can become variable, its magnitude dependent on the channel selected. This is according to the relation

$$\text{Gain} = R_{feedback} / R_{input}$$

Although the instrument is currently configured for a constant gain of 100, operation of this additional amplifier stage as a variable one would require only minor software adjustment. Detailed electronic connections of the interface are listed in Table II.3.

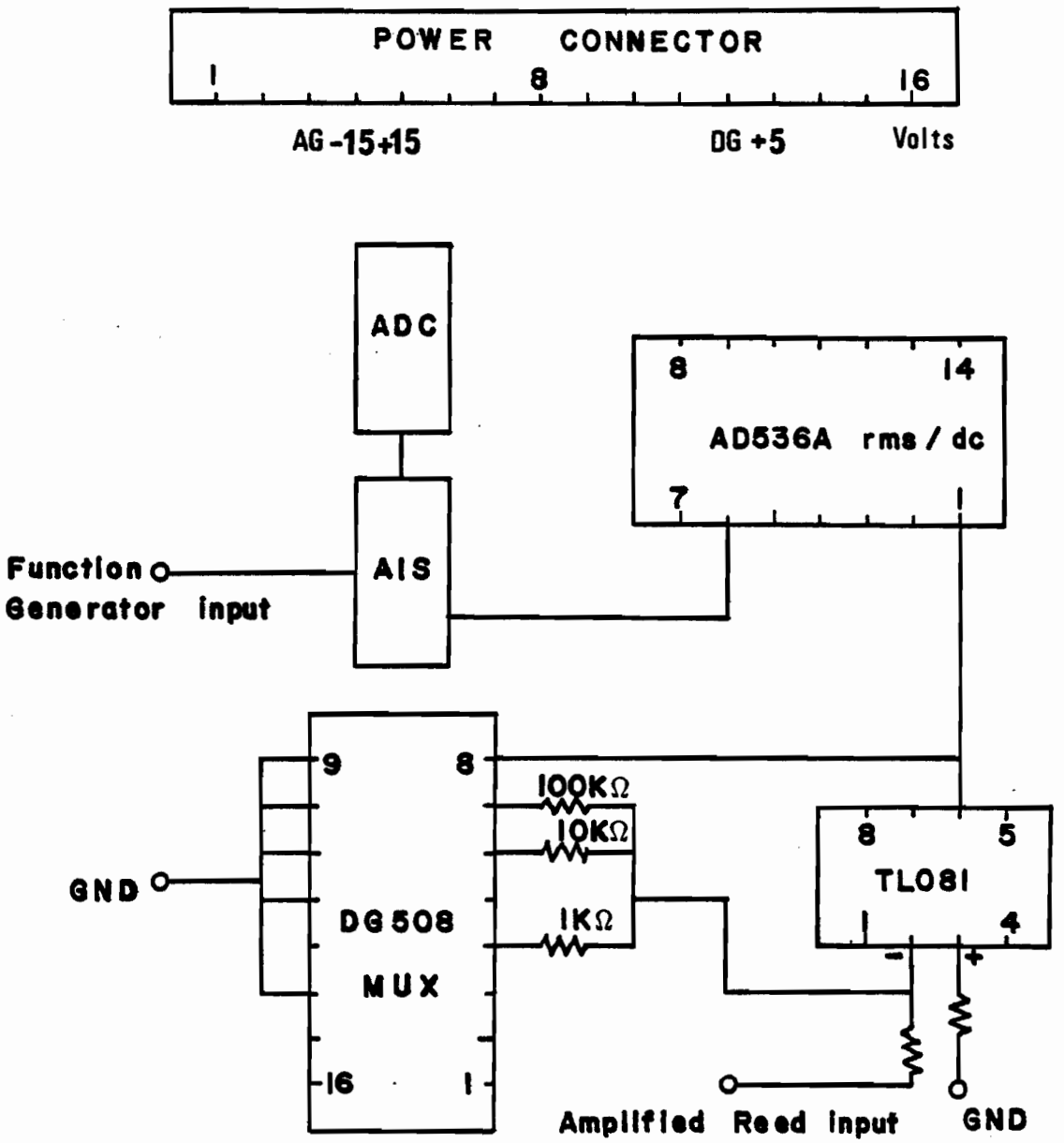

Figure II-3: Detailed schematic of the AIM-65/vibrating reed interface
AIS - AD363KD Analog Input Section
ADC - AD363KD analog-to-digital converter section
MUX - multiplexer

Table II.3 Details of the AIM-65 / ADC interface

AIS363KD Pin #	A/D Pin #	Connector Description	AIM-65 J-1 Pin #	Connector ID
1	38	digital ground		
2	37	digital ground		
3	42	+ 5 V		
4 - 7		unused		
8	4/59	VR input to ADC		
9	63	FG input to ADC		
10 -16		unused		
17	48	analog ground		
18 -19		unused		
20	34	- 15 V		
21	30	+ 15 V		
22 - 27		unused		
28	38	digital ground		
29	71	input channel select	13	PB4
30	44	+ 5 V		
31	38	digital ground		
32	67	channel select latch	16	PB5
	10	input to op amp TL081 (VR input)		
	16	input of VR signal to rms-to-dc converter		
	4/59	output of rms-to-dc converter		
ADC363KD Pin #				
1	72	least significant bit	14	PA0
2	70		4	PA1
3	68		3	PA2
4	66		2	PA3
5	64		5	PA4
6	62		6	PA5
7	60		7	PA6
8	58		8	PA7
9	56		9	PB0
10	54		10	PB1
11	52		11	PB2
12	50	most significant bit	12	PB3
14	42	+ 5 V		
15	38	digital ground		
16	42	+ 5 V		
17	51	handshake line	20	CA1
18 - 20		unused		
21	55	handshake line	21	CA2
22 - 25		unused		
26	48	analog ground		
28	30	+ 15 V		
31	34	- 15 V		
13,27,29,30		unused		

II.2 Software

The AIM-65 user software comprises 20K bytes of ROM distributed in the following manner. An 8K Monitor controls AIM-65 operation and allows memory examination, register display, program editing and debugging among other functions. An Assembler, taking up 4K bytes, allows programming in machine code with the use of mnemonics. The remaining 8K of ROM are occupied by the BASIC interpreter.

The specific software developed for this application consists of a BASIC master program which makes use of a machine language subroutine to control the ADC and acquire data points. The software incorporates several user alterable parameters which can broadly be classified into two types. The first class consists of those necessary to specify experimental conditions such as temperature and resonance frequency of the sample. The parameters of the second class are those necessary to optimize the quality of the data acquired, for example an offset parameter used to reduce the effect of noise in the experimental curve. The data used to perform the calculations leading to the loss tangent are stored in a BASIC array in decimal form.

The experimental curve is stored in memory through the acquisition of 252 points, each specifying two coordinates, these being frequency and amplitude of vibration. Data acquisition is performed in machine language to ensure adequate speed. Typically, an experimental curve is swept out in a time period ranging

between 10 and 20 seconds. This gives the program a maximum of 39 milliseconds to acquire each point, in the case of a 10-second sweep. This acquisition rate could not be achieved by BASIC. The delay necessary between the acquisition of subsequent points is controlled by the software, so as to optimize curve definition.

The values obtained for tan delta at one fixed temperature yield a relative precision of 0.3 %. This value may be improved by increasing the number of points used to define the experimental curve.

A listing of the BASIC master program, identified by the file names VIB20 or VIB22 (for hardcopy output on the AIM-65 printer or on the Decwriter, respectively), is given below. It is followed by the listing of the Machine Language subroutine, identified by the file name ADC14.

The software listings are followed by a detailed user guide for the operation of the computerized vibrating reed assembly. This user guide was not intended to be a complete manual for the method of operation of the Vibrating Reed instrument. For a complete description of the instrument and method of operation, the reader is referred to Appendix II in Williams (1978). To the exclusion of the computer interface components, the apparatus described therein was changed in one respect only. The X-Y recorder was replaced by a dual trace storage oscilloscope (Tektronix model 5111), the hardcopy of acquired data being provided by the associated printer.

II.3 SOFTWARE LISTINGS

II.3.1 Commented BASIC Master Program

File VIB20 uses the AIM-65 printer for the output

File VIB21 uses the DECwriter for output

```
3   REM AIM 65 KEYBOARD CONTROLLED VERSION USING DECWRITER
4   REM FILE NAME VIB21, OF AIM 65/VIBRATING REED OPERATION
5   REM PROGRAM FOR THE ACQUISITION OF 252 POINTS PER CURVE
6   REM REFERENCE IS INTERFACING NOTEBOOK II
8   REM
10  REM WRITTEN BY ERICA BESSO, OCTOBER 1981
12  POKE 43010,63; This sets PB3 of Z3232 VIA as output
16  POKE 43008,244; Selects DECwriter as output
17  PRINT "TEMPERATURE","TAN D X 10E+6","RESONANCE F","VMAX"
18  POKE 43008,252; Returns control to AIM 65 keyboard
19  POKE 42001,0; Turns printer OFF
20  POKE 04,00:POKE 05,55
40  Z = 2.44142E-3:A = 9.48683981
41  REM Z is a factor to convert 12-bit ADC data to real
42  REM voltages; A is a factor representing frequency
43  REM increment resulting from the Function Generator
44  REM triangular wave
45  INPUT "SWEEP T, SEC";S:D = ((S/2.52E-4)-10)/1546
46  REM D is the delay between Machine Language aquisition
47  REM of points
50  POKE 14077,D: ST = 1.732051:ST is the square root of 3
60  DIM A1(252,2): Specifies the dimensions of BASIC array A1
65  INPUT"TEMPERATURE"; INPUT "BASE PERIOD";BF
70  BF = 1/(BF*1E-6): BF is the base frequency
75  INPUT "CAD CONTROLS";DIV
76  REM Now go to Machine Language subroutine which collects
77  REM and stores 504 data points
80  W = USR(1): B = 15868
81  REM B is the base address where HEX numbers are stored
100 FOR K = 0 TO 62: FOR L = 1 TO 2: GOSUB 420
101 REM This stores in array A1 the data in decimal form
110 A1(K,1) = N*Z: NEXT: NEXT
120 B = 15612: FOR K = 63 TO 125: FOR L = 1 TO 2: GOSUB 420
130 A1(K,L) = N*Z: NEXT: NEXT
140 B = 15356: FOR K = 126 TO 188: FOR L = 1 TO 2:GOSUB 420
150 A1(K,L) = N*Z: NEXT: NEXT
160 B = 15100: FOR K = 189 TO 252:FOR L = 1 to 2: GOSUB 420
170 A1(K,L) = N*Z: NEXT: NEXT
180 MX = 0: RF = 0
185 REM Now search array for highest amplitude of vibration
190 FOR K = 0 TO 252: IF MX ≥ A1(K,2) GO TO 210
200 MX = A1(K,2): W = K: RF = A1(K,1)
```

```
210 REM Calculate frequency at maximum amplitude of vibration
220 RF = BF + (((RF * 2)-10)*DIV/A)
240 MV = MX
245 REM Specify voltage offset if necessary
250 INPUT"OFFSET?";S
255 REM Find exact value of amplitude at half-width
260 MX = (((MX-5)+S)/2)+5: HF = 0
261 REM To print out vibration amplitude values, insert
262 REM the following line: 265 PRINT A1(K,L)
270 FOR K = 0 TO 252: L = 2: NEXT: HK = 0.1
275 REM Find the value of first halfwidth frequency, HF
280 FOR K = 0 TO 252: HL = ABS (MX-A1(K,2))
281 IF HL < 0.1 GO TO 290: NEXT
285 REM HL holds the last absolute difference,HL the present one
290 IF HK > HL THEN HK = HL: IF HK < HL GO TO 520
300 HF = A1(K,1): NEXT: HF = BF + (((HF*2)-10)*DIV/A)
310 HG = BF + (((HG*2)-10)*DIV/A)
320 TD = ABS ((HF-HG)/ST/RF/MV*10)
321 REM TD is Tan Delta which is calculated with a VMAX
322 REM scaled to 10 Volts for all runs
323 TD = INT (TD*1E+6): Converts TD to a more common form
325 REM Retain only 5 significant figures in RF value for print
326 RF = RF*10: RG = (RF - INT(RF))/10: RF = (RF/10) - RG
328 INPUT "TEMPERATURE";T: POKE 43008,244: POKE 42001,128
330 PRINT T, ,TD, ,RF, ,MV: POKE 43008,252: POKE 42001,0
331 STOP
340 INPUT "COMMENT";C$: Print a comment if desired
342 IF LEN(C$) = 0 THEN 350: POKE 43008,244: POKE 42001,128
344 PRINT C$: POKE 43008,252: POKE 42001,0
350 STOP
400 REM Routine to convert a 12-bit HEX number to decimal form
420 LB = PEEK (B): C = LB: T = 0
421 REM LB is low byte of 12-bit number, T is coefficient of 10
430 IF C > 16 THEN 460:T = 16*T:LB = C + T:B = B - 1:HB = PEEK(B)
440 IF HB>15 THEN 470: HB holds value of bits 8 - 12
460 C = C - 16: T = T + 1: GO TO 430
470 HB = HB AND 15: GO TO 450
519 REM Find value of second halfwidth frequency, HG
520 HK = 0.1: FOR I = W TO 252: HL = ABS (MX - A1(I,2))
530 IF HL<0.1 GO TO 540: NEXT
540 IF HK>HL THEN HK = HL: IF HK<HL GO TO 300
550 HG = A1(I,1): NEXT
```

II.3.2 Disassembled version of Machine Language subroutine

```
3700 A2 LDX #FC
3702 20 JSR 37DA
3705 20 JSR 380B
3708 20 JSR 37F3
370B 20 JSR 3803
370E 20 JSR 3814
3711 20 JSR 37EA
3714 20 JSR 37F3
3717 20 JSR 3803
371A 20 JSR 3814
371D 20 JSR 37C5
3720 E0 CPX #00
3722 D0 BNE 3705
3724 A2 LDX #FC
3726 20 JSR 380B
3729 20 JSR 37F3
372C 20 JSR 3803
372F 20 JSR 3823
3732 20 JSR 37EA
3735 20 JSR 37F3
3738 20 JSR 3803
373B 20 JSR 3823
373E 20 JSR 37C5
3741 E0 CPX #00
3743 D0 BNE 3726
3745 A2 LDX #FC
3747 20 JSR 380B
374A 20 JSR 37F3
374D 20 JSR 3803
3750 20 JSR 3832
3753 20 JSR 37EA
3756 20 JSR 37F3
3759 20 JSR 3803
375C 20 JSR 3832
375F 20 JSR 37C5
3762 E0 CPX #00
3764 D0 BNE 3747
3766 A2 LDX #FC
3768 20 JSR 380B
376B 20 JSR 37F3
376E 20 JSR 3803
3771 20 JSR 3841
3774 20 JSR 37EA
3777 20 JSR 37F3
377A 20 JSR 3803
377D 20 JSR 3841
3780 20 JSR 37C5
3783 E0 CPX #00
3785 D0 BNE 3768
3787 A2 LDX #FC
3789 8E STX 36FF
378C A9 LDA #91
378E 85 STA 04
3790 60 RTS
3791 AE LDX 36FF
3794 20 JSR 386E
3797 E0 CPX #00
3799 F0 BEQ 379C
379B 60 RTS
379C 4C JMP 3850
379F 60 RTS
37A0 AE LDX 36FF
37A3 20 JSR 3880
37A6 E0 CPX #00
37A8 F0 BEQ 37AB
37AA 60 RTS
37AB 4C JMP 385A
37AE 60 RTS
37AF AE LDX 36FF
37B2 20 JSR 3892
37B5 E0 CPX #00
37B7 F0 BEQ 37BA
37B9 60 RTS
37BA 4C JMP 3864
37BD 60 RTS
37BE AE LDX 36FF
37C1 20 JSR 38A4
37C4 60 RTS
37C5 AC LDY 36FD
37C8 8C STY 36FE
37CB A0 LDY #00
37CD 18 CLC
37CE C8 INY
37CF C0 CPY #FF
37D1 90 BCC 37CE
37D3 AC LDY 36FE
37D6 88 DEY
37D7 D0 BNE 37C8
37D9 60 RTS
37DA A9 LDA #00
37DC 8D STA A003
37DF A9 LDA #D0
37E1 8D STA A002
37E4 A9 LDA #03
37E6 8D STA A00B
37E9 60 RTS
37EA AD LDA A000
```

```
37ED 09 ORA #10
37EF 8D STA A000
37F2 60 RTS
37F3 A9 LDA #0D
37F5 8D STA A00C
37F8 A9 LDA #0F
37FA 8D STA A00C
37FD A9 LDA #0D
37FF 8D STA A00C
3802 60 RTS
3803 AD LDA A00D
3806 29 AND #02
3808 F0 BEQ 3803
380A 60 RTS
380B AD LDA A000
380E 29 AND #EF
3810 8D STA A000
3813 60 RTS
3814 AD LDA A001
3817 9D STA 3D00,X
381A CA DEX
381B AD LDA A000
381E 9D STA 3D00,X
3821 CA DEX
3822 60 RTS
3823 AD LDA A001
3826 9D STA 3C00,X
3829 CA DEX
382A AD LDA A000
382D 9D STA 3C00,X
3830 CA DEX
3831 60 RTS
3832 AD LDA A001
3835 9D STA 3B00,X
3838 CA DEX
3839 AD LDA A000
383C 9D STA 3B00,X
383F CA DEX
3840 60 RTS
3841 AD LDA A001
3844 9D STA 3A00,X
3847 CA DEX
3848 AD LDA A000
384B 9D STA 3A00,X
384E CA DEX
384F 60 RTS
3850 A2 LDX #FC
3852 8E STX 36FF
3855 A9 LDA #A0
3857 85 STA 04
3859 60 RTS
385A A2 LDX #FC
385C 8E STX 36FF
385F A9 LDA #AF
3861 85 STA 04
3863 60 RTS
3864 A2 LDX #FC
3866 8E STX 36FF
3869 A9 LDA #BE
386B 85 STA 04
386D 60 RTS
386E BD LDA 3D00,X
3871 A8 TAY
3872 CA DEX
3873 BD LDA 3D00,X
3876 29 AND #0F
3878 CA DEX
3879 8E STX 36FF
387C 20 JSR C0D1
387F 60 RTS
3880 BD LDA 3C00,X
3883 A8 TAY
3884 CA DEX
3885 BD LDA 3C00,X
3888 29 AND #0F
388A CA DEX
388B 8E STX 36FF
388E 20 JSR C0D1
3891 60 RTS
3892 BD LDA 3B00,X
3895 A8 TAY
3896 CA DEX
3897 BD LDA 3B00,X
389A 29 AND #0F
389C CA DEX
389D 8E STX 36FF
38A0 20 JSR C0D1
38A3 60 RTS
38A4 BD LDA 3A00,X
38A7 A8 TAY
38A8 CA DEX
38A9 BD LDA 3A00,X
38AC 29 AND #0F
38AE CA DEX
38AF 8E STX 36FF
38B2 20 JSR C0D1
38B5 60 RTS
38B6 20 JSR C0D1
38B9 60 RTS
```

II.3.3 Editor version of Machine Language subroutine

```
        *=$3700
==3700
A2FC    LDX #$FC
20DA37  JSR SETUP
==3705 W1
200B38  JSR FGSET
20F337  JSR SC
200338  JSR WAIT
201438  JSR STR1
20EA37  JSR VRSET
20F337  JSR SC
==3717
200338  JSR WAIT
201438  JSR STR1
20C537  JSR DLAY
E000    CPX #$00
D0E1    BNE W1
A2FC    LDX #$FC
==3726 W2
200B38  JSR FGSET
20F337  JSR SC
200338  JSR WAIT
202338  JSR STR2
20EA37  JSR VRSET
20F337  JSR SC
==3738
200338  JSR WAIT
202338  JSR STR2
20C537  JSR DLAY
E000    CPX #$00
D0E1    BNE W2
A2FC    LDX #$FC
==3747 W3
200B38  JSR FGSET
20F337  JSR SC
200338  JSR WAIT
203238  JSR STR3
20EA37  JSR VRSET
20F337  JSR SC
==3759
200338  JSR WAIT
203238  JSR STR3
20C537  JSR DLAY
E000    CPX #$00
D0E1    BNE W3
A2FC    LDX #$FC
==3768 W4
200B38  JSR FGSET
20F337  JSR SC
200338  JSR WAIT
204138  JSR STR4
20EA37  JSR VRSET
20F337  JSR SC
```

```
==377A
200338  JSR WAIT
204138  JSR STR4
20C537  JSR DLAY
E000    CPX #$00
D0E1    BNE W4
A2FC    LDX #$FC
8EFF36  STX $36FF
==378C
A995    LDA #$95
8504    STA $04
60      RTS
;SEND FIRST 128 PTS
AEFF36  LDX $36FF
206E38  JSR SEND1
E000    CPX #$00
F001    BEQ *+3
60      RTS
==379C
4C5038  JMP DONE1
60      RTS

;SEND NEXT 128 PTS
AEFF36  LDX $36FF
208038  JSR SEND2
E000    CPX #$00
F001    BEQ *+3
60      RTS
4C5A38  JMP DONE2
==37AE
60      RTS

AEFF36  LDX $36FF
209238  JSR SEND3
E000    CPX #$00
F001    BEQ *+3
60      RTS
4C6438  JMP DONE3
60      RTS

==37BE
AEFF36  LDX $36FF
20A438  JSR SEND4
60      RTS
```

```
;DELAY LOOP
==37C5 DLAY
ACFD36  LDY $36FD
==37C8 LP2
8CFE36  STY $36FE
A000    LDY #$00
18      CLC
==37CE LP1
C8      INY
C0FF    CPY #$FF
90FB    BCC LP1
ACFE36  LDY $36FE
88      DEY
D0EF    BNE LP2
60      RTS

;SET UP DDR'S & ACR
==37DA SETUP
A900    LDA #$00
8D03A0  STA $A003
A9D0    LDA #$D0
8D02A0  STA $A002
A903    LDA #$03
8D0BA0  STA $A00B
60      RTS

==37EA
;SELECT VR INPUT
==37EA VRSET
AD00A0  LDA $A000
0910    ORA #$10
8D00A0  STA $A000
60      RTS

;START CONVERSION
==37F3 SC
A90D    LDA #$0D
8D0CA0  STA $A00C
A90F    LDA #$0F
8D0CA0  STA $A00C
A90D    LDA #$0D
8D0CA0  STA $A00C
60      RTS

==3803
;WAIT UNTIL DONE
==3803 WAIT
AD0DA0  LDA $A00D
2902    AND #$02
F0F9    BEQ WAIT
60      RTS
```

```
;SELECT FG CHANNEL
==380B FGSET
AD00A0 LDA $A000
29EF   AND #$EF
8D00A0 STA $A000
60     RTS

;STORE FIRST 128 PTS
==3814 STR1
AD01A0 LDA $A001
9D003D STA $3D00,X
CA     DEX
AD00A0 LDA $A000
9D003D STA $3D00,X
CA     DEX
60     RTS

;STORE NEXT 128
==3823 STR2
AD01A0 LDA $A001
9D003C STA $3C00,X
CA     DEX
AD00A0 LDA $A000
9D003C STA $3C00,X
CA     DEX
60     RTS

;NEXT 128 STORED
==3832 STR3
AD01A0 LDA $A001
9D003B STA $3B00,X
CA     DEX
AD00A0 LDA $A000
9D003B STA $3B00,X
CA     DEX
60     RTS

;STORE LAST 128 PTS
==3841 STR4
AD01A0 LDA $A001
9D003A STA $3A00,X
CA     DEX
AD00A0 LDA $A000
9D003A STA $3A00,X
CA     DEX
60     RTS

==3850 DONE1
A2FC   LDX #$FC
8EFF36 STX $36FF
A9A4   LDA #$A4
8504   STA $04
60     RTS

==385A DONE2
A2FC   LDX #$FC
8EFF36 STX $36FF
A9B3   LDA #$B3
8504   STA $04
60     RTS

==3864 DONE3
A2FC   LDX #$FC
8EFF36 STX $36FF
A9C2   LDA #$C2
8504   STA $04
60     RTS

;SEND 1ST 128 PTS
   TO BASIC ARRAY A1
(K,L)
==386E SEND1
BD003D LDA $3D00,X
A8     TAY
CA     DEX
BD003D LDA $3D00,X
290F   AND #$0F
CA     DEX
8EFF36 STX $36FF
20D1C0 JSR $C0D1
==387F
60     RTS

;SEND NEXT 128 PTS
==3880 SEND2
BD003C LDA $3C00,X
A8     TAY
CA     DEX
BD003C LDA $3C00,X
290F   AND #$0F
CA     DEX
8EFF36 STX $36FF
20D1C0 JSR $C0D1
==3891
60     RTS

==3892 SEND3
BD003B LDA $3B00,X
A8     TAY
CA     DEX
BD003B LDA $3B00,X
290F   AND #$0F
CA     DEX
8EFF36 STX $36FF
20D1C0 JSR $C0D1
==38A3
60     RTS

;SEND LAST 128 PTS
==38A4 SEND4
BD003A LDA $3A00,X
A8     TAY
CA     DEX
BD003A LDA $3A00,X
290F   AND #$0F
CA     DEX
8EFF36 STX $36FF
20D1C0 JSR $C0D1
==38B5
60     RTS
       RTS
 ERRORS= 0000
```

II.4 Operating Instructions for VR/AIM-65 Assembly

1. Turn VR components and computer system power ON.

2. Toggle the printer to OFF by depressing CTRL and PRINT keys simultaneously.

3. Load Machine language and BASIC programs from tape to memory

4. If using the DECWRITER, select 150 baud transmission rate. Ascertain that the RS-232 connector is out and the AIM-65 connector is plugged into the printer.

5. Connect one channel of the oscilloscope to the LOW output of the Function Generator

6. Connect the other channel of the oscilloscope to the output of the rms-to-dc converter (line 4 or 59)

   The oscilloscope should be operated in storage mode; Typical settings would be 2 V/div and 5 sec/div

7. Observe the bell-shaped curve of vibrational amplitude as a function of time. Note the time, in seconds, necessary for the entire frequency scan.

8. To RUN the program, ONE MUST BE in BASIC

   Type RUN, followed by "Return"

9. To "SWEEP T" prompt, enter the value observed (step 7) on the oscilloscope, followed by "Return"

10. To "BASE PERIOD" prompt, enter the period, in microseconds, at maximum amplitude of reed vibration followed by "Return"

    This should be the period displayed on the frequency counter when the function generator is OFF

11. To "CAD CONTROLS" prompt, enter the frequency decade controlled by the CAD dial of the frequency synthesizer

12. If using the AIM-65 printer, toggle the printer ON

    DO NOT PRESS "Return" UNTIL READY TO ACQUIRE DATA

13. Start Function Generator sweep, if necessary, and watch the trace on the oscilloscope.

    Once the signal reaches a minimum, press the "Return" key to start data acquisition.

14. Note the temperature

15. Wait for points to be acquired, approximately 3 minutes

16. To "OFFSET" prompt, enter the desired voltage offset value followed by "Return"

    This value is a correction for a vibration amplitude minimum value which differs from 0 Volts.

17. To "TEMPERATURE" prompt, enter temperature recorded at the start of data acquisition, followed by "Return"

18. To "COMMENTS" prompt, enter desired comments and follow by "Return"

19. The calculated values will be output on the printer

    The value of Tan Delta printed out is (TAN D) x 10^6

20. To start another run, repeat procedure starting at step 8

II.5 REFERENCES

Horio, M.; Onogi, S. J. Appl. Phys., 22, 977 (1951)

Nolle, A. W. J. Appl. Phys., 19, 753 (1948)

APPENDIX III

ADDITIONS TO THE TENSILE TESTING APPARATUS

The temperature-controlled chamber designed to allow measurements on samples in solution is shown schematically in Figure III.1. The immersion heater is connected to a digital temperature controller (D921, Omega Engineering). The controller regulates the heater action by continual comparison between the chosen set-point and the solution temperature which is input by the thermocouple.

The design of the tube furnace is analogous to that of the bath, the two being completely interchangeable. They differ in that the movable 3-zone furnace has a thicker layer of insulation around the internal wall on which the three 250 W band heaters are mounted. Three thermocouples are placed in the chamber wall, each in close proximity to one of the band heaters. The temperatures of the three heaters are directly input to three temperature controllers (D921). Thus each band heater is monitored independently. Sample temperature, sensed by the thermocouple located within the furnace, is displayed on a digital temperature indicator. Typically, the controller set-points must be set at ca. 15^{o}C above the temperature desired within the furnace.

For the tube furnace, the stationary lid contains neither stirrer nor immersion heater, but only the thermocouple well.

The vertical movement of either chamber along the

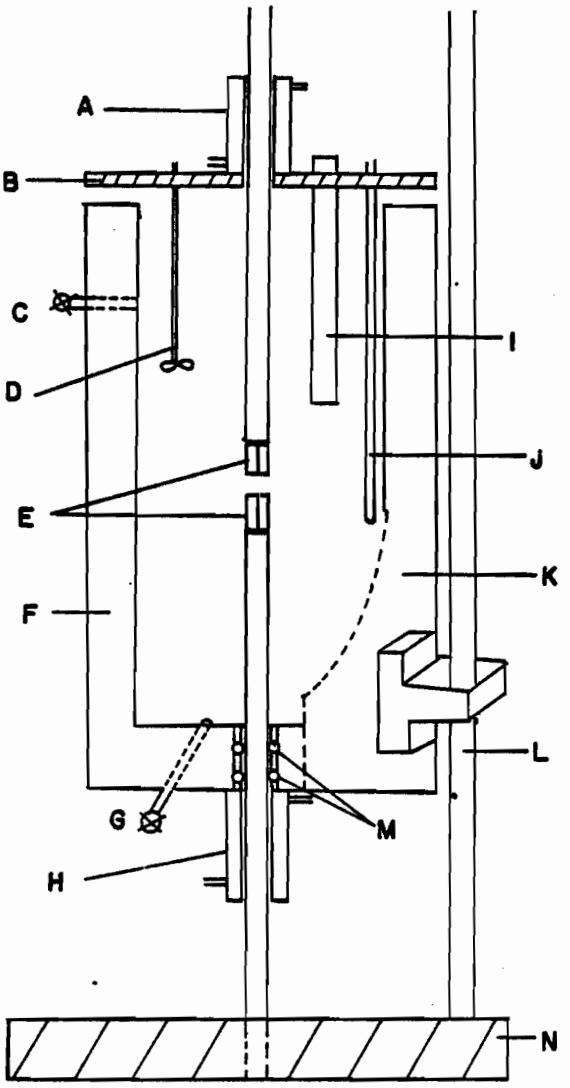

Figure III-1: Temperature-controlled bath designed for stress-strain testing apparatus

A	cooling water circulating in copper tubing
B	stationary lid
C	solution inlet
D	stirrer
E	sample grips
F	insulation
G	solution outlet
H	cooling water
I	immersion heater, 500 W
J	thermocouple well
K	mobile bath
L	elevator guiding rod
M	Viton O-rings
N	Instron base

guiding rod is activated by a momentary switch. The direction of movement is specified by placing an SPDT switch in the UP or DOWN position. The maximum travel distance is of approximately 17 cms and is covered in 40 seconds. The upper and lower limits of travel are microswitch protected.

The controls for chamber travel, stirring, and furnace or solution heating are mounted on a single panel which also holds a temperature indicator. The temperature indicator is necessary in the case of the high temperature experiments because the temperature within the furnace differs from that indicated by the controllers. As mentioned previously, the thermocouples connected to the temperature controllers are located in close proximity to the band heaters.

The electrical connections were designed for ease of interchangeability of the bath and high temperature chambers. The procedure to follow in going from the bath assembly to the high temperature chamber is given below.

1. Verify that water circulation in cooling coils is turned OFF. Disconnect the tubing
2. Position the empty chamber to the lowest point of travel
3. Disconnect the stirrer
4. Disconnect the thermocouple input to the temperature controller
5. Disconnect the immersion heater from the temperature controller
6. Disconnect the elevator circuit
7. Remove bath chamber and cover assembly

8. Position high temperature chamber and cover assembly

9. Connect band heaters to temperature controllers

10. Connect band heater thermocouples to temperature controllers

11. Connect sample thermocouple to temperature indicator

12. Connect elevator circuit

13. Verify alignment by using the elevator controls. Correct if necessary

APPENDIX IV

HIGH TEMPERATURE STRESS RELAXOMETER

The instrument is shown schematically in Figure IV-1. The film sample is clamped between an upper stationary grip (not shown) and a lower movable grip connected to a linear variable differential transformer (LVDT). The LVDT output is fed to an amplifier/indicator via a six-conductor shielded cable. The digital display indicates the force exerted on the sample in grams. The force is also output to a strip chart recorder. The connections between the LVDT and the amplifier/indicator are shown in Table IV.1.

Table IV.1 Electronic connections between force transducer and amplifier/indicator (A/I)

Description	LVDT Pin	A/I Edge Connector
Primary, - Excitation	E	1
Primary, + Excitation	F	2
Secondary 1	C	3
Secondary 2	A	4
Secondary 1	D	5
Secondary 2	B	E
Shield		9

The 500 W main heater (not shown) consists of a Nichrome winding with an electrical insulation of ceramic fish-spine beads. It is supplemented by five auxiliary band heaters having a power of 100 W each.

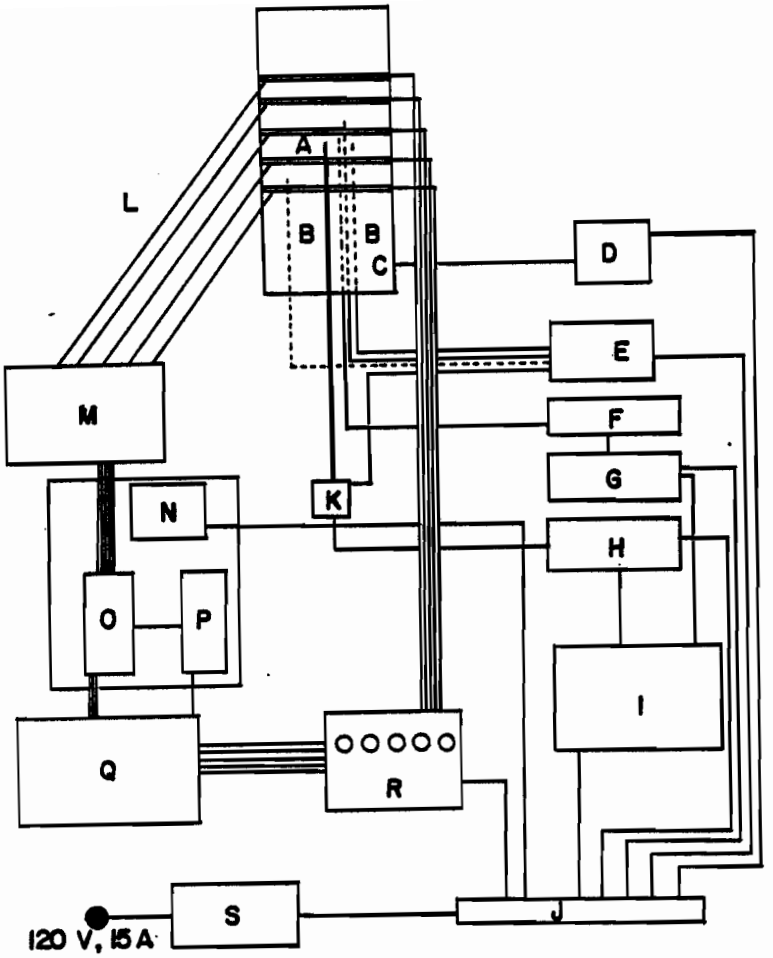

Figure IV-1: Block diagram of high-temperature stress relaxometer

A lower sample grip
B thermocouples (TC)
C main block heater, 500W (not shown)
D autotransformer (Variac)
E temperature readout (Doric Trendicator 412A)
F cold junction compensator (Omega Engineering)
G zero suppression circuit for TC output
H load amplifier/indicator (Daytronic 3230)
I strip chart recorder (Fisher Recordall)
J power bar
K LVDT (Daytronic 152A-10)
L TC's monitoring 5 auxiliary band heaters (Watlow 9859LX)
M multichannel reference junction (Omega OM-101)
N power supply (Power-One HTAA-16W)
O multiplexer (Analog Devices AD7501)
P voltage to frequency converter (Analog Devices AD537)
Q SYM microcomputer (6502 processor, 1K RAM)
R solid state relays (Opto-22, P120D2)
S voltage regulator

Three iron-constantan thermocouples are positioned near the sample. Two of these connect to the temperature indicator and the third is used as the input to the zero-suppression circuit. Two additional thermocouples monitor the temperature of the main block and of the LVDT chamber.

The zero-suppression module allows the suppression of integral millivolt values input from the cold junction compensator so that its output may consist of the fraction of input millivolts only. For example, for an input of 9.3 mV, the 9 mV can be suppressed to allow an output of 0.3 mV. On a recorder set to display 1 mV full scale, the temperature can easily be followed to $\pm$ 0.1^{o}C, since an interval of 0.1 mV spans 2^{o}C. This permits very precise monitoring of temperature fluctuations in the course of an experiment.

The temperature is kept constant by the electronic circuit designed around the SYM microcomputer. The temperature is monitored continually and input to the computer. The detailed components of the temperature input section are shown in Figure IV-2. These were mounted on a printed circuit board. The band heaters are turned ON or OFF by the computer through relays designed for TTL control of AC loads. The software developed for this temperature controller is given in Appendix V, in commented version, together with a list of the parameters to be input by the user.

Figure A4-2: Electronic circuit built for SYM-based temperature controller

Connections of Multiplexer (MUX) AD7501:

1	select line A1 to SYM
2	ground (GND)
3	enable line to SYM
4	select line A2 to SYM
5	GND
6	GND
7	thermocouple 5 (TC5)
8	TC4
9	TC3
10	TC2
11	TC1
12	output signal to V/F
13	output to OM101 reference line
14	+5 V
15	GND
16	select line A0 to SYM

Connections of Voltage to Frequency Converter (V/F) AD537

1	GND
2	sync line to SYM
3	I_{in}
4	$-V_{in}$
5	$+V_{in}$
6	GND
7	V_{ref}
8	GND
9	+5 V
10	+5 V
11	
12	
13	+5 V
14	output to SYM

All dashed lines connect to OM-101 reference junction

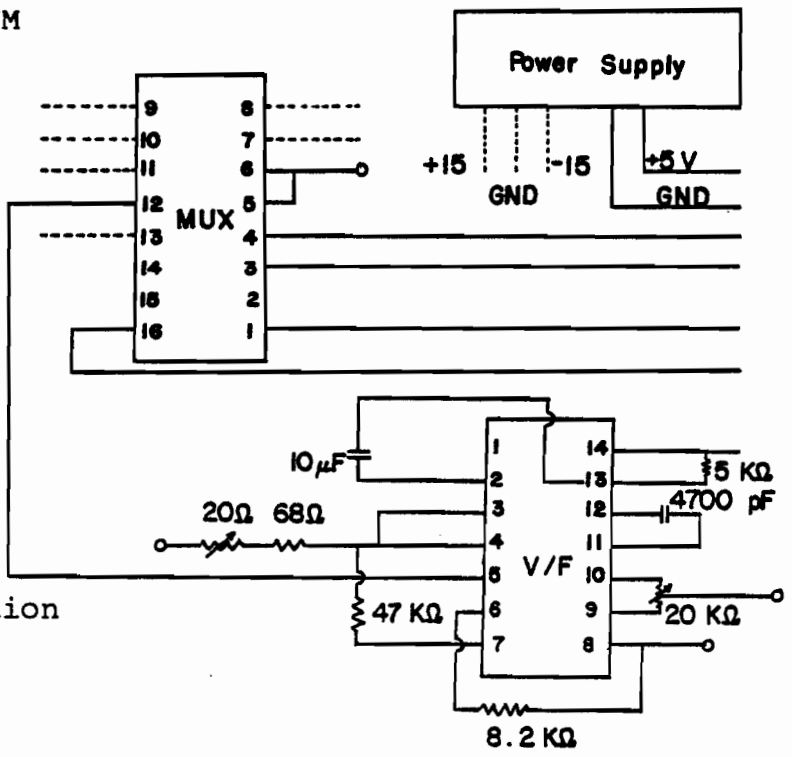

Calibration of the instrument is necessary to establish the Variac setting and the values to input for frequency in order to maintain a particular temperature. The values determined in the temperature range used in this work are given in Table IV.2. They were determined in conjunction with the program in the ON/OFF mode. The same settings used with the program in the CONTINUOUS mode generally yielded a temperature higher by approximately 25°. The width of the acceptable frequency range was always chosen to be 5 Hz.

Table IV.2 Relationship between temperature and instrumental settings with 1 second heating period for the auxiliary heaters (ON/OFF mode)

Variac (V)	Frequency Hz	Frequency Hexadecimal input to SYM	Temperature (°C ±0.1)
30	3300	0CE4	210.0
35	3400	0D48	223.0
35	3800	0ED8	230.0
38	3600	0E10	234.2
38	3800	0ED8	235.8
40	3800	0ED8	246.5
42	4000	0FA0	257.0
45	4200	1068	267.7
50	4400	1130	288.9
53	4400	1130	294.9

APPENDIX V

SYM MACHINE LANGUAGE PROGRAM FOR TEMPERATURE CONTROL FOR HIGH TEMPERATURE STRESS RELAXOMETER

C. G. BAZUIN & E. BESSO
MARCH 1983

DESCRIPTION

THE TEMPERATURE OF 5 AUXILIARY BAND HEATERS IS CONTINUALLY MONITORED SO AS TO KEEP THE SAMPLE AT A CONSTANT (±0.1 C) TEMPERATURE. A THERMOCOUPLE IS LOCATED CLOSE TO EACH BAND HEATER. FOLLOWING PASSAGE THROUGH A REFERENCE JUNCTION COMPENSATOR, THE MULTIPLEXED THERMOCOUPLE INPUTS REACH THE SYM MICROCOMPUTER THROUGH A VOLTAGE TO FREQUENCY (V/F) CONVERTER.

IN THE CASE WHERE A HEATER'S TEMPERATURE FALLS BELOW THE SPECIFIED RANGE, THE PROGRAM ACTIVATES A CORRESPONDING SOLID STATE RELAY WHICH ALLOWS VOLTAGE TO GO THROUGH THE HEATER. TWO VERSIONS OF THE SOFTWARE ALLOW THIS TO BE DONE EITHER IN CONTINUOUS HEATING MODE OR IN ON/OFF HEATING MODE. IN THE LATTER CASE, THE USER MAY SELECT THE DURATION OF THE ON CYCLE OF THE HEATER.

IN THE CASE OF A TEMPERATURE INPUT WHICH FALLS ABOVE THE SPECIFIED RANGE, THE RELAY OPENS AND THE HEATER IS INACTIVATED. A V/F CONVERTER IS USED INSTEAD OF AN ADC BECAUSE THE FORMER HAS A LINEAR, TEMPERATURE PROPORTIONAL OUTPUT WHICH ALLOWS DIRECT TEMPERATURE TO FREQUENCY CONVERSION. THE V/F CONVERTER DELIVERS AN OUTPUT OF 10 Hz/DEGREE C.

PARAMETERS TO BE INPUT BY THE USER:

LOW BYTE OF DESIRED FREQUENCY	MEMORY LOCATION	$14
HIGH BYTE OF DESIRED FREQUENCY		$15
WIDTH OF ACCEPTABLE FREQUENCY RANGE		$16
DURATION OF HEATER ON CYCLE (OPTIONAL)		$3BB

FOR 1 SECOND (DEFAULT VALUE)	INPUT	04
2 SECONDS		03
3 SECONDS		02
4 SECONDS		01

PROGRAM ORGANIZATION

```
MAIN:          $200 - $206          CALLING THE SUBROUTINES:

CONFIG:        $270 - $298

HCNTL2:        $2B0 - $2C6          INCORPORATING:
               $2D8 - $32A          MORE
               $3A0 - $3E7          LOOP2, LOOP3
               $3B9 - $3C4          HONOFF (ON/OFF MODE ONLY)

MEAST:         $330 - $375

MULT:          $400 - $487


LIST OF REGISTERS: DDRA=$A803
                   DDRB=$A802
                   PCR =$A80C
                   IORA=$A801
                   ACR =$A80B
                   IORB=$A800
                   T1CL=$A804
                   T2CL=$A808
                   T1CH=$A805
                   T2CH=$A809
                   IFR =$A80D


VARIABLES:     NUMHTR=$10   NUMBER OF HEATERS
               CYCLES=$11   SETS SAMPLING TIME OF THERMOCOUPLES
               COUNTR=$12   SAME FUNCTION AS CYCLES
               TIN    =$14  LOW BYTE (LB) DESIRED FREQUENCY
               TIN+1  =$15  HIGH BYTE (HB) DESIRED FREQUENCY
               TSUB2  =$16  WIDTH OF ACCEPTABLE FREQUENCY RANGE
               TLOW   =$1A  FREQUENCY LOWER LIMIT, LB ($1B,HB)
               THIGH  =$1E  FREQUENCY UPPER LIMIT, LB ($1F,HB)
               TMEAS  =$22  FREQUENCY MEASURED, LB ($23,HB)
               MUL    =$26  REFERENCE TEMP CORRECTION,LB($27,HB)
               STOREL=$30
               STOREH=$40
```

COMMENTED VERSION

MAIN is the master program which calls the subroutines CONFIG and HCNTL2

```
MAIN:          JSR CONFIG                  200  20 70 02
```

```
                JSR HCNTL2              203  20 B0 02
                BRK                     206  00
```

ON/OFF OPERATING MODE (SEE MARGIN FOR CONTINUOUS MODE CHANGES)

Set up input/output lines, timer controls, constants, etc.

```
CONFIG:   CLD           270  D8
          LDA #$0F      271  A9 0F      Sets PA0 to PA3 as outputs
          STA DDRA      273  8D 03 A8   (PA0-2 MUX channel select,
                                        PA3 MUX enable)
          LDA #$3F      276  A9 3F      Sets PB1 to PB5 as outputs
          STA DDRB      278  8D 02 A8   to auxiliary heaters, PB6
                                        as input from V/F converter
          LDA #$00      27B  A9 00      PCR control lines set as
          STA PCR       27D  8D 0C A8   inputs

          STA IORA      280  8D 01 A8   Multiplexer disabled

          LDA #$60      283  A9 60      Sets timer controls: T1 to
          STA ACR       285  8D 0B A8   operate in free-running mode
                                        T2 to count pulses on PB6
          LDA #$05      288  A9 05      Number of auxiliary heaters
          STA NUMHTR    28A  85 10      specified

          LDA #$14      28C  A9 14      Number of T1 cycles (20)
          STA CYCLES    28E  85 11      specified

          LDA #$4E      290  A9 4E      Value stored in T1 counter
          STA COUNTR    292  85 12      (50,000)
          LDA #$C3      294  A9 C3
          STA COUNTR+1  296   85 13     Total period of counting :
                                        20*50,000*1E-6 = 1 second
                                        for  a 1 MHz clock rate
                                        i.e. sampling time per
                                        thermocouple is 1 second

          RTS           298  60         End of CONFIG

HCNTL2    SEC           2B0  38
          LDA TIN       2B1  A5 14      Get lo byte of frequency
          STA  THIGH    2B3  85 1E      input by  user - this is
                                        upper frequency of range
          SBC TSUB2     2B5  E5 16      Range
          STA TLOW      2B7  85 1A      Lower frequency of range
          LDA TIN+1     2B9  A5 15      Hi byte frequency input
          STA THIGH+1   2BB  85 1F      Hi byte upper frequency
          SBC #$00      2BD  E9 00
          STA TLOW+1    2BF  85 1B      Hi byte lower frequency
          CLC           2C1  18

          LDX NUMHTR    2C2  A6 10      Get number of auxiliary
                                        heaters to be controlled
```

```
          JMP LOOP2    2C4   4C A0 03

                                              CONT.MODE
                                              $3A0-$3A4
                                              ALL  "EA"

LOOP2     LDA #$00     3A0   A9 00      Turn off heater that
          JSR HONOFF   3A2   20 B9 03   may have been turned on
                                        1 - 4 seconds earlier
          LDA #$08     3A5   A9 08      Enable MUX for sampling
          STA IORA     3A7   8D 01 A8   of channel 0 (reference T)

          JSR MEAST    3AA   20 3B 03   Get frequency
                                        corresponding
                                        to reference temperature
          JMP MULT     3AD   4C 00 04   Multiply by correction
                                        factor



HONOFF    SEC          3B9   38         Routine to turn off a
          SBC #$04     3BA   E9 04      heater
          BPL SHUTDOWN 3BC   10 03
          CLC          3BE   18
          ADC #$06     3BF   69 06
SHUTDOWN  JSR HEATOF   3C1   20 19 03
          RTS          3C4   60            End of HONOFF

                                              CONT. MODE
                                              $3CB-$3CE
                                              ALL  "EA"

LOOP3     TXA          3CB   8A
          JSR HONOFF   3CC   20 B9 03
          TXA          3CF   8A         Get frequency representing
          ORA #$08     3D0   09 08      temperature of one of the
          STA IORA     3D2   8D 01 A8   thermocouples (one of
          JSR MEAST    3D5   20 3B 03   channels 1-5 of multiplexer)

          CLC          3D8   18         Add reference temperature
          LDA MUL      3D9   A5 26      correction
          ADC TMEAS    3DB   65 22
          STA TMEAS    3DD   85 22
          LDA MUL+1    3DF   A5 27
          ADC TMEAS+1  3E1   65 23
          STA TMEAS+1  3E3   85 23

          JMP MORE     3E5   4C D8 02

MORE      SEC          2D8   38         Compare measured frequency
          LDA TMEAS    2D9   A5 22      with minimum frequency of
          SBC TLOW     2DB   E5 1A      range
          LDA TMEAS+1  2DD   A5 23
          SBC TLOW+1   2DF   E5 1B
          TXA          2E1   8A         If measured frequency is
          BCC ONHEAT   2E2   90 14      lower, turn on corresponding
```

```
                                                    heater

          LDA TMEAS    2E4   A5 22      Compare measured frequency
          SBC THIGH    2E6   E5 1E      with maximum frequency of
          LDA TMEAS+1  2E8   A5 23      range
          SBC THIGH+1  2EA   E5 1F
          TXA          2EC   8A         If measured frequency
          BCS OFHEAT   2ED   B0 0F      higher,turn corresponding
                                        heater off
CONTIN    CLC          2EF   18
          DEX          2F0   CA         Next thermocouple
          BNE JUMP     2F1   D0 38

          LDX NUMHTR   2F3   A6 10      Repeat sampling of
          JMP LOOP2    2F5   4C A0 03   thermocouples

ONHEAT    JSR HEATON   2F8   20 06 03
          JMP CONTIN   2FB   4C EF 02
OFHEAT    JSR HEATOF   2FE   20 19 03
          JMP CONTIN   301   4C EF 02
          RTS          304   60         End of HCNTL2

          NOP               305  EA
HEATON    TAY               306  A8         Routine to turn
          CLC               307  18         a heater ON
          LDA #%00000001    308  A9 01
LOOPON    DEY               30A  88
          BMI ON            30B  30 04
          ROL A             30D  2A
          JMP LOOPON        30E  4C 0A 03
ON        ORA IORB          311  0D 00 A8
          STA IORB          314  8D 00 A8
          RTS               317  60         End of HEATON
          NOP               318  EA

HEATOF    TAY               319  A8         Routine to turn
          SEC               31A  38         a heater OFF
          LDA #%11111110    31B  A9 FE
LOOPOF    DEY               31D  88
          BMI OFF           31E  30 04
          ROL A             320  2A
          JMP LOOPOF        321  4C 1D 03
OFF       AND IORB          324  2D 00 A8
          STA IORB          327  8D 00 A8
          RTS               32A  60         End of HEATOF

JUMP      JMP LOOP3         32B  4C CB 03
```

The following subroutine MEASures Temperature. T1 is set up in free-running mode (which determines the time interval of counting per cycle). T2 counts negative pulses on PB6 by decrementing its counter (T2CL & T2CH) with each pulse. The number of PB6 pulses counted never exceeds $FFFF in our application.

```
MEAST     LDY CYCLES   33B  A4 11      Get number of cycles
                                       for timing
          LDA COUNTR   33D  A5 12      Get number of counts
                                       per cycle
          STA T1CL     33F  8D 04 A8   of T1 (lo byte)

          LDA #$FF     342  A9 FF      Load T2 counter (lo byte)
          STA T2CL     344  8D 08 A8

          LDA COUNTR+1  347  A5 13       Get hi byte of counts
                                         for T1
          STA T1CH       349  8D 05 A8   T1 starts

          LDA #$FF     34C  A9 FF      Test T1 flag for end of
          STA T2CH     34E  8D 09 A8   cycle(50 msec per cycle)

TEST      LDA #$40     351  A9 40      Test T1 flag for end of
          BIT IFR      353  2C 0D A8   cycle(50 msec per cycle)

          BEQ TEST     356  F0 F9
          LDA T1CL     358  AD 04 A8   Dummy read to clear T1
                                       interrupt flag
          DEY          35B  88         Repeat "CYCLES" times for
                                       total of 1 second
          BNE TEST     35C  D0 F3      of sampling

          LDA T2CL     35E  AD 08 A8   Store value of T2 counter.
          STA STOREL   361  85 30      This stops timer.
          LDA T2CH     363  AD 09 A8
          STA STOREH   366  85 40

          SEC          368  38         Convert to actual
          LDA #$FF     369  A9 FF      number ofpulses
          SBC STOREL   36B  E5 30      counted during the
          STA TMEAS    36D  85 22      1 second of sampling
          LDA #$FF     36F  A9 FF
          SBC STOREH   371  E5 40
          STA TMEAS+1  373  85 23

          RTS          375  60         End of MEAST

HALT      BRK          3FF  00
```

The following subroutine MULTiplies a hexadecimal number by 0.0517

```
MULT      LDA TMEAS    400  A5 22
          STA MUL      402  85 26
          LDA TMEAS+1  404  A5 23
          STA MUL+1    406  85 27
          SEC          408  38
          SBC #$1C     409  E9 1C
          BPL HALT     40B  10 F2      Number (T) too high.
                                       Stop program
          JMP AHEAD    40D  4C 23 04
```

```
AHEAD     LSR TMEAS+1 423   46 23      Shift right one time
          ROR TMEAS   425   66 22
          JSR ADD           427  20 7B 04      Add, store
          LSR TMEAS+1       42A  46 23          Shift right
          ROR TMEAS         42C  66 22          two times
          LSR TMEAS+1       42E  46 23
          ROR TMEAS         430  66 22
          JSR ADD           432  20 7B 04      Add, store
          LSR TMEAS+1       435  46 23          Shift right
          ROR TMEAS         437  66 22          three times
          LSR TMEAS+1       439  46 23
          ROR TMEAS         43B  66 22
          LSR TMEAS+1       43D  46 23
          ROR TMEAS         43F  66 22
          JSR ADD           441  20 7B 04      Add, store
          LSR TMEAS         444  46 22
          JSR ADD           446  20 7B 04
          LSR TMEAS         449  46 22
          JSR ADD           44B  20 7B 04
          LSR TMEAS         44E  46 22
          JSR ADD           450  20 7B 04
          LSR MUL+1         453  46 27
          ROR MUL           455  66 26
          LSR MUL+1         457  46 27
          ROR MUL           459  66 26
          LSR MUL+1         45B  46 27
          ROR MUL           45D  66 26
          LSR MUL+1         45F  46 27
          ROR MUL           461  66 26
          LSR MUL+1         463  46 27
          ROR MUL           465  66 26
          NOP               467  EA
          NOP               468  EA
          BCC ENDMU         469  90 0D
          CLC               46B  18
          LDA #$01          46C  A9 01
          ADC MUL           46E  65 26
          STA MUL           470  85 26
          LDA #$00          472  A9 00
          ADC MUL+1         474  65 27
          STA MUL+1         476  85 27
ENDMU     JMP LOOP3         478  4C CB 03

ADD       CLC               47B  18
          LDA TMEAS         47C  A5 22
          ADC MUL           47E  65 26
          STA MUL           480  85 26
          LDA TMEAS+1       482  A5 23
          ADC MUL+1         484  65 27
          STA MUL+1         486  85 27
          RTS               488  60            End of ADD
```

NOTES

The sequence of shifts for multiplying by X = 0.0517 was obtained by using the following BASIC program :

```
10    X = 0.0517000
20    FOR I = 0  TO  -20  STEP -1
30    IF X >  2E*I, THEN PRINT X = X - {2E*I}
40    NEXT
```

To MULTIPLY a hexadecimal number by 0.051696 (see OM101 Reference Junction manual - Omega Engineering):

The sequence of total arithmetic shifts to the right of the original number is:

5,6,8,11,12,13,14;

or, at each step, on current number,

5,1,2,3,1,1,1;

ADD the numbers that are the result of each step.

It has been found that sufficient accuracy is obtained when

1. the original number is first shifted left 5 times before the shift right and the adds are performed

2. the final result is incremented by 1 if the last bit shifted out, right, is high (i.e. if carry was set by the last 6 or 7 right shifts).

Outline of MULT routine

1. Test high byte of number. If higher than $1C - out of range for our set-up. Stop program.

2.
```
                                store # as is
                                shift right 1 time
                                add to number in store
                                store
                                shift right 2 times
                                add
                                store
                                shift right 3 times
                                add
                                store
   Do these 3 operations 3 times:    shift right 1 time
                                     add
                                     store
```

3. Shift right 5 times

4. If carry set, INCrement result by 1.

APPENDIX VI

TABLES OF SUPPORTING DATA FOR FIGURES

Figure 9; p. 44

	T (°C)	% weight loss
600EW ester	366	0
	385	0.5
	390	0.7
	394	0.9
	399	1.4
	403	1.8
	406	2.3
	408	2.5
	412	2.7
	421	4
	430	5.5
	439	7
	448	9
	457	12
	466	14
	475	15
	493	16
	511	17
	528	20
	546	23
600EW-f	366	0
	376	0.1
	381	0.5
	385	0.7
	394	1
	403	1.4
	412	1.7
	421	2
	430	3
	439	4
	448	5
	457	6.5
	475	8.5
	493	10
	502	12
	511	13
	528	15.7
	546	19

Figure 10; p. 45

	Temperature (°C)	% Weight Loss
600EW ester	100	0
	150	0
	185	1.5
	220	1.5
	260	4.5
	300	24.4
	345	49.8
600EW-f	222	0
	257	3
	304	10.3
	350	20.8
	370	30

Figure 23; p. 64

	time (sec)	Contact angle (± 1°)
Nafion precursor	30	89
	60	89
	90	89
	150	88
Nafion 1200	30	78
	60	74
	90	69
	150	67
600EW ester	30	66
	65	62
	150	54
600EW-f	20	79
	60	55
	90	43
	150	11

Figure 27; p. 69 800EW ester

T (°C)	Tan x 10^2	Frequency (Hz)	T (°C)	Tan x 10^2	Frequency (Hz)
-190	.45	323	-82	2.23	296
-187	.46	322	-80	2.27	295
-184	.47	321	-78	2.33	295
-182	.48	321	-76	2.32	294
-180	.49	321	-74	2.37	292
-178	.49	321	-72	2.41	291
-176	.50	321	-70	2.43	291
-174	.52	321	-68	2.49	289
-172	.53	321	-66	2.55	289
-170	.53	321	-63	2.63	288
-168	.55	321	-60	2.63	286
-166	.58	320	-58	2.62	283
-164	.59	320	-55	2.50	283
-162	.60	320	-52	2.45	282
-160	.62	320	-50	2.38	282
-158	.64	319	-48	2.35	281
-156	.65	319	-46	2.32	279
-154	.67	319	-43	2.23	279
-152	.68	319	-40	2.17	277
-150	.69	319	-31	1.86	273
-148	.71	319	-28	1.77	273
-146	.73	318			
-144	.75	318			
-142	.76	318			
-140	.79	318			
-139	.81	318			
-136	.83	317			
-134	.85	316			
-132	.86	316			
-130	.90	316			
-128	.93	315			
-126	.97	314			
-124	1.01	314			
-121	1.07	313			
-118	1.12	312			
-116	1.16	312			
-114	1.20	311			
-112	1.22	310			
-110	1.27	309			
-108	1.34	308			
-105	1.39	307			
-102	1.44	306			
-100	1.52	305			
-98	1.60	304			
-94	1.73	303			
-92	1.81	302			
-89	1.92	300			
-87	1.99	298			
-85	2.10	298			

Figure 27; p. 69 600EW ester

T (°C)	Tan x 10^2	Frequency (Hz)	T (°C)	Tan x 10^2	Frequency (Hz)
-193	1.58	225	-60	2.29	218
-191	1.56	228	-58	2.36	215
-187	1.52	227	-56	2.38	217
-182	1.46	230	-54	2.41	213
-179	1.44	229	-51	2.50	215
-176	1.39	230	-49	2.47	215
-173	1.37	229	-47	2.57	214
-171	1.33	229	-45	2.65	210
-166	1.31	230	-42	2.64	213
-161	1.26	229	-40	3.99	211
-159	1.28	230	-37	3.04	213
-157	1.23	229	-35	2.61	211
-155	1.24	229	-33	2.85	208
-153	1.23	230	-31	2.67	208
-151	1.25	229	-28	2.58	208
-147	1.20	230	-26	2.58	207
-145	1.16	230	-24	2.59	207
-143	1.20	228	-20	2.60	203
-141	1.20	228			
-139	1.19	228			
-137	1.20	228			
-134	1.2	228			
-132	1.18	229			
-127	1.22	228			
-125	1.23	228			
-123	1.19	227			
-120	1.24	227			
-118	1.19	229			
-116	1.35	229			
-114	1.27	227			
-112	1.31	226			
-109	1.25	226			
-107	1.30	226			
-104	1.30	226			
-101	1.37	225			
-99	1.43	226			
-97	1.44	225			
-93	1.50	224			
-91	1.56	224			
-89	1.58	224			
-87	1.67	223			
-85	1.71	223			
-79	1.85	222			
-77	1.94	222			
-74	2.04	221			
-72	2.08	220			
-70	2.14	220			
-67	2.21	219			
-65	2.25	216			
-63	2.26	219			

Figure 28; p. 71

	Stress (MPa)	Strain (%)
600EW ester	7	0.8
	14	1.4
	23	2.3
	29	3.1
	32	3.5
	35	4.3
	37	5.0
	38.2	6.2
	38.4	7.8
	36	23
	37	47
	39	70
	41	94
	43	113
	46	137
	49	164
600EW-f, 70 % neutralized	9	1.6
	18	3.2
	28	5.2
	37	7.2
	46	9.6
	55	13
	64	17
Nafion 1200	7	2.5
	13	4
	17	11
	19	20.5
	20	32
	22	51
	24	76
	27	105
	30	128
	33	152
	35	175

Figure 29; p. 72

	Stress (MPa)	Strain (%)
600EW-f, 25°C	5.2	0.7
	10	1.0
	15	1.3
	21	1.7
	24	1.9
	26	2.1
	27	2.3
100°C	5.6	0.4
	11	0.9
	17	1.3
	22	1.8
200°C	5.8	0.3
	12	0.5
	17	0.7
	20	1.0
290°C	0.3	0.4
	0.5	0.7
	0.8	0.95
	1.0	1.1
	1.3	1.3
	1.8	1.6
	2.6	1.9

Figure 30; p. 75

	Stress (MPa)	Strain (%)
600EW ester	7	0.5
	14	0.9
	25	1.7
	32	2.5
	34.9	3.6
	34.6	7.3
	35.6	17.5
	36	23.0
	37	28.0
	37.7	32.1
	38	36.8
600EW-f, 70 % neutralized	9	1.3
	20	3.5
	27	5.3
	29.7	7.7
	29.2	42.0
	30	50.4
	31	55.7
600EW-f, >85 % neutralized	4	2
	8	5
	10	6
	12	9
	13	12
	15	22
	16.5	38
	17.1	46
	17.8	57
	17.8	58

Figure 31; p. 77

	Stress (MPa)	Strain (%)
600EW-f-I	6	2.4
	12	4
	18	5.6
	24	8.4
	28	12.8
	29	21.6
	29.7	28
	30.3	33.6
	31.5	48
	31.9	56
600EẆ-f-II	1	0.4
	2	0.9
	5	1.9
	6	2.8
	7	3.9
	8	5.4
	9	7.1
	11	9.1
	13	14
	14	16.2
	15	18.6
	17	21
	17	23

Figure 32; p. 78

		Stress (MPa)	Strain (%)
600EW-f,	a	2	2.9
		4	6.9
		6	12
		7.5	18
		9	25
		11	32
	b	2	1.6
		4	3.5
		5	4.8
		5.7	6.1
		6.6	7.7
		7.5	9.6
		8.5	11.7
		9	14
		10	17
		11.3	19.7
		11.6	21.3
	c	1.6	1.9
		3	4.3
		5	7.2
		6.5	12.8
		8	19
		8.2	20

Figure 33; p. 79 600EW-f

	Stress (MPa)	Strain (%)
kept at ambient conditions	4	3.2
	8	5.6
	10	7.2
	11	9
	13	12.8
	15	19.2
	17	29.6
	18.9	46.4
	19.1	47.2
dried *in. vacuo*.	1	0.4
	2	0.9
	5	1.9
	6	2.8
	7	3.9
	8	5.4
	9	7.1
	11	9.1
	12	11.3
	13	14
	14	16.2
	15	18.6
	16.5	21
	17.1	23
continuously kept in water	- same values as in Fig. 30, for 600EW-f, >85 % neutralized	

Figure 34; p. 82

in 5.6 % (0.1 *M*) KOH	- same values as in Fig. 30, for 600EW-f, >85 % neutralized	
in 20 % KOH	5	1.3
	7	3.8
	9	5.2
	12	7
	15	11.8
	16	17
	17	26
	18.1	38.1
	18.5	42.8
	18.6	44.7

Figure 35; p. 83 Nafion 1200

	Stress (MPa)	Strain (%)
in water	2	2
	4	8
	6	16
	7	40
	7.5	56
	8	84
	10	120
	11	156
	13	204
	14	240
	17	324
	18	336
	18.5	352
	19	372
	20	388
	20.6	395
in 5.6 % (0.1 M) KOH	3	4
	7	8
	8	18
	9	34
	11	74
	14	140
	16	192
	18.1	242
	18.6	264
in 20 % KOH	2	1.3
	5	2.6
	7	4
	8	5.3
	9	10.6
	10	17
	11	29
	12	41
	13	67
	15	100
	16.5	135
	17.5	155

dry state - same values as given for Figure 28

Figure 36; p. 84

	T (°C)	E (MPa)
600EW-f	28	175
	50	139
	80	75
Nafion 1200	27	230
	50	175
	80	120

Figure 37; p. 86 600EW ester , stress relaxation

Temperature (°C)	Log Time (sec)	Log E (MPa)
223.0	0.4771	8.6536
	0.6990	8.6370
	0.8451	8.6081
	1.0000	8.5991
	1.2304	8.5774
	1.3979	8.5647
	1.5441	8.5449
	1.8451	8.5102
	2.0170	8.4728
	2.1818	8.4325
	2.3979	8.3746
	2.5933	8.3089
	2.8089	8.2326
	3.0017	8.1568
	3.2052	8.0380
	3.3986	7.8906
	3.5893	7.7681
229.1	0.6021	8.5510
	0.7782	8.5210
	1.0000	8.4839
	1.2041	8.4448
	1.3979	8.3889
	1.6021	8.3187
	1.7993	8.2391
	2.0000	8.1540
	2.1987	8.0786
	2.3979	7.9581
	2.6021	7.8066
	2.7993	7.6216
	3.0000	7.4826
	3.2000	7.3085
	3.3997	7.2460
	3.5999	7.0158
	3.8000	6.9091

Temperature (°C)	Log Time (sec)	Log E (MPa)
235.9	0.4771	8.2385
	0.8451	8.0532
	1.0000	7.9526
	1.1761	7.8314
	1.3979	7.6623
	1.5911	7.5077
	1.7993	7.3397
	1.9956	7.1624
	2.1847	7.0369
	2.4065	6.9574
	2.6010	6.8602
246.8	0.6021	7.2834
	0.7782	7.0699
	1.0000	6.9369
	1.2041	6.8698
	1.3979	6.7904
	1.6021	6.7446
	1.7993	6.6934
	2.1987	6.6353
	2.3979	6.5683
	2.6021	6.5683
	2.7993	6.4890
	3.2000	6.3920
	3.3997	6.3920
	3.5999	6.3920
	3.8000	6.2670
256.6	0.6021	6.7728
	0.7782	6.7350
	1.0414	6.6935
	1.2041	6.6635
	1.3979	6.6312
	1.6021	6.5779
	1.7993	6.5384
	1.9823	6.5172
	2.1875	6.4714
	2.4378	6.4202
	2.6085	6.3921
	2.8102	6.3299
	3.0000	6.2951
	3.1976	6.2573
	3.3990	6.2159
	3.5994	6.1701
	3.8004	6.0609
	4.0003	6.0609
	4.2002	5.9147
	4.3269	5.9147
	4.4253	5.8178
	4.5055	5.8178

Figure 24; p. 65 & Figure 26; p.68

TEMP.	TAN DELTA	G′	G′′	FREQ.
-190.4	0.00973	8.945E+08	8.703E+06	2.3889
-189.5	0.00978	8.924E+08	8.728E+06	2.3861
-187.2	0.00985	8.906E+08	8.772E+06	2.3837
-183.9	0.00986	8.859E+08	8.735E+06	2.3775
-180.0	0.01001	8.802E+08	8.811E+06	2.3699
-177.5	0.01016	8.756E+08	8.896E+06	2.3638
-174.7	0.01010	8.725E+08	8.812E+06	2.3595
-172.0	0.01026	8.658E+08	8.883E+06	2.3505
-170.0	0.01035	8.612E+08	8.913E+06	2.3443
-168.0	0.01023	8.594E+08	8.792E+06	2.3419
-166.2	0.01030	8.813E+08	9.077E+06	2.3364
-164.0	0.01038	8.484E+08	8.806E+06	2.3269
-160.5	0.01038	8.444E+08	8.765E+06	2.3215
-157.4	0.01058	8.405E+08	8.892E+06	2.3162
-156.0	0.01062	8.385E+08	8.905E+06	2.3135
-153.8	0.01070	8.349E+08	8.933E+06	2.3085
-152.0	0.01086	8.315E+08	9.030E+06	2.3038
-150.0	0.01095	8.284E+08	9.071E+06	2.2995
-146.5	0.01130	8.193E+08	9.258E+06	2.2870
-144.2	0.01154	8.191E+08	9.452E+06	2.2867
-141.2	0.01194	8.125E+08	9.701E+06	2.2776
-140.0	0.01217	8.100E+08	9.858E+06	2.2740
-137.4	0.01268	8.035E+08	1.019E+07	2.2650

800EW ESTER, FILE EB800.EST

TEMP.	TAN DELTA	G'	G''	FREQ.
-136.0	0.01308	8.027E+08	1.050E+07	2.2638
-134.0	0.01359	7.963E+08	1.082E+07	2.2548
-131.0	0.01426	7.930E+08	1.131E+07	2.2504
-128.0	0.01532	7.835E+08	1.200E+07	2.2368
-125.5	0.01614	7.811E+08	1.261E+07	2.2334
-123.5	0.01700	7.746E+08	1.317E+07	2.2241
-122.0	0.01761	7.726E+08	1.361E+07	2.2212
-120.0	0.01871	7.674E+08	1.436E+07	2.2138
-118.0	0.01952	7.617E+08	1.487E+07	2.2057
-116.0	0.02047	7.548E+08	1.545E+07	2.1857
-114.2	0.02119	7.511E+08	1.592E+07	2.1903
-112.0	0.02231	7.448E+08	1.662E+07	2.1812
-110.2	0.02287	7.364E+08	1.684E+07	2.1690
-108.0	0.02382	7.332E+08	1.746E+07	2.1643
-106.0	0.02449	7.263E+08	1.779E+07	2.1541
-104.0	0.02518	7.197E+08	1.812E+07	2.1443
-102.2	0.02570	7.134E+08	1.833E+07	2.1351
-100.0	0.02635	7.057E+08	1.860E+07	2.1235
-96.5	0.02726	6.958E+08	1.897E+07	2.1087
-95.0	0.02744	6.912E+08	1.897E+07	2.1019
-92.0	0.02812	6.823E+08	1.919E+07	2.0884
-90.0	0.02837	6.761E+08	1.918E+07	2.0790
-88.0	0.02873	6.702E+08	1.925E+07	2.0700

800EW ESTER, FILE EB800.EST

TEMP.	TAN DELTA	G′	G′′	FREQ.
-86.0	0.02881	6.642E+08	1.914E+07	2.0607
-84.0	0.02908	6.596E+08	1.918E+07	2.0536
-80.5	0.02907	6.468E+08	1.880E+07	2.0338
-76.6	0.02906	6.356E+08	1.847E+07	2.0162
-75.0	0.02865	6.322E+08	1.811E+07	2.0109
-72.0	0.02810	6.270E+08	1.762E+07	2.0027
-69.2	0.02755	6.187E+08	1.705E+07	1.9895
-67.0	0.02660	6.143E+08	1.634E+07	1.9825
-64.5	0.02573	6.102E+08	1.570E+07	1.9759
-61.3	0.02392	6.025E+08	1.441E+07	1.9636
-59.8	0.02394	6.036E+08	1.445E+07	1.9653
-58.0	0.02327	5.992E+08	1.394E+07	1.9582
-55.4	0.02190	5.978E+08	1.309E+07	1.9560
-52.7	0.02033	5.940E+08	1.208E+07	1.9498
-50.0	0.01938	5.925E+08	1.148E+07	1.9474
-46.5	0.01794	5.897E+08	1.058E+07	1.9429
-42.5	0.01645	5.848E+08	9.620E+06	1.9348
-39.8	0.01543	5.833E+08	9.000E+06	1.9325
-33.6	0.01348	5.797E+08	7.814E+06	1.9265
-30.0	0.01234	5.778E+08	7.130E+06	1.9233
-26.5	0.01160	5.769E+08	6.692E+06	1.9219
-22.8	0.01063	5.779E+08	6.143E+06	1.9236
-20.0	0.00994	5.767E+08	5.732E+06	1.9216

800EW ESTER, FILE EB800.EST

TEMP.	TAN DELTA	G'	G''	FREQ.
-17.6	0.00986	5.740E+08	5.660E+06	1.9171
-15.0	0.00941	5.724E+08	5.386E+06	1.9145
-12.4	0.00890	5.740E+08	5.109E+06	1.9171
-10.0	0.00851	5.733E+08	4.879E+06	1.9160
-7.4	0.00815	5.697E+08	4.643E+06	1.9100
-5.0	0.00800	5.697E+08	4.558E+06	1.9100
-2.7	0.00782	5.687E+08	4.447E+06	1.9084
0.0	0.00767	5.687E+08	4.362E+06	1.9084
2.8	0.00757	5.672E+08	4.294E+06	1.9058
5.0	0.00726	5.688E+08	4.129E+06	1.9086
8.3	0.00726	5.675E+08	4.120E+06	1.9064
10.0	0.00712	5.672E+08	4.038E+06	1.9058
15.0	0.00720	5.653E+08	4.070E+06	1.9028
20.5	0.00726	5.615E+08	4.076E+06	1.8964
25.0	0.00735	5.598E+08	4.115E+06	1.8936
33.0	0.00739	5.580E+08	4.124E+06	1.8906
40.2	0.00770	5.546E+08	4.270E+06	1.8848
47.8	0.00820	5.500E+08	4.510E+06	1.8771
53.0	0.00860	5.457E+08	4.693E+06	1.8698
42.0	0.00756	5.307E+08	4.012E+06	2.1549
57.0	0.00940	5.146E+08	4.837E+06	2.1221
65.0	0.01056	5.093E+08	5.378E+06	2.1112
70.0	0.01182	5.026E+08	5.941E+06	2.0972

800EW ESTER, FILE EB800.EST

TEMP.	TAN DELTA	G'	G''	FREQ.
75.0	0.01120	4.992E+08	5.591E+06	2.0902
80.0	0.01393	4.911E+08	6.841E+06	2.0732
88.0	0.01289	4.897E+08	6.312E+06	2.0703
103.5	0.01500	4.832E+08	7.248E+06	2.0566
110.0	0.01606	4.784E+08	7.683E+06	2.0463
116.5	0.01915	4.679E+08	8.960E+06	2.0238
120.5	0.02014	4.597E+08	9.258E+06	2.0059
126.0	0.02277	4.458E+08	1.015E+07	1.9755
131.5	0.02498	4.380E+08	1.094E+07	1.9582
137.1	0.02633	4.268E+08	1.124E+07	1.9331
145.2	0.02687	4.178E+08	1.123E+07	1.9126
150.0	0.02709	4.124E+08	1.117E+07	1.9002
155.0	0.02734	4.091E+08	1.118E+07	1.8928
160.2	0.02816	4.087E+08	1.151E+07	1.8917
168.2	0.02855	3.965E+08	1.132E+07	1.8634
175.2	0.02970	3.859E+08	1.146E+07	1.8383
188.5	0.03289	3.702E+08	1.218E+07	1.8007
195.0	0.03404	3.664E+08	1.247E+07	1.7915
200.5	0.03693	3.643E+08	1.345E+07	1.7864
205.5	0.03832	3.583E+08	1.373E+07	1.7716
211.0	0.03879	3.245E+08	1.259E+07	1.6664
215.0	0.04062	3.162E+08	1.284E+07	1.6647
218.0	0.04480	3.079E+08	1.379E+07	1.6427

800EW ESTER, FILE EB800.EST

TEMP.	TAN DELTA	G′	G′′	FREQ.
220.0	0.04889	3.030E+08	1.481E+07	1.6296
222.0	0.05600	2.973E+08	1.665E+07	1.6141
224.0	0.06912	2.914E+08	2.014E+07	1.5979
226.0	0.08449	2.809E+08	2.373E+07	1.5686
228.5	0.11385	2.670E+08	3.040E+07	1.5284
236.5	0.40452	1.776E+08	7.184E+07	1.2239
238.0	0.46003	1.379E+08	6.344E+07	1.0727
259.5	0.73482	2.505E+06	1.841E+06	0.1843
263.5	0.49768	1.820E+06	9.058E+05	0.1714
264.7	0.43431	1.716E+06	7.453E+05	0.1692
266.5	0.36626	1.478E+06	5.413E+05	0.1634
269.5	0.30795	1.351E+06	4.160E+05	0.1603
274.0	0.26181	1.117E+06	2.924E+05	0.1540
279.5	0.25746	9.479E+05	2.440E+05	0.1491
283.5	0.26831	8.450E+05	2.267E+05	0.1461
289.0	0.29058	7.433E+05	2.160E+05	0.1431
294.2	0.31418	6.550E+05	2.058E+05	0.1404
297.5	0.33963	5.852E+05	1.988E+05	0.1382
302.0	0.34822	5.626E+05	1.959E+05	0.1375
306.0	0.36090	5.349E+05	1.930E+05	0.1366

Figure 25; p. 67 & Figure 26; p.68

TEMP.	TAN DELTA	G′	G′′	FREQ.
-134.0	0.01071	1.344E+09	1.440E+07	3.3225
-132.0	0.01038	1.345E+09	1.397E+07	3.3237
-130.0	0.01110	1.337E+09	1.484E+07	3.3133
-128.0	0.01075	1.326E+09	1.426E+07	3.2998
-126.0	0.01074	1.327E+09	1.426E+07	3.3011
-125.0	0.01085	1.319E+09	1.432E+07	3.2918
-122.7	0.01117	1.316E+09	1.470E+07	3.2878
-122.5	0.01119	1.316E+09	1.473E+07	3.2880
-120.5	0.01146	1.310E+09	1.501E+07	3.2802
-117.3	0.01194	1.304E+09	1.557E+07	3.2723
-114.6	0.01217	1.290E+09	1.571E+07	3.2555
-112.5	0.01264	1.293E+09	1.634E+07	3.2584
-110.0	0.01284	1.279E+09	1.642E+07	3.2416
-107.5	0.01348	1.275E+09	1.719E+07	3.2359
-105.0	0.01417	1.265E+09	1.793E+07	3.2236
-102.5	0.01489	1.256E+09	1.870E+07	3.2124
-100.0	0.01540	1.253E+09	1.930E+07	3.2087
-97.3	0.01635	1.242E+09	2.030E+07	3.1938
-95.0	0.01664	1.235E+09	2.056E+07	3.1855
-92.5	0.01738	1.231E+09	2.140E+07	3.1801
-90.0	0.01804	1.222E+09	2.205E+07	3.1681
-87.5	0.01872	1.212E+09	2.268E+07	3.1549
-85.0	0.01929	1.204E+09	2.322E+07	3.1443

800EW IONOMER, MOLDED

TEMP.	TAN DELTA	G'	G''	FREQ.
-82.0	0.01925	1.193E+09	2.298E+07	3.1312
-80.0	0.01936	1.188E+09	2.300E+07	3.1241
-77.5	0.01885	1.183E+09	2.231E+07	3.1182
-75.0	0.01892	1.174E+09	2.221E+07	3.1053
-72.5	0.01791	1.168E+09	2.092E+07	3.0981
-70.0	0.01755	1.157E+09	2.031E+07	3.0837
-67.5	0.01668	1.153E+09	1.924E+07	3.0784
-65.0	0.01580	1.150E+09	1.817E+07	3.0740
-62.5	0.01521	1.144E+09	1.741E+07	3.0665
-60.0	0.01401	1.136E+09	1.591E+07	3.0553
-57.5	0.01348	1.133E+09	1.527E+07	3.0511
-55.0	0.01284	1.129E+09	1.449E+07	3.0460
-52.5	0.01215	1.125E+09	1.367E+07	3.0407
-50.0	0.01155	1.122E+09	1.296E+07	3.0363
-47.5	0.01093	1.117E+09	1.221E+07	3.0303
-45.0	0.01088	1.111E+09	1.209E+07	3.0221
-42.5	0.01042	1.109E+09	1.155E+07	3.0184
-40.0	0.00974	1.106E+09	1.078E+07	3.0148
-37.5	0.00978	1.104E+09	1.079E+07	3.0115
-35.0	0.00966	1.100E+09	1.062E+07	3.0064
-32.5	0.00978	1.094E+09	1.070E+07	2.9988
-32.0	0.01145	1.096E+09	1.255E+07	3.0012
-30.0	0.00994	1.089E+09	1.082E+07	2.9913

800EW IONOMER, MOLDED

TEMP.	TAN DELTA	G'	G''	FREQ.
-27.2	0.00955	1.087E+09	1.038E+07	2.9895
-25.0	0.00981	1.083E+09	1.063E+07	2.9833
-22.0	0.00983	1.080E+09	1.061E+07	2.9787
-20.0	0.00946	1.076E+09	1.018E+07	2.9744
-15.5	0.00892	1.072E+09	9.557E+06	2.9682
-15.0	0.01053	1.061E+09	1.117E+07	2.9525
-13.5	0.00948	1.060E+09	1.005E+07	2.9513
-12.0	0.00972	1.053E+09	1.024E+07	2.9426
-9.5	0.00947	1.052E+09	9.964E+06	2.9409
-8.0	0.00906	1.053E+09	9.538E+06	2.9424
-6.0	0.00959	1.049E+09	1.006E+07	2.9370
-3.0	0.00931	1.047E+09	9.750E+06	2.9343
0.0	0.00988	1.039E+09	1.027E+07	2.9228
4.3	0.01065	1.034E+09	1.101E+07	2.9158
7.0	0.01083	1.027E+09	1.113E+07	2.9061
10.0	0.01148	1.025E+09	1.176E+07	2.9026
15.0	0.01210	1.015E+09	1.227E+07	2.8882
18.0	0.01255	1.011E+09	1.269E+07	2.8834
20.5	0.01304	1.006E+09	1.312E+07	2.8759
24.0	0.01365	9.959E+08	1.360E+07	2.8614
30.0	0.01463	9.861E+08	1.443E+07	2.8475
33.0	0.01521	9.801E+08	1.490E+07	2.8388
36.4	0.01528	9.755E+08	1.490E+07	2.8321

800EW IONOMER, MOLDED

TEMP.	TAN DELTA	G'	G''	FREQ.
40.4	0.01564	9.669E+08	1.512E+07	2.8198
43.0	0.01602	9.636E+08	1.543E+07	2.8148
46.1	0.01622	9.592E+08	1.556E+07	2.8085
50.0	0.01650	9.552E+08	1.576E+07	2.8026
54.5	0.01661	9.491E+08	1.577E+07	2.7938
60.0	0.01669	9.427E+08	1.573E+07	2.7843
65.0	0.01658	9.398E+08	1.558E+07	2.7800
70.0	0.01679	9.317E+08	1.565E+07	2.7681
75.7	0.01658	9.258E+08	1.535E+07	2.7595
80.0	0.01663	9.214E+08	1.532E+07	2.7529
85.0	0.01663	9.175E+08	1.526E+07	2.7470
90.0	0.01685	9.130E+08	1.539E+07	2.7404
95.0	0.01630	9.097E+08	1.483E+07	2.7354
100.0	0.01623	9.064E+08	1.471E+07	2.7304
105.0	0.01624	9.020E+08	1.465E+07	2.7238
110.0	0.01634	8.992E+08	1.470E+07	2.7197
115.5	0.01641	8.960E+08	1.471E+07	2.7148
120.0	0.01667	8.906E+08	1.484E+07	2.7067
125.0	0.01678	8.885E+08	1.491E+07	2.7035
130.0	0.01730	8.821E+08	1.526E+07	2.6938
135.0	0.01761	8.779E+08	1.546E+07	2.6874
140.0	0.01818	8.721E+08	1.586E+07	2.6786
145.0	0.01932	8.659E+08	1.673E+07	2.6691

800EW IONOMER, MOLDED

TEMP.	TAN DELTA	G'	G''	FREQ.
150.0	0.02032	8.606E+08	1.748E+07	2.6609
155.0	0.02208	8.519E+08	1.881E+07	2.6474
160.0	0.02390	8.453E+08	2.020E+07	2.6372
165.0	0.02602	8.350E+08	2.173E+07	2.6211
170.0	0.02747	8.282E+08	2.275E+07	2.6105
175.0	0.02957	8.130E+08	2.404E+07	2.5866
180.0	0.02901	8.068E+08	2.340E+07	2.5767
185.0	0.03004	7.916E+08	2.378E+07	2.5524
190.0	0.03153	7.839E+08	2.472E+07	2.5400
195.0	0.03177	7.725E+08	2.454E+07	2.5217
200.0	0.03198	7.660E+08	2.450E+07	2.5111
205.0	0.03272	7.552E+08	2.471E+07	2.4934
212.0	0.03309	7.453E+08	2.466E+07	2.4770
217.5	0.03394	7.339E+08	2.490E+07	2.4581
225.0	0.03457	7.239E+08	2.502E+07	2.4415
233.0	0.03550	7.068E+08	2.509E+07	2.4126
241.0	0.03636	6.898E+08	2.508E+07	2.3836
251.0	0.03902	6.681E+08	2.607E+07	2.3460
262.0	0.04220	5.950E+08	2.511E+07	2.6720
271.0	0.04400	5.820E+08	2.561E+07	2.6440
276.0	0.04660	5.730E+08	2.670E+07	2.6230
281.0	0.05020	5.620E+08	2.821E+07	2.5970
286.0	0.05530	5.510E+08	3.047E+07	2.5730

800EW IONOMER, MOLDED

TEMP.	TAN DELTA	G'	G''	FREQ.
291.0	0.06200	5.330E+08	3.305E+07	2.5280
295.0	0.07310	5.090E+08	3.721E+07	2.4720
300.0	0.08340	4.860E+08	4.053E+07	2.4140
305.0	0.10500	4.380E+08	4.599E+07	2.2910
310.0	0.13000	3.990E+08	5.187E+07	2.1850
313.0	0.14500	3.810E+08	5.525E+07	2.1340
317.0	0.17200	3.110E+08	5.349E+07	1.9270
320.0	0.19200	3.060E+08	5.875E+07	1.9110
323.0	0.21600	2.500E+08	5.400E+07	1.7260
330.0	0.26400	1.900E+08	5.016E+07	1.5020
334.0	0.25900	1.470E+08	3.807E+07	1.3230
337.0	0.25700	1.370E+08	3.521E+07	1.2760
340.0	0.26000	1.000E+08	2.600E+07	1.0940
345.0	0.25300	1.010E+08	2.555E+07	1.0990
350.0	0.23000	7.510E+07	1.727E+07	0.9500
352.0	0.21400	7.800E+07	1.669E+07	0.9690
355.0	0.21600	7.120E+07	1.538E+07	0.9260
360.0	0.20800	6.030E+07	1.254E+07	0.8540
365.0	0.19600	4.340E+07	8.506E+06	0.7270
370.0	0.19900	4.080E+07	8.119E+06	0.7060
371.0	0.18200	4.080E+07	7.426E+06	0.7060
375.0	0.20500	3.060E+07	6.273E+06	0.6160
378.0	0.21200	2.720E+07	5.766E+06	0.5800
386.0	0.27100	1.430E+7	3.875E+6	0.4270